2 Physics Objectives

(We acknowledge contributions by: G. Amelino-Camelia, R. Baier, J. Bartels, G. Baur, M. Beneke, A. Berera, A. Capella, F. Close, C. Costa, J-R. Cudell, Yu. Dokshitzer, A. Donnachie, R. Engel, K. Geiger, A. Giovannini, K. Goulianos, K. Hencken, M.M. Islam, A.B. Kaidalov, Y. Kharlov, V. Khoze, S. Klein, K. Kowalski, P.V. Landshoff, A.H. Mueller, G. Marchesini, R. Orava, E. Papageorgiou, D. Rainwater, J. Ranft, G.P. Salam, S. Sadovsky, D. Schiff, D. Treleani, R. Ugoccioni, A. White, Z. Wlodarczyk, V. Yakovlev, D. Zeppenfeld, M. Zhalov.)

2.1. New hard QCD phenomena at the LHC

2.1.1. Motivations for hard, small x physics at the LHC

2.1.1.1. Large parton densities and a new QCD regime

Recent data from HERA show that the proton's quark and gluon distributions grow fairly rapidly with decreasing x-values for a fixed value of Q^2, in qualitative agreement with expectations. This means that the number of partons, quarks and gluons, in a high energy proton becomes remarkably large at very small values of x. Present indications are that the number of gluons per unit rapidity having spatial transverse size $\Delta x_\perp \propto 1/Q$, is around 25 for moderate $Q^2 \sim 20$ GeV^2 at the smallest $x \sim 10^{-4}$ available at HERA. Parton densities cannot grow indefinitely at small x at fixed Q^2, since this violates unitarity for hard processes. Exactly how this contradiction is resolved is currently the subject of vigorous study by theorists. But clearly new mechanisms beyond the standard hard-scattering picture are necessary. Why this is a fundamental and exciting question is not hard to see [1]. Gluons having longitudinal momentum fraction x and transverse size $\Delta x_\perp \propto 1/Q$ may give a contribution to the typical QCD field strength in the light cone wave function of the proton so large that perturbation theory ceases to be reliable and a new nonperturbative regime of QCD is reached. This is a regime where α_s is small, and so the usual nonperturbative effects of QCD associated with gluon and/or chiral condensates should be unimportant. Nevertheless, the field strengths are so large that interactions are highly nonlinear.

Although parton number densities at HERA and Fermilab energies are large, they do not appear to be large enough to reach a truly high density regime where perturbation theory breaks down while α_s is still small. Deep inelastic scattering on nuclei at HERA may allow one to reach saturation in the $Q^2 \approx$ 3-6 GeV^2 region [2] but studies of very high density, small x partonic systems where α_s is clearly small can only be done at the LHC both for pp and for pA collisions using a forward detector. Such a detector would allow one to extend the previously studied x range by three orders of magnitude.

The consequences for LHC collisions are enormous: at the perturbative QCD scale of 5-10 GeV, literally many thousands of gluon pairs from the projectiles are available for semi-hard collisions. As discussed later, visible jets at this scale may become commonplace even in typical minimum-bias interactions.

2.1.1.2. The BFKL regime; high energy scattering of small color dipoles

For conventional hard-collision processes, the Q^2 evolution is the basic phenomenon. The hard scale is supplied by the virtuality of jets, while there is a soft scale determined by the proton size of ≈ 1 fm.

For the total cross-section of deep inelastic scattering and for typical hadron-hadron hard collisions, the well-known DGLAP equations describe the evolution of the hard-collision rate from the large Q^2 scale to the scale of soft QCD processes. Soft physics then enters in terms of the boundary conditions for these equations. On the other hand, the consideration of the growth of parton densities with energy at fixed Q^2 is attacked within perturbative theory via a different kind of evolution equation, the BFKL formalism [3]. A prototypical process here is the high-energy scattering of two small objects, such as "onium-onium" scattering. For such processes, the strong coupling α_s has a fixed momentum scale Q which is defined by the transverse size of the colliding objects. If the onia are sufficiently small, then α_s is small and this justifies the use of perturbation theory. However, in spite of the smallness of the coupling constant, the lowest order approximation in α_s is still insufficient at very large energies $\sqrt{s}$ and relatively small momentum transfers $|t| = Q^2$. For example, within the leading logarithmic $\alpha_s(Q)\ln s$ approximation, the forward elastic scattering amplitude of the two small-size colorless objects, and thus the total cross-section, increases strongly with energy [3]:

$$T_{el}(s,0) \sim is^{1+\omega} \tag{2.1}$$

where

$$\omega = \omega_{BFKL} = \frac{4N_c \ln 2}{\pi}\alpha_s \quad \approx \quad 0.5 \qquad \text{for} \quad \alpha_s = 0.19. \tag{2.2}$$

Next to leading order corrections are being calculated, and these corrections may reduce substantially the growth of $T_{el}(s,0)$, see e.g. [4].

The Feynman diagrams that contribute to this approximation can be represented as gluon ladder diagrams. This means that, roughly speaking, the growth in energy of the onium-onium interaction is created by multiregge-like production of gluon jets, of typical transverse momentum scale Q or larger. This multijet structure requires extremely large energies and very large acceptance to become manifest experimentally, and will be a major object of study for FELIX.

2.1.1.3. Quark-quark scattering at very large values of s

To clearly study the BFKL process, one ideally wants to maximize the sub-energy $\sqrt{s}$, keeping the transverse scale $p_T \sim Q \geq 5 - 10$ GeV in order to clearly identify parton jets in the final state. An optimal choice for doing this at the LHC is by studying the interaction of valence quarks, with $\sqrt{s} \sim 5$ -10 TeV. At $p_T \geq 10$ GeV, this implies production angles of 2 - 4 mrad.

The naive expectation for the BFKL enhancement mechanism over the one-gluon-exchange process is the associated emission of the multiregge "ladder" of gluons. The cross-section enhancement might be crudely expected (Eqns.(2.1,2.2)) to be $(s/t)^{\omega} \sim 30$, with the average number of emitted gluons being

$$\bar{n} \sim \omega \ln \frac{s}{t} \sim 3 - 4. \tag{2.3}$$

This implies that the original quark dijet coplanarity will be destroyed by the presence of the intermediate gluons. It will, of course, be important to measure the acoplanarity as well as the yield of these multijet configurations in full acceptance. This again requires the FELIX detector.

In addition to this inelastic process the naive expectation for *elastic* quark-quark scattering via color-singlet two-gluon exchange is that it should be enhanced by the square of the BFKL factor $\sim (s/t)^{2\omega} \approx 10^3$.

At moderate energies this two-gluon cross-section is suppressed by two powers of α_S (but enhanced by a factor $\ln s$), and is only a ten percent contribution. However its rapid energy dependence could make it comparable to the inelastic contribution for the above conditions at FELIX. This elastic contribution consists of coplanar dijets occasionally accompanied by a rapidity gap, and is therefore distinguishable from the inelastic contribution. Note that if the elastic contribution does overtake the inelastic, this signals the onset of a "blackness" of the "pointlike" quarks of perturbative QCD physics.

Unfortunately, at present there are no reliable, well-normalized predictions available for these cross-sections. Some detailed estimates, taking into account realistic kinematic effects omitted in the leading order analytic calculations, greatly reduce the naive expectations. Nevertheless a significant enhancement over lowest-order estimates can be anticipated. The measurement of the scattering of valence quarks as a function of angle, at the highest $\sqrt{s}$, therefore is a fundamental empirical probe of this new regime of nonperturbative short-range QCD.

2.1.1.4. Resolving the theoretical uncertainties

While the physics of the BFKL enhancement originates within perturbative QCD, it should be already clear that its role in phenomenology, present and future, remains uncertain. The normalization problem alluded to in the previous section may in time be solved by more detailed calculations. But there are other uncertainties. One is that the quarks of the previous section are not onia or small color dipoles (although arguably such configurations will exist within the valence-parton wave functions of the projectiles), so the applicability of the enhancement factor to quark-quark scattering may not be completely justified.

But the most serious problem is more fundamental, and it is called diffusion in p_T. With increasing energy, the relevant phase space of the gluons inside the BFKL ladder spreads out into both the infrared and the ultraviolet region. So even if the external transverse momentum scale is chosen to be very large, there is a contribution due to the infrared part of the internal phase space which will become important at sufficiently high energy. In other words, in contrast to the DGLAP calculations, the BFKL ladder has no strict separation of short and large distance physics. By choosing sufficiently small sizes of the external particles one can suppress the infrared effects, but with increasing energy these contributions will always grow. At some high energy the perturbative QCD approximation becomes inapplicable. This transition from perturbative to non-perturbative physics defines a *new frontier* in QCD which already is moving into the center of theoretical and experimental interest. It should be clear that to make progress, one will need a large and comprehensive experimental data base.

2.1.1.5. Event structure in the high parton-density regime

The above perturbative QCD ideas should be applicable in the p_T range of 1 - 2 GeV to 10 GeV; however in this regime it will not be easy to clearly isolate gluon jets. This is the "minijet" region, where hadronization effects partially (but not completely) obscure what is happening at the parton level. The phenomena discussed above will have very strong effects on phenomenology in this region of p_T scales at the LHC, and in particular lead to average large dispersion in the multiplicity.

Although BFKL contributions to semi-hard collisions, producing jets of about 5 GeV transverse momentum, occur with a cross-section of only 1 mb or so at LHC energies (including its rapid increase with energy), the parton densities at small x are so large that there can be a large probability for producing several pairs of jets via multiple pair-wise interactions of the partons of the colliding protons. This probability for multiple parton interactions remains high up to $p_T^{min} \sim 10$ GeV/c [5]. Moreover, when the gluon densities become high, the pairwise interaction of small color dipoles (or partons with large virtualities) leads by itself to enhanced multiplicities of produced secondaries [1]. Finally, soft "spectator" interactions may also become much stronger, as discussed in the next section. This is yet another source of large dispersion in multiplicity.

Therefore one can expect that *typical events* at the LHC will be characterized by a significant average density of minijets per unit of rapidity, by large fluctuations in the number of such minijets, and by fluctuations in the multiplicity of soft particles, both for central and for forward rapidities. Long-range correlations even stronger than those seen at the $Sp\bar{p}S$ and Tevatron are expected for the whole rapidity range at the LHC. Correlations between the multiplicity in the fragmentation regions and the central regions should in particular be strong. The pattern of these correlations should be highly sensitive to the pattern of parton correlations in the nucleons and the parton evolution at high densities. Thus even the basic phenomenology of generic central collisions may be quite different at the LHC.

Besides having a lot of jets contained in several units of rapidity, other signals can be expected from such high field strength "hot spots". For example, there may be a significant amount of charm and bottom quark production associated with the gluon jets, with bottom production perhaps only mildly suppressed compared to charm. All of this is a subject still in its infancy and one can expect new ideas and experimental signatures to emerge in the course of the theoretical development of the subject, a development which is receiving impetus also from the importance of understanding the earliest stages of heavy ion collisions [6].

2.1.1.6. Hard coherent phenomena in small x processes

Hard processes at moderate x correspond to small space-time intervals $1/Q$ and to small distances $\leq$ 1 fm. With decreasing x, the transverse space-time intervals remain small but typical longitudinal distances, l_c, in the target rest frame become extremely large [7,8], proportional to the beam energy or equivalently x^{-1}. At the LHC when $x = 10^{-6}$, the value of l_c in the proton rest frame is $l_c = 10^5$ fm. Thus the wave function of a fast projectile is built up over macroscopic distances (on the scale of hadron physics), and is "frozen", due to time dilation, during the collision.

Sometimes the incident-projectile configuration may be a small, colorless wave packet. The interaction of such a configuration with hadronic media is analogous to Fraunhofer diffraction in optics. This limit is different from the BFKL limit discussed above where both objects are small, and has a closer connection to DGLAP evolution. The total cross-section for such "onium"-hadron interactions is still small (color transparency). This follows from the fact that hard high energy processes are dominated by gluon exchanges, and that the cross-section for a small $q\bar{q}$ configuration is proportional to b^2, its size in impact parameter space [9,10]:

$$\sigma^{q\bar{q}}(inel) = \alpha_s(\mu^2)\frac{\pi^2 b^2}{3}\ xG(x,\mu^2). \tag{2.4}$$

Here $G(x,\mu^2)$ is the gluon distribution in the target, and the hard scale μ^2 to be used in the above formula is related to b^2 at the energy scale $x \in 10^{-2} - 10^{-4}$ by the relation $b^2\mu^2 \approx 9$ and $x = \mu^2/s$. The decrease of the cross-section with b is partly compensated by the increase of the gluon density. At fixed size b and at very high energy, when the number of gluons becomes very large, Eq.(2.4) leads to large interaction cross sections and what may be called perturbative color opacity.

An important consequence of color transparency is that, in the region of its applicability, initial and final state interactions are suppressed and cross-sections for hard diffractive processes are calculable in terms of parton densities in a model independent way. So such processes can be used to investigate the three-dimensional distribution of color within hadrons rather than the one-dimensional distribution of deep inelastic scattering.

A number of such processes have been studied at HERA: $\gamma_L^* + p \to \rho(\phi) + p$, $\gamma(\gamma^*) + p \to J/\psi + p$ [11]. These studies find the expected strong increase of the cross-sections for hard diffractive processes $\propto \left[xG(x,Q^2)\right]^2$ and a tendency for restoration of the flavor SU(3) symmetry at large Q^2. FELIX will be able to extend substantially the energy range of measurements for J/ψ photoproduction and also measure Υ photoproduction in a large energy range via AA collisions. Related hard pp and pA processes calculable in perturbative QCD, only possible to study with a forward detector such as FELIX, include diffraction of a proton into three high p_T jets and diffraction dissociation of a pion into two jets in baryon-tagged processes (see Section 2.1.5.2, page 25). In such hard diffractive processes it may also be possible to measure the part of the wave function of a proton relevant for proton decay calculations.

2.1.2. Measurement of parton distributions at small x

2.1.2.1. Kinematics of hard processes to be measured at FELIX

HERA measurements of parton distributions in nucleons have greatly expanded our knowledge about perturbative QCD in the new domain of very small x and large Q^2. They confirm the predicted rapid increase of the parton densities. However the kinematic range available at HERA barely touches the domain where linear QCD evolution equations are expected to break down (see discussion in Section 2.1.1, page 9). A program aimed at measuring parton densities over a wide range of small x and over a range of virtualities Q will be necessary to probe the non linear, high density regime described in Section 2.1.1, page 9; the onset of the regime is signaled by a failure in the consistency of the parton density measurements.

In principle, studies of hard processes at the LHC will allow one to cover a very large x, Q^2 region

$$x_1 \geq \frac{4p_T^2}{x_2 s}, \quad Q^2 \sim p_T^2. \tag{2.5}$$

Here x_1 and x_2 are the momentum fractions of the colliding partons, and p_T is the transverse momentum of the produced jets. In a dijet event, with two jets at large positive rapidities y_1 and y_2, the momentum fractions of the initial partons can be approximately reconstructed as

$$x_1 = \frac{p_T}{\sqrt{s}}\left(e^{y_1} + e^{y_2}\right), \tag{2.6}$$

$$x_2 = \frac{p_T}{\sqrt{s}}\left(e^{-y_1} + e^{-y_2}\right). \tag{2.7}$$

For $p_T^{min} \sim 10$ GeV, Eq. (2.5) indicates that at the LHC the range in x can be extended by at least three orders of magnitude down from the HERA limit to $x \sim 10^{-6}$.

However, the detector should meet at least three requirements:

- The detector should have good acceptance in as large a rapidity interval as possible. Losing two units of rapidity is approximately equivalent to losing one order of magnitude in the x-range.
- The detector should have fine enough angular and momentum resolution to resolve and to measure these jets in the forward region down to $p_T \sim 10$ GeV to ensure that one can probe parton distributions at sufficiently small virtualities.
- To discriminate between quark and gluon densities, the detector should be able to detect prompt photons and preferably also heavy flavor particles as well as electrons and muons.

All of these requirements are satisfied for FELIX. There are several reactions which can be used for the measurements of the parton densities and studies of the related physics:

$$\begin{aligned} pp &\to \mathrm{jet}_1 + \mathrm{jet}_2 + X, \\ &\to \mathrm{jet} + \gamma + X, \\ &\to Q + \bar{Q} + X, \\ &\to l^+ + l^- + X, \\ &\to \mathrm{Z(W)} + X, \\ &\to \gamma + \gamma + X, \end{aligned} \tag{2.8}$$

where $Q(\bar{Q})$ denotes a heavy quark (antiquark), and l stands for an electron or muon. The cross-sections for these processes are straightforward convolutions over parton densities of elementary hard-collision cross-sections $d\sigma/dt$. Details of the cross-sections in lowest order may be found in [12] and relevant parton distributions may be found in [13,14].

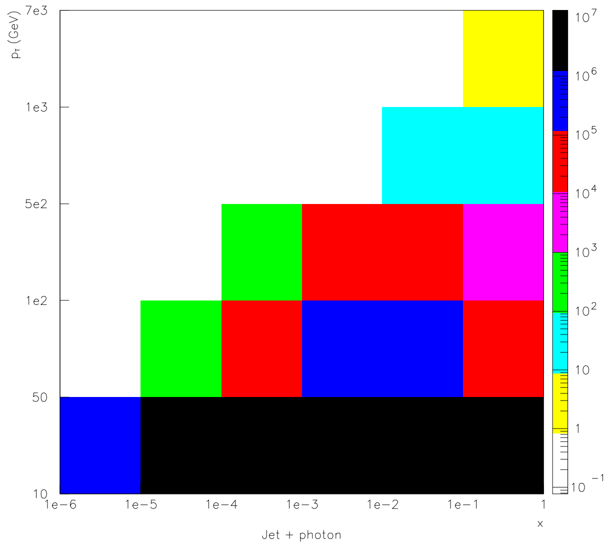

Figure 2.1. A plot of the number of events in (p_T, x) bins for jet + γ production.

To probe the parton distributions at the smallest x possible, it is necessary to choose highly asymmetric kinematics: $x_1 \gg x_2$ (or $x_2 \gg x_1$). In this case the hard subsystem is produced in the nucleon fragmentation region at very large rapidities y. An important advantage of these kinematics is that, for such large y (especially for y corresponding to $|y - y_{max}| \leq 3$), soft interactions result in substantially smaller backgrounds than for $y \sim 0$. Hence we chose $p_T^{min} = 10$ GeV in our estimates. In this case, for $\sqrt{s} = 14$ TeV, the momentum fractions x_i obey $x_1 x_2 \geq 2 \times 10^{-6}$. In fact, for the production of heavy flavors one can probably take p_T^{min} even smaller. For Drell-Yan dileptons, one may go all the way down to $p_T \geq 2 - 3$ GeV, allowing a probe of considerably smaller x. We find that the various reactions in (2.8) allow the measurement of both quark and gluon distributions with a number of cross checks.

2.1.2.2. Jet plus photon

For $p_T \sim p_T^{min}$, one of the safest probes is the production of a jet plus photon. In this case the uncertainties in the reconstruction of a jet of relatively low p_T are minimized. Since we are interested in probing the small x behavior of parton densities, we can consider the cross-section in bins of p_T and x_1, with the parameter x_2 integrated up to 0.8.
Fig. 2.1 shows the number of events in bins of (p_T, x_1) calculated for an integrated luminosity of 100 pb^{-1} where the color bar on the right gives the number of events. One readily observes that large counting rates are expected over the entire range of x_1 with 10 GeV $\leq p_T \leq$ 50 GeV. This will guarantee the statistical accuracy of the measurements to be better than 1%. The cross-section (solid curve)

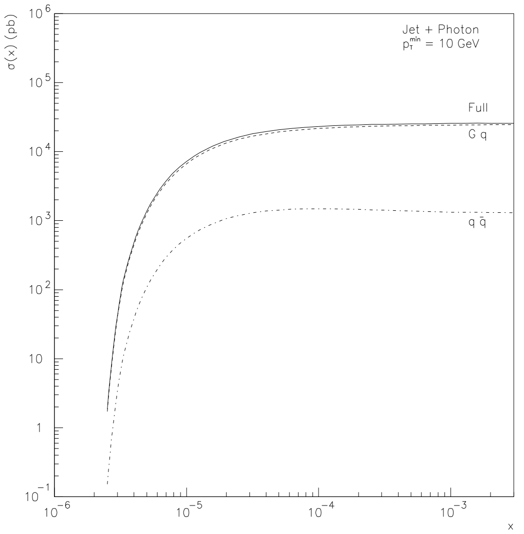

Figure 2.2. The cross-section $\sigma(x)$ for $pp \to jet + \gamma$ + X as a function of $x = x_1$. It is integrated over $p_T > 10$ GeV, max$(x_1, x_2) < 0.8$, and $x/\Delta <$ min$(x_1, x_2) < x\Delta$ where $\Delta = 10^{1/20}$. The choice of Δ corresponds to 10 bins per decade of x.

in bins of x_1 is shown in Fig. 2.2, where the separate contributions from the gq (dashed curve) and $q\bar{q}$ (dot-dashed curve) channels are also shown. The cross-section is dominated by the gq channel, which is at least 10 times larger than the contribution of the $q\bar{q}$ channel over the entire x_1 range. Using large x quark distributions which are known from HERA experiments with an accuracy of better than 10%, it would be possible to extract the gluon density for $x \geq 2.6 \times 10^{-6}$ from this process, (Fig. 2.3). The information from the angular distribution of the jet-γ system for fixed x_1 and x_2 is also of importance for the separation of the gluon and quark contributions [15].

2.1.2.3. Heavy quarks

We next consider the cross-section for the production of charm quarks for the same cut in p_T. As mentioned above, this may be somewhat too conser-

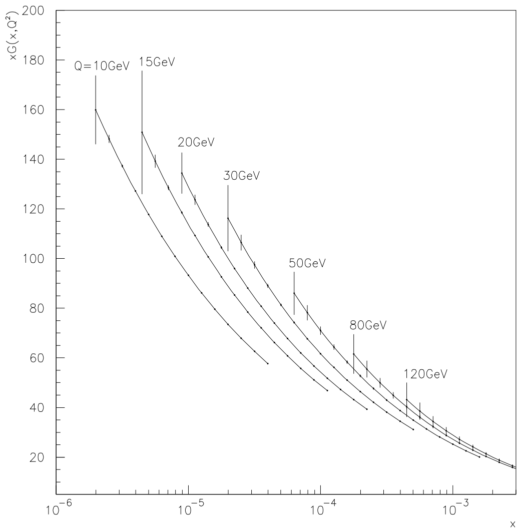

Figure 2.3. The gluon momentum distribution with error bars as determined from the jet + γ cross-section.

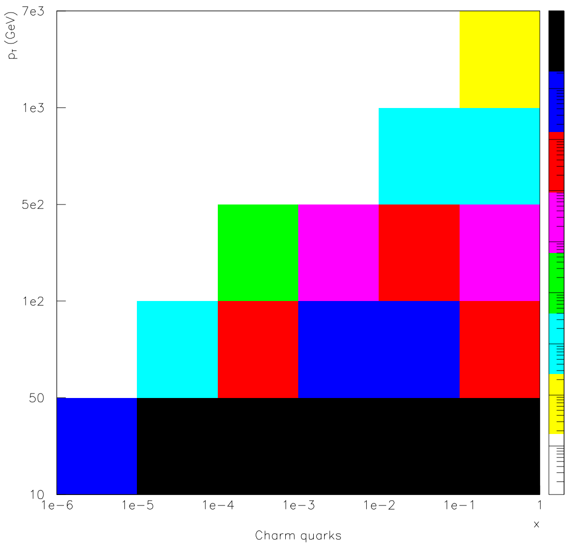

Figure 2.4. A plot of the number of events in (p_T, x) bins for charm quark production.

vative, since the leading particle effect in charm production may allow one to define jets adequately at smaller transverse momenta. We need not consider separately b-particle production, since for $p_T^{min} = 10$ GeV the cross-sections for the production of $b\bar{b}$ and $c\bar{c}$ are comparable. Fig. 2.4 shows a plot of the number of events in bins of (p_T, x_1), with x_2 integrated up to 0.8 for an integrated luminosity of 100 pb^{-1}.

Again, one observes that large counting rates are expected in the entire range of x_1 and $p_T \leq 50$ GeV, as well as for parts of the x_1 range up to $p_T \leq 500$ GeV. In analogy with the jet-γ process, the dominant contribution is given by the $gg \to Q\bar{Q}$ channel, with the $q\bar{q} \to Q\bar{Q}$ channel generally giving less than a 10% correction.

However, in the region $2.5 \times 10^{-6} \leq x \leq 4 \times 10^{-6}$ the $q\bar{q}$ contribution dominates (Fig. 2.5). In this bin the counting rate is about 10^5 events per year, with the $q\bar{q}$ contribution being twice that of gg. Hence, using gluon densities obtained from other reactions as well as from the study of charm at smaller x_2 it should be possible to determine quark densities at $x \leq 10^{-5}$ with a reasonable accuracy.

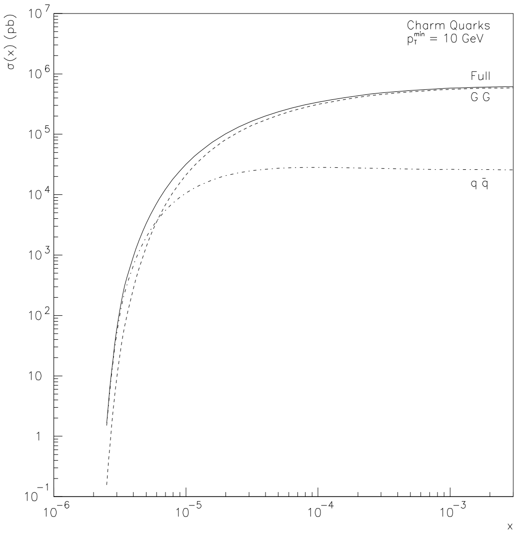

Figure 2.5. The cross-section $\sigma(x)$ for $pp \to Q\overline{Q}$ + X as a function of $x = x_1$. It is integrated over $p_T >$ 10 GeV, max$(x_1, x_2) < 0.8$, and $x/\Delta <$min$(x_1, x_2) < x\Delta$ where $\Delta = 10^{1/20}$. The choice of Δ corresponds to 10 bins per decade of x

2.1.2.4. Two jets

The cross-section for two jet production is about 100 times larger than $Q\bar{Q}$ production. At $p_T \geq 20 - 30$ GeV [16], uncertainties in the determination of the jet p_T become small enough so that this process can be used to study gluon parton densities with only a small correction from the gq process. Obviously this would allow a measurement of the gluon density at small x for much larger virtualities than via the other processes considered above. For $p_T \leq 100$ GeV this process will also provide an independent consistency check of the gluon distributions obtained from the other processes (Fig. 2.6).

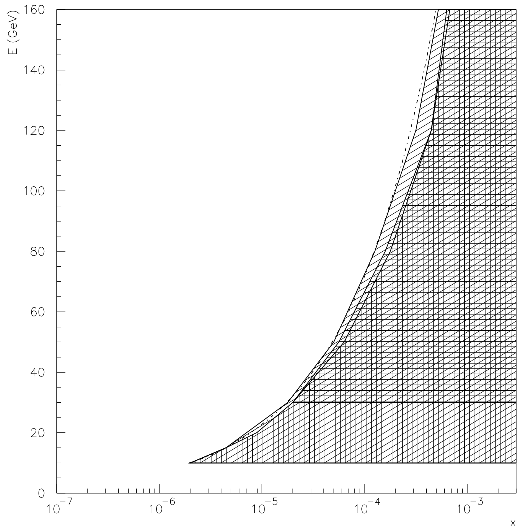

Figure 2.6. A contour plot showing the region in $(E = p_T,\ x)$ where measurements of the gluon density in the proton can be made to within 20% accuracy. The regions marked with vertical, horizontal and slanted lines correspond to jet plus γ, charm quark and dijet production, respectively.

2.1.2.5. Drell-Yan lepton pair production and production of W and Z bosons

The ability of FELIX to identify events with heavy-flavor production should allow a measurement of the Drell-Yan process down to rather small invariant masses – probably down to dilepton masses ~ 4 GeV. Dilepton backgrounds from heavy-flavor processes, in general very serious, are expected to be substantially reduced for the forward kinematics. Consequently it appears possible to probe quark distributions down to $x \sim 2 \times 10^{-7}$ and cover a broad range of x, Q^2 (Fig. 2.7). A study of W and Z boson production will allow one to probe a rather large range of $x_1 \geq 5 \times 10^{-5}$ (Fig. 2.8).

Note also that a measurement of the W^-/W^+

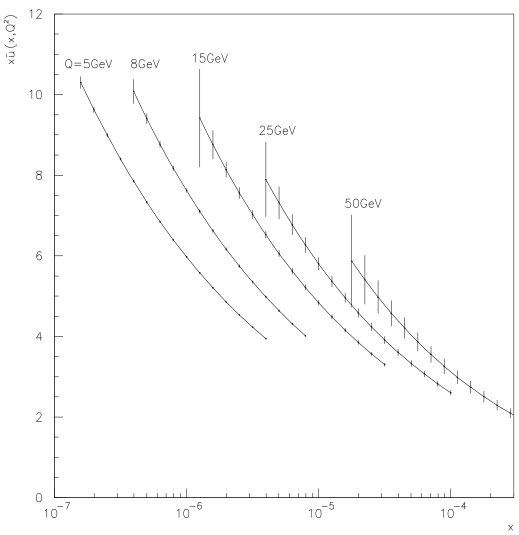

Figure 2.7. The $\bar{u}$ antiquark momentum distribution with error bars as calculated from the Drell-Yan cross-section.

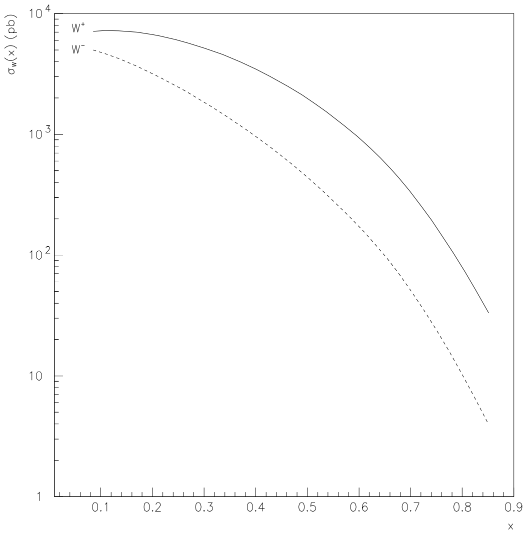

Figure 2.8. The cross-section $\sigma(x)$ for $pp \to W^{\pm}$ + X as a function of $x = x_1$. It is integrated over max$(x_1, x_2)<$ 0.8, and $x/\Delta < min(x_1, x_2) < x\Delta$ where $\Delta = 10^{1/20}$. The choice of Δ corresponds to 10 bins per decade of x.

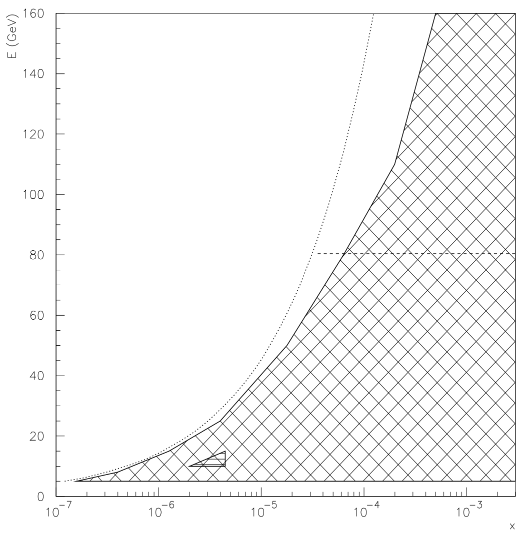

Figure 2.9. A contour plot showing the region in ($E = p_t$, x) where measurements of the anti-quark densities in the proton can be made to within 20% accuracy. The region marked with cross-hatch shading corresponds to the Drell-Yan process. The dashed horizontal line is where W production dominates. The small triangle with horizontal shading shows where charm production is dominated by the $q\bar{q} \to c\bar{c}$ subprocess.

ratio at large x_F would allow a measurement of the $d(x, Q^2)/u(x, Q^2)$ ratio for $x \geq 0.5$, where current determinations are affected by uncertainties from nuclear effects.

Summary

To summarize, we find that due to its unique forward acceptance and to its capability for lepton and heavy-flavor identification, FELIX offers an excellent opportunity for the measurement of quark and gluon parton densities in nucleons down to $x \sim 10^{-7}$ and 10^{-6}. This can be done in several independent ways, with a number of cross checks for the perturbative QCD interpretation of the measurements - (see Fig. 2.6 for gluons and Fig. 2.9 for anti-quarks). These measurements will be able to establish the presence of nonlinear effects in QCD evolution at extremely small x by seeing the breakdown of the predictions of cross-sections via the DGLAP evolution equations.

2.1.3. Diffractive hard scattering at FELIX

By definition, diffraction is the set of phenomena associated with nonexponentially suppressed rapidity gaps. In high-energy collisions, hadrons appear to be fragile objects, their breakup typically resulting in high final-state particle multiplicities. Nevertheless, about half of all hadronic collisions should be diffractive (elastic scattering + inelastic diffraction-dissociation).

In the two decades since QCD was discovered, there has been a noticeable lack of interest in diffraction. This can be perhaps ascribed to the difficulty of relating the phenomena to the fundamental microscopic theory. But now this situation is changing. Diffraction processes represent a primary challenge to theorists: how to understand the phenomena from first principles.

A new subject of active investigation is that of hard diffraction: diffractive processes that contain a hard (short-distance) collision, with visible jets in the final state. Experiments at $p\bar{p}$ colliders and at HERA have provided first evidence of the existence of these processes. This opens up new possibilities for experimentally probing the space-time structure of hadronic scattering.

There are a large variety of basic hard diffractive processes to be studied. There can be more than one rapidity gap in the final state; the most common example is "double Pomeron exchange". A single gap can reside between high-p_T jets ("perturbative Pomeron exchange"). Also, dijet final states can be found in single diffraction dissociation. Each of these basic processes has variants, exhibited in Fig. 2.10. They are all linked logically together, irrespective of how one views the underlying dynamics. How this works will be mentioned again in Section 2.1.4.2, page 22. But to begin we restrict our attention to the relatively well-studied case of single, hard diffractive dissociation.

We will use the variables $x_{I\!P}$ and t to describe diffractive processes ($p + p \to p + X$). $x_{I\!P}$ is the fractional energy loss of the proton, and t is the invariant momentum transfer from the proton to the rest of the system. The squared mass of the rest of the system is then $x_{I\!P}s$. The momentum fraction of the diffracted proton is $x_F = 1 - x_{I\!P}$.

The same definitions can be used if an excited state $n\pi^+, p\pi^+\pi^-$ or ΛK^+ is detected instead of a final proton. It is important to realize that when $x_{I\!P}$ is small it can be measured from the structure of rapidity gap events (e.g. the location in rapidity of the edge of the gap) without using information

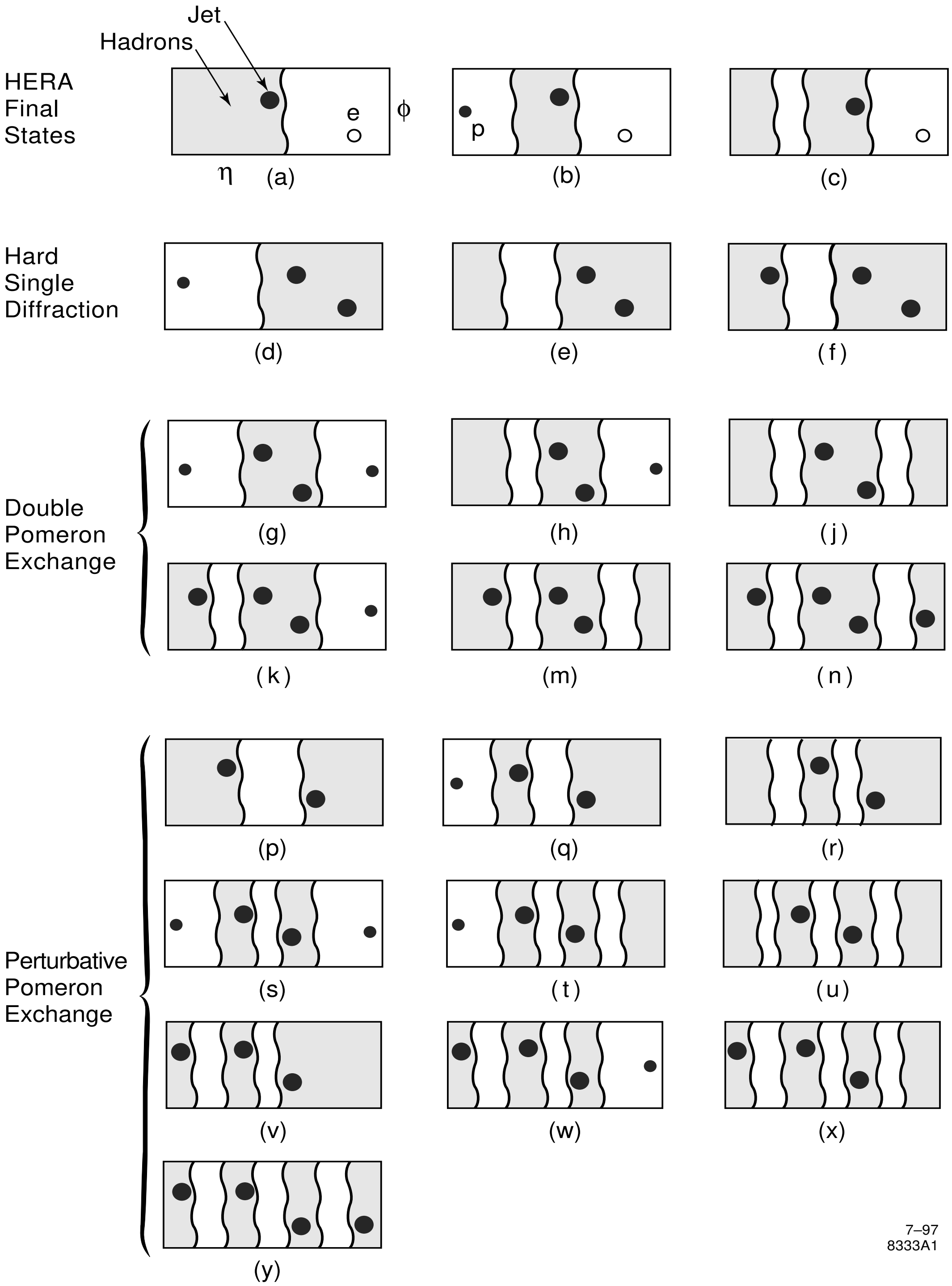

Figure 2.10. Lego plots for the basic class of hard-diffraction events containing jets plus rapidity-gaps. The top row illustrates (a) the generic HERA nondiffractive, high Q^2 final state, (b) the diffractive final state with an undissociated proton, and (c) the diffractive final state with the proton dissociated into a soft, high mass final state. The next row illustrates hard single diffraction for pp collisions, in a hopefully clear notation. Note that the final state in process (f) corresponds to diffraction off a parton in the proton with large p_T, leading to a tagging-jet, and a subsystem similar to the generic HERA final state. The next two rows illustrate the same categories for double-Pomeron-exchange. Finally, the last four rows, beginning with the basic hard process (p) with a gap between jets, adds gaps to the left - and/or right-moving subsystems in a way analogous to the previous cases. Note also that, for example, processes (n) and (y) are closely related. Many other such relationships can be identified.

about the momentum of the leading nucleon (or the diffractively excited system).

The kinematics alone suggests a possible description in which there is an exchange of an entity, the soft Pomeron, between the proton and the system X. Regge-pole theory makes this possibility manifest: the amplitude for the diffractive process factors into 3 pieces: the t-dependent coupling of the Pomeron Regge-pole to the proton, the "propagator" of the Reggeon, containing an energy dependent factor $\left(\frac{s}{M_X^2}\right)^{\alpha(t)}$, and finally the amplitude for the Pomeron to be "absorbed" by the other nucleon and produce the system X.

While this language is widely used in hard-diffraction phenomenology, it is far from established as an appropriate one. As discussed in Section 2.2.2.1, page 35, soft diffraction and elastic scattering may not be simply described by Regge-pole theory at all. In addition it should be remembered that there are two distinct uses for the word *factorization.* One is in the sense of Regge factorization as used above, and the other one is in the sense of hard-scattering factorization. Diffractive hard-scattering is concerned with both kinds of factorization, and one must be careful to distinguish them. As mentioned above and discussed in Section 2.2.2.5, page 38, experimental data appear to show a breakdown of Regge factorization in single diffraction excitation [17,18]. Nevertheless, despite these reservations, the concept of Pomeron-exchange is widely used to describe hard-diffraction processes. In the present case, following the pioneering theoretical work of Ingelman and Schlein and of the UA8 experimental program, one considers the diffractive dijet process as occurring via a Pomeron-proton collision, within which a parton in the Pomeron interacts with another in the proton, producing the dijets in the final state. This picture provides an operational definition of the parton distribution of the Pomeron, although it is not at all guaranteed that the parton distribution so defined can be successfully applied to a different process. It also implies a Regge factorization for the single hard diffraction process itself, again something which needs experimental verification.

In any case, irrespective of the language used, FELIX would allow a systematic study and extension of the studies carried out by UA8 and now extended at CDF and D0 to a broader range of single diffractive processes, containing the hard final states of the nondiffractive processes of Eq.(2.8), as discussed in Section 2.1.2, page 12.

2.1.3.1. Diffractive hard factorization

A generic property of most of the current models for hard diffraction is the assumption of factorization of hard scattering from the soft processes [19–29], see summary in [30]. For example, one writes for nondiffractive dijet production the familiar formula

$$\frac{d\sigma}{dp_T^2\, d\eta_1 d\eta_2} = \sum_{i,j} f_{i/A}(x_a,\mu) f_{j/B}(x_b,\mu)\, \frac{d\hat{\sigma}_{ij}}{dp_T^2\, d\eta_1 d\eta_2}, \tag{2.9}$$

where the momentum fractions x_a, x_b are determined from the kinematics of the collision, i.e. the rapidities η_1 and η_2 of the observed jets. $f_{i/A}$ is the ordinary parton density in the non-diffracted hadron, and μ is the usual renormalization/factorization scale.

For the diffractive process one writes a direct generalization:

$$x_{I\!P} \frac{d\sigma}{dx_{I\!P} dt dp_T^2\, d\eta_1 d\eta_2} = \sum_{i,j} f_{i/A}(x_a,\mu) \frac{x_{I\!P} df^D_{j/B}}{dx_{I\!P} dt}(\frac{x_b}{x_{I\!P}}, x_{I\!P}, t, \mu)\, \frac{d\hat{\sigma}_{ij}}{dp_T^2\, d\eta_1 d\eta_2} \tag{2.10}$$

The ratio of these two cross-sections is the (differential) probability for finding the single-diffractive final state, or differential gap fraction r :

$$x_{I\!P} \frac{dr}{dx_{I\!P} dt} = \frac{1}{\sum_j f_{j,b}(x_b,\mu)} \sum_j x_{I\!P} \frac{df^D_{j,b}}{dx_{I\!P} dt}(x_b/x_{I\!P}, x_{I\!P}, t, \mu). \tag{2.11}$$

The hard factorization hypothesis is that this quantity is indeed dependent only on the properties of the diffracted proton B and not on those of the undiffracted proton A or on hard the collision parameters η_1, η_2, p_T^2.

An even simpler expression can be written down for a gap fraction appropriate to HERA electroproduction, and experimentally this gap fraction, integrated over t, is found to be about 5% (per unit rapidity). The corresponding quantity for UA8 and Fermilab single hard-diffraction data appears to be considerably smaller, of order $(0.5-1)\%$.

For processes like this, where both colliding particles are hadrons, one indeed expects such a substantial reduction of the hard diffractive cross section relative to the hard factorization predictions, given diffractive densities from fits to deep inelastic electroproduction processes. The physics of the reduction is simply the possibility for spectator partons in the hadron projectiles to interact via soft collisions. A necessary condition for the diffractive final state to survive is that no inelastic spectator collisions occur. This obviously leads to a strong reduction of the diffractive cross-section. Indeed in this case factorization can be proven [31] not to hold, at least as a statement about perturbation theory. But it may be possible to prove hard-scattering factorization [27,28] for the class of diffractive hard processes in which there is only one hadron in the final state e.g., diffractive deep inelastic scattering [32]. Hence it is natural to use these processes as a benchmark for determining diffractive quark and gluon distributions [33].[1]

Figs. 2.11 and 2.12 show the cross-sections calculated from Eq.(2.10) for diffractive dijet and W production, respectively, at the LHC using diffractive densities obtained from fits to HERA diffractive DIS data.

It is convenient to represent the measured cross-section as a factorizing cross-section times a suppression factor:

$$\sigma_{\text{true}} = \sigma_{\text{fact}} \times S(x_{I\!P}, t, s). \tag{2.12}$$

Estimates of the value of S typically give a value $S \sim \frac{1}{10}$.

S may actually be a slowly varying, but rather complicated function of initial energy, $x_{I\!P}$, t, and x_B. For example, one can expect that it will decrease with an increase of $\sigma_{tot}(pp)$ (stronger spectator effects), increase with increasing $|t|$ (selection of more weakly interacting configurations in the intact nucleon [39]), and increase as x_B becomes large (due to a selection of smaller size configurations in B).

It would be also interesting to study diffraction to inelastic low-mass final states B in the process:

$$p(p_1) + p(p_2) \to (\text{jet}_1 + \text{jet}_2 + X) + B \tag{2.13}$$

which may select configurations with an interaction strength rather different from the average one. Several examples of the channels feasible with FELIX include the aforementioned $B = n\pi^+, p\pi^+\pi^-$ and ΛK^+, each of which can be studied as a function of p_T of the produced jets for fixed $t \sim 0$. A hard factorization combined with Regge factorization would lead to

$$\frac{\sigma(p(p_1) + p(p_2) \to (\text{jet}_1 + \text{jet}_2 + X) + B)}{\sigma(p(p_1) + p(p_2) \to (\text{jet}_1 + \text{jet}_2 + X) + p)} = \frac{\sigma(p(p_1) + p(p_2) \to p + B)}{\sigma(p(p_1) + p(p_2) \to p + p)} \tag{2.14}$$

It is natural to expect that at least for large enough p_T this factorization would be broken, with the cross-section of diffractive jet production in the inelastic diffraction channel substantially enhanced compared to the expectations of Eq.(2.14).

2.1.3.2. The super-hard Pomeron

One of the striking features of the UA8 diffractive jet data [40] is that in a substantial proportion of the events almost all of the momentum associated with the Pomeron exchange goes into the jet system. The H1 collaboration [37] has presented a fit to their diffractive-electroproduction data in which a similar peak appears in the gluon distribution in the Pomeron.

If the diffractive process is modeled in terms of color-singlet two-gluon exchange, then this contribution can be interpreted as exchange of configurations where almost all the momentum is carried by one or the other of the gluons, but not both. It is even possible that the soft gluon is really nonperturbative in character, perhaps better described as a color-octet system of gluon degrees of freedom which is exchanged. On the other hand, such super-hard terms might be accountable within a perturbative QCD framework [39], especially at reasonably large t and at not too large p_T.

In any case, the phenomenology and theory of these super-hard terms is in its infancy. One should look for them under as large a range of conditions as possible (large and small t, large and small jet p_T). Any experiment that is capable of seeing the kinds of cross-section predicted by factorization will also be able to investigate the super-hard terms. As data from CDF and D0 are analyzed over the next year or two, it should become apparent whether or not they confirm UA8's measurement of a super-hard component to diffractive hard processes.

2.1.4. Rapidity gaps between jets

2.1.4.1. One gap events

An important characteristic of scattering events at the LHC is the color flow in the underlying partonic process. In forward scattering, where the t-

[1] A number of theorists and experimentalists are actively involved in fitting diffractive parton densities to data and in predicting further cross-sections (e.g., [28,34–37]). Coordination of the diffractive physics between the HERA, the Tevatron and the FELIX experiments ensures that predictions made for other processes (e.g., [36,38]) are properly normalized, and known QCD effects (particularly evolution) are taken into account.

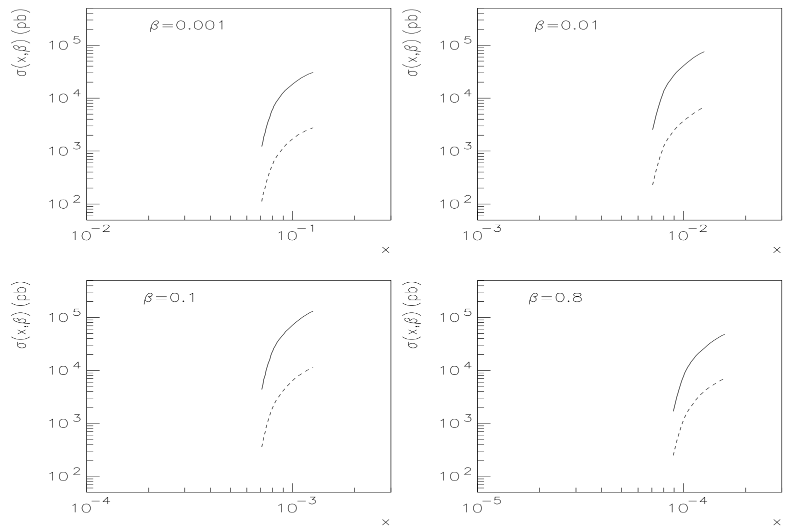

Figure 2.11. The cross-section $\sigma(x,\beta)$ for diffractive dijet production at the LHC for different values of $\beta = |t|/(M_X^2 + |t|)$. The solid (dashed) curves correspond to the fits to the current diffractive data assuming that the Pomeron structure function is dominated by gluons (quarks) at Q_0^2 =4 GeV^2 [38,36]. The cross-section is given as a function of $x = x_2$ and is integrated over $p_T > 10$ GeV, $\beta/\Delta < x_1 < \beta\Delta$, $x/\Delta < x_2 < x\Delta$ and $0.002 < x_{pom} < 0.03$, with $\Delta = 10^{1/40}$. Here, x_1, x_2 are the longitudinal momentum fractions of the dijet relative to the Pomeron and the nondiffracted proton, respectively.

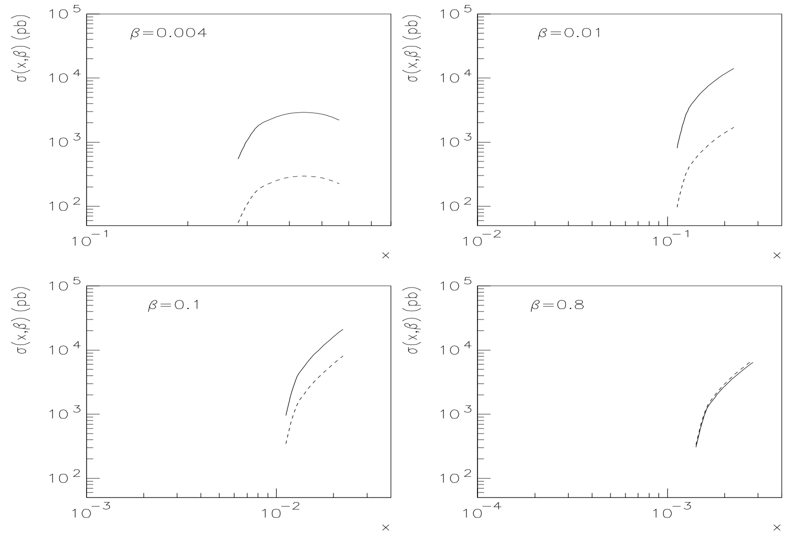

Figure 2.12. The cross-section $\sigma(x,\beta)$ for diffractive W production at the LHC for different values of β. The curves correspond to the same model as in Fig. 2.11. The cross-section is given as a function of $x = x_2$ and is integrated over $\beta/\Delta < x_1 < \beta\Delta$, $x/\Delta < x_2 < x\Delta$ and $0.002 < x_{pom} < 0.03$, with $\Delta = 10^{1/40}$. Here, x_1, x_2 are the longitudinal momentum fractions of the W relative to the Pomeron and the nondiffracted proton, respectively.

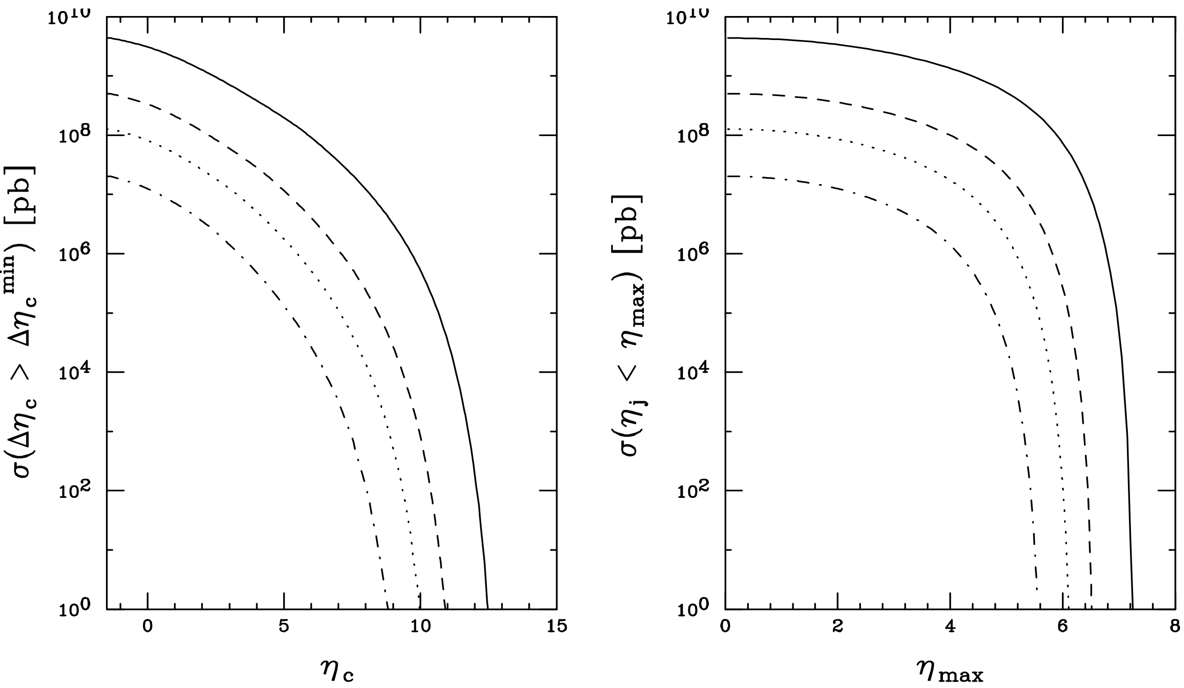

Figure 2.13. Dependence of the dijet cross-section on (a) the rapidity distance η_c between the jet cones and (b) the rapidity range covered by the detector. Curves are for minimal jet p_T's of 10 (solid), 20 (dashed), 30 (dotted), and 50 GeV (dash-dotted lines).

channel exchange of light quanta dominates, color-octet exchange of gluons versus color-singlet exchange of electroweak bosons or Pomerons is expected to lead to very different hadronization patterns. In t-channel color-singlet exchange, color coherence between initial and final state gluon radiation leads to soft gluon emission preferentially into the region between the beam and the forward scattered parton. This leaves the central region (between the two jets in a dijet event) free of gluons and their hadronization products. In t-channel color-octet exchange, on the other hand, gluon radiation into the central region is preferred. Consistently t-channel color-singlet exchange can lead to a rapidity gap, *i.e.* a rapidity region of exceptionally low hadronic activity, for the fraction of pp collisions which produce no underlying event containing soft inelastic spectator interactions.

An excess of dijet events with rapidity gaps has already been observed at the Tevatron [41]. About 1% of all dijet events with rapidity separations $|\eta_{j_1} - \eta_{j_2}| \geq 4$ exhibit anomalously low hadronic activity in the rapidity region between the jet cones. At the LHC, FELIX, with its unique angular coverage, can continue and extend these studies of rapidity gaps in dijet events and, among other things, study the energy dependence of the gap survival probability. Within the DGLAP and BFKL approximations, it is expected that the probability of the hard subprocess would increase with the length of the rapidity interval. On the other hand, since $\sigma_{tot}(pp)$ is expected to increase by nearly 50% between the Tevatron collider and the LHC, one may expect a substantial decrease of the gap survival probability at the LHC for the same η_{j_1}, η_{j_2}.

Fig. 2.13 shows the dijet cross-section as a function of the separation of jet definition cones, $\eta_c = |\eta_{j_1} - \eta_{j_2}| - 1.4$, and as a function of the maximal jet rapidity η_{max}, for p_T thresholds defining a jet of $p_T > 10$, 20, 30, and 50 GeV. For an integrated luminosity of 100 pb^{-1} and a 1% fraction of rapidity gap events, the dijet cross-section in pb corresponds to the total number of rapidity gap events. From Fig. 2.13 it is then clear that FELIX can record meaningful samples of gap events with gaps which are 8 or even 10 units of rapidity wide. What is perhaps more important, FELIX can study the continuous transition from soft diffraction, mediated by Pomeron exchange with $|t|$ in the 1 GeV^2 range or below, to the hard gap events considered here, with a momentum transfer $|t|$ in excess of $t \approx p_{Tj}^2 \geq 100$ GeV^2. Symmetric events with $x_1 \approx x_2$ will be dominated by the scattering of valence quarks for $x_1 \geq 0.3$ and by glue-glue scattering for $x_1, x_2 \ll 0.01$. Asymmetric events with large x_1 but small x_2 on the other hand will be dominated by quark-gluon scattering. The large acceptance in rapidity of the FELIX detector will be vital in separating these samples. Such a study will allow measurements of the fraction of rapidity gap events separately for quark-quark, quark-gluon and gluon-gluon scattering, an issue which is crucial for distinguishing different models of hard rapidity gap events. A model [42] based upon perturbative, color-singlet two-gluon exchange predicts, due to the stronger coupling of the gluons to the color-octet charge of the scattered gluons, an enhanced rapidity gap fraction in glue-glue scattering. A color evaporation model, on the other hand, makes it more difficult for the color-octet charge of scattered gluons to be "bleached" and implies that the rapidity gap fraction is largest for quark-quark scattering [43]. Another possibility considered in [44] is the suppression of the gap survival probability by Sudakov type form factors. FELIX will be able to discriminate in great detail these possibilities. The preliminary evidence from D0 [45] appears to favor the latter mechanism, implying that, even when the momentum transfer is tens of GeV, nonperturbative effects are of great importance.

We also emphasize the importance of investigating the gap-survival probability in the situation when one of the jets is generated by a quark or gluon with $x \geq 0.4 - 0.5$. In this situation relatively compact, weakly interacting configurations in the colliding hadron may be preferentially selected. This could lead to an increase in the gap survival probability to a level closer to what is observed at HERA for γp collisions [46].

2.1.4.2. Multigap events

Hard diffraction events containing more than one rapidity gap should occur and, thanks to the very large FELIX rapidity acceptance, be readily observable. The most familiar example of this class is double-Pomeron exchange, with both undissociated beam protons being detected in Roman pots. This process will be discussed in the next subsection. However, as already illustrated in Fig. 2.10, there are a variety of other quite fundamental processes to be considered.

A convenient starting point for considering these is the hard double-diffraction process discussed above, and observed at the Tevatron, consisting of a rapidity gap between jets. As discussed in the previous section, about 1% of all coplanar dijet events contain such a gap. Theoretically, one expects that there is a 10% chance per event that the hard process be color-singlet exchange, with the remaining 10% factor being due to the requirement that spectator degrees of freedom at other locations in the impact plane do not interact inelastically. This is essentially the factor S in Eq.(2.12).

The event structure in such events is closely related to what is seen in ordinary deep inelastic events at HERA. In particular the left-moving system looks like the entire HERA hadron final state, with the right-moving hadron system being a reflected copy which replaces the single positron in the HERA right-moving system. Since these final states are so similar, it is not at all unreasonable to expect that in the pp or $p\bar{p}$ reactions there will also be a diffractive component. Furthermore, in terms of the gap fractions introduced in Section 2.1.3.1, page 18, it is also reasonable that the fraction of events which contain the extra gaps will be similar to what is seen at HERA, namely 5% per unit rapidity. Therefore of order 10^{-3} dijet events should have an extra rapidity gap. These are by definition a subclass of single-diffraction dijet events which contain a rapidity gap between the jets. A more quantitative estimate is simply found by multiplying 1% by 5%, and by the rapidity interval over which the second gap edge can occur (a number which will be between 3 and 10 in practice). There is of course another factor of two from choosing which of the incident protons is diffractive.

If both left- and right-moving systems choose to be diffractive, then the final state system contains three rapidity gaps. This is a special case of a hard double-Pomeron process. Multiplication of 1%, $(5\%)^2$, and a factor 10 for the rapidity acceptance of the two new gap edges, gives for the fraction of dijet events with this rich topology a number of order 3×10^{-4}. Note that now one can remove the central gap, and obtain an estimate for the number of ordinary double-Pomeron hard-diffraction coplanar dijet events of the order of 3×10^{-3}. Again, a more precise prediction would be in terms of a gap fraction differential in the locations of the two gap edges; this number is evidently $1\% \times (5\%)^2 \times 10 = 3 \times 10^{-4}$. Likewise, one can remove the central gap in the double-gap, hard-single diffraction example, and get for the gap fraction, differential in the location of the gap edge, the value $1\% \times 5\% \times 10 = 5 \times 10^{-3}$. This number is quite consistent with what is observed, as quoted in Section 2.1.3.1, page 18.

It is very important to recognize that this line of argument, based in large part on the HERA phenomenology, is only appropriate for the hard collision process being a quark-quark interaction; there is little doubt that this is what generates the "quark-jet" in the HERA final state. Furthermore, the diffracted mass at HERA at a given Q^2 is typically of order Q or more; the contribution with $M_X^2 \ll Q^2$ is higher-twist. What this means kinematically is that, in the HERA laboratory-frame, the diffractive gap edge cannot be too close to the quark-jet seen in the final state. The distance in the lego plot from gap edge to jet core is bounded below by $ln\ Q$. This feature should persist, for quark-quark processes, in the FELIX context as well.

However we already noted in Section 2.1.4.1, page 19, that both from experiment and theory there are expected to be important differences between quark-initiated processes and gluon-initiated ones. The gap fraction for quarks may be larger than that for gluons. However, in the case of gluons there is the evidence from UA8 that, in the Pomeron-exchange language, there is a super-hard component to the Pomeron structure function. What this means in practice is that kinematically the Pomeron exchange acts as if it is a single-gluon exchange. This is just what is in fact observed in the Tevatron hard double-diffraction process. The rapidity-gap edges are seen to be at the edge of the jet cores (0.7 units away), and the final state is as if there were photon exchange between the left-moving and right-moving systems.

This is also the phase-space signature of the super-hard Pomeron contribution to hard single-diffraction production of dijets as observed by UA8. The superhard contribution puts the rapidity gap at the edge of the dijet system. So, in summary, for quark-induced hard collisions the gap edge is separated from the quark jet by at least $ln\ p_T$, but for gluon-induced hard collisions, there need not be such a constraint. In terms of the microscopic dynamics, this distinction has to do with the fact that when color triplets are produced in distant parts of phase space (as in electron-positron annihilation), rapidity gap production in the intermediate phase-space region is exponentially suppressed. For color-octet systems, however, extra (possibly nonperturbative) soft gluon exchanges allow the screening of the octet color and therefore allow larger rapidity gaps to form. However, the systematic theoretical development of these ideas is still in its infancy. And if nonperturbative mechanisms are involved (as the recent D0 data suggest [45]; cf Section 2.1.4.1, page 19) it may take some time as well as considerable data to create the full picture.

Experimentally, it will be important to systematize the gap-fraction contributions from the quarks and from the gluons and, in the case of the gluons, to determine what fraction of their contribution is superhard. At present there are only the rough beginnings of this phenomenology.

For FELIX, even the triple-gap process fits rather comfortably into its acceptance. If the dijets are produced at 50 mrad with a p_T of 20 GeV, then the central gap extends from +100 mrad to -100 mrad, an interval of six units of rapidity. If the process is quark induced, the gap edge must be roughly at least 3 units of rapidity beyond the jet-core rapidity, namely at an angle of 2.5 mrad. So the study of the distribution of the gap edges should be possible over a broad range relative to this central value.

There are clearly a variety of lines of generalization for this approach. An important one is to vary the momentum transfer to the diffracted proton; there may be a distinctly different behavior in the soft region of $|t| < 0.4$ GeV^2 and the semihard region $|t| > 1$ GeV^2. One may also see what happens when the proton is softly dissociated into a low mass system like $p\pi^+\pi^-$, $n\pi^+$, ΛK^+, etc. (This is probably a small fraction of the gap events, perhaps of order 1%.) Next, one should look at what happens when the proton dissociates softly into a high-mass system. This is harder experimentally, although do-able. Theoretical expectations based on existing data from HERA and the Tevatron suggest that this component is perhaps $5-20\%$ of the contribution from undissociated protons. Finally there is the contribution from very high momentum transfers, high enough to create a tagging-jet in the diffracted-proton system. This subprocess should of course have a much smaller cross-section (for fixed kinematics of the central dijet, etc., system). It should be estimated by taking the perturbative cross-section calculation for the full multijet system without gaps (including the aforementioned tagging jets), and then appending the differential gap-fraction estimates for each rapidity gap, with one final factor of the gap survival-probability S. It is important to note that the survival probability factor S is applied once, and only once, since it once and for all requires all spectators not to interact inelastically.

From a practical point of view, the gap-fraction approach allows one to estimate cross-sections and construct simulations from the existing theoretical Monte-Carlo data base. One may simulate in general the hard processes without gaps, and then analytically estimate the fraction of those processes which will contain the gaps of interest. Also, from the point of view of triggering, it is clear that one will take as primary trigger the jet structure (p_T, existence of jet cores, etc). Certainly in many if not most cases, this will give a low enough trigger rate that the gap search can be done offline or at Level 2. In the remaining cases, lack of activity at very large rapidities, or existence of a Roman pot tag, should easily suffice to reduce the trigger rate to a reasonable value.

2.1.4.3. Double-Pomeron exchange

The ideas applied to single diffractive hard scattering and to single gap events can be applied to double-Pomeron induced processes as well:

$$pp \to p + X + p, \tag{2.15}$$

with a large rapidity gap on opposite sides of the central system X, *i.e.*, between X and each of the two diffracted beam particles. Because of the information obtainable from the Roman-pots, this process is especially accessible to detailed experimental scrutiny. Recently, first evidence for the occurrence of such processes, with dijets in the central system X, has been reported by D0 [45]. The gap fraction, however, is quite low, and it is not yet clear whether the yield is consistent with the estimates made in the previous subsection.

More detailed estimates of cross-sections for this class of processes exist, but at present the spread in the predictions covers several orders of magnitude. The basic underlying mechanism assumed in most calculations is perturbative color-singlet two-gluon exchange, something which itself is not above suspicion. But even so, estimation of the cost of suppression of soft gluon radiation, etc., creates major uncertainties.

If super-hard Pomeron collisions occur, then they will result in a spectacular signature in double-Pomeron exchange events: the final state consists of a proton going down each beam pipe plus a central two-jet system and absolutely nothing else. The shadowing effects already observed for single diffraction probably strongly reduce the rate as compared to the expectations based on perturbative QCD, without taking shadowing into account. It is not yet clear whether the hard double-Pomeron-exchange processes seen at the Tevatron contain superhard contributions. The next collider run at Fermilab should create a much improved data base.

2.1.5. Hard exclusive diffraction

2.1.5.1. Diffraction into three jets

It is possible that a nucleon (meson) has a significant amplitude to be in a configuration where valence partons are localized in a small transverse area together with the rest of the partons. These configurations are usually referred to as *minimal* Fock space configurations - $|3q\rangle$ ($|q\bar{q}\rangle$). Strong evidence for the importance of such configurations in the wave function of vector mesons has been obtained recently at HERA from the observation of the rather rapid increase with energy of the cross-sections for exclusive electroproduction of ρ, ϕ and especially J/ψ-mesons at small x. Hadrons in such a configuration occupy a small transverse area with a larger probability than in the case of nonminimal configurations, because, e.g. the long range pion field is very weak. Therefore, such initial configurations are expected to interact with other hadrons, even at high energy, with a small cross-section. In the case of the "elastic scattering" of such a proton configuration off another proton, this three-quark system with large relative momenta should preferentially diffractively dissociate into a system of three jets with large transverse momenta $p_{Ti} \sim \pi\ b^{-1}$, where b is the transverse size of the minimal configuration. The production cross-section for the three jets can be estimated [47] to leading order in $(\alpha_s \ln M^2_{3jet})$. As in the case of diffractive vector meson production in deep inelastic scattering, the cross-section is proportional to the square of the gluon density in the nucleon at $x \approx M^2_{3jets}/s$, and virtuality $\sim p^2_{T\ jet}$. The distribution over the fractions of the momentum carried by the jets is proportional to the square of the light cone wave function of the $|3q\rangle$ configuration. Hence the diffraction of a proton into three jets provides important information about the short-distance quark structure of the proton, and also provides unique information about the longitudinal momentum distribution in the $|3q\rangle$ configuration. From an analysis of diffraction data [47,48], numerical estimates lead to a value of the cross-section integrated over everything except a $p_{T\ jet}$ threshold for one jet,

$$\sigma_{3\ jets} \sim (10^{-4} - 10^{-5}) \left(\frac{5\ \text{GeV}}{p_{T\ jet}}\right)^8 \text{mb}. \tag{2.16}$$

The probability of the $|3q\rangle$ configuration is estimated using a phenomenological fit to the probability of configurations of different interaction strengths in a nucleon (cf. [47,48]). One can see from the estimate (2.16) that FELIX should be able to collect more than 10^7 events/year in this interesting kinematic regime. Studies of this reaction in pA collisions (Section 2.3, page 43) will allow one to enhance this signal.

Another interesting group of hard processes is proton diffraction into 2 high p_T jets and one collinear jet. These processes are dominated by parton configurations when only 2 quarks in the projectile proton are close to each other, i.e., have large transverse momenta. Such quark configurations are relevant for estimates of proton decay rates. The wave function describing such a configuration can be measured in the double-diffraction process where each of the protons fragments into 3 high p_t jets: $pp \to jet(k_t) + jet(-k_t - q_t) + jet(q_t) + jet(l_t) + jet(-l_t - r_t) + jet(r_t)$. Note that to measure the cross-section for such diffractive processes, both arms of the FELIX spectrometer are needed.

2.1.5.2. Tagged-pion diffraction dissociation

Reactions containing a very forward neutron or a Δ-isobar can be dominated by the scattering off the pion cloud of the nucleon. In this way the proton beam is effectively converted into a pion beam; the leading baryon is effectively a pion tag. A necessary condition that one-pion exchange dominates this process is that the transverse momentum of the forward baryon be small compared to 300 MeV and, in the case of the Δ, that its x_F exceed 0.9. The precise condition is

$$|t| = (\frac{M_B^2}{x_F} - m_N^2)(1 - x_F) + \frac{k_t^2}{x_F} \leq 0.1\mathrm{GeV}^2. \quad (2.17)$$

One must still deal with absorptive corrections due to the simultaneous interactions of the projectile with a nucleon and a pion. These are expected to be corrections no larger than a factor two.

Two types of processes would be of special interest:

Pion diffraction into two jets:

In analogy with the process of nucleon diffraction into three jets it is expected that a pion can dissociate into two jets in the process $\pi + p \to jet_1 + jet_2 + p$ [49,50] (Fig. 2.14).

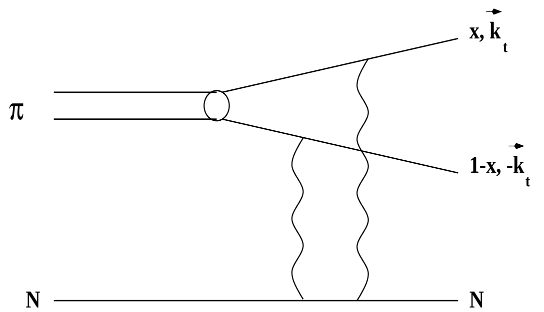

Figure 2.14. Illustrative diagram for hard diffractive production of jets when an incident pion dissociates into a $q\bar{q}$ pair before hitting the nucleon. The exchanged gluons are represented by wavy lines.

The cross-section for this process has a similar structure [50,51]: due to the rapid increase of the gluon density with energy one expects the cross-section for pion diffraction into two jets to be much larger than in the case of the fixed target experiment E791 at FNAL which has just reported first evidence for this effect [52].

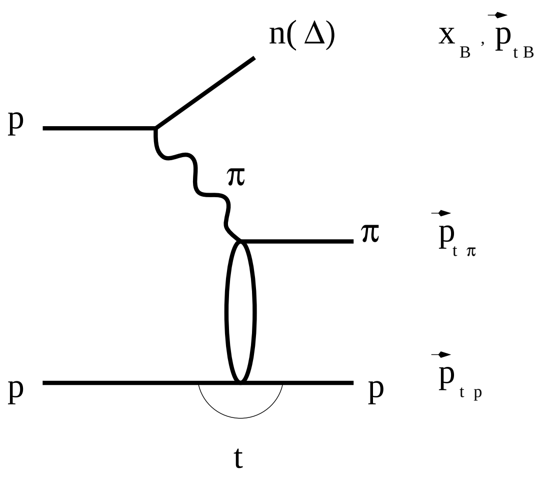

Figure 2.15. Diagram corresponding to large $|t|$ elastic scattering off the pion cloud.

Two → three hard reactions:

It is also interesting to study large $|t|$ elastic scattering off the pion cloud in a number of reactions [53] like(Fig. 2.15):

$$pp \to B(p_{T\ B}) + \pi(p_{T\ \pi}) + p(p_{T\ p}), \qquad (2.18)$$

for $B = N, \Delta$, $x_F(B) \geq 0.9$, $p_{T\ B} \sim 0$, and $p_{T\ \pi} \sim -p_{T\ p} \gg 1$ GeV, which corresponds to the proton elastic scattering off the pion cloud. Although the flux of such pions in the proton is only $\sim 1\%$, at large $|t| \approx p_{T\ p}^2$ the cross-section for elastic πp scattering is expected to be substantially larger than the cross-section for elastic pp scattering. [2] Hence the cross-sections for reaction (2.18) and elastic pp scattering at $|t|$ larger than 10 GeV^2 should be comparable.

One may also consider elastic scattering of two pions in processes like

$$pp \to B(p_{T\ B}) + \pi(p_{T\ \pi}) + \pi(p_{T\ \pi'}) + B'(p_{T\ B'}) \quad (2.19)$$

for $B, B' = N, \Delta$, $x_B, x_{B'} \geq 0.9$, $p_{T\ B} \sim p_{T\ B'} \sim 0$, and $p_{T\ \pi} \sim -p_{T\ \pi'} \gg 1$ GeV. Again the much slower decrease of the $\pi\pi$ elastic scattering with $|t|$ helps to compensate the small probability of finding both nucleons in configurations with pions.

Many generalizations of such processes can be estimated. These include channels with strange par-

[2] The high-energy data on large $|t|$ πp elastic scattering [54] are consistent with this expectation.

ticles in the final state like

$$pp \to (\Lambda K^+, \Sigma^+ K^0) + p$$

as well as kinematics for which the transverse momentum of the proton is balanced by a baryon, not a meson. Such processes are of interest, both for the study of high-energy scattering and for the structure of color correlations in hadrons, especially in relation to the question of intrinsic strangeness in nucleons, see e.g. [55]. Note that at sufficiently large $|t|$, where the colliding-hadron configurations are sufficiently small for the applicability of perturbative QCD, new factorization relations are expected to be valid. The ratio of elastic cross-sections at large $|t|$ should be equal to the ratio of the probabilities for small configurations in the colliding hadrons. For example

$$\frac{\frac{d\sigma^{el}}{dt}(Kp)}{\frac{d\sigma^{el}}{dt}(\pi p)} \to \left(\frac{f_K}{f_\pi}\right)^4 \sim 3. \tag{2.20}$$

Here f_π, f_K are the leptonic decay constants of the π- and K-mesons.

2.1.6. Quarkonium physics with FELIX

2.1.6.1. Problems with the theory of quarkonium production

There is of course a long history of quarkonium production in hadron-hadron collisions, with quite a rich data base, especially for the S-wave spin-triplet states $J/\psi, \psi', \Upsilon(nS)$. Because these states are made of heavy degrees of freedom, it is expected that their production properties will reveal important information on an underlying hard production process. However, the mechanism of quarkonium formation has stubbornly resisted the theoretical interpretations based upon the simplest perturbative QCD mechanisms. Even after twenty years of development, until recently theory and experiment on high-p_T charmonium hadroproduction differed by one to two orders of magnitude.

However, there have been promising recent developments in the theory. In particular, aside from the question of how to describe in detail the underlying dynamics, it has been explicitly recognized that the ratio of bound-charm production to low-mass open-charm production for the same external kinematics, e.g. pseudorapidity and p_T, is a slow function of such variables and typically of order 10 percent. This feature is a central element of the color-evaporation model of charmonium production, but is not limited to this theoretical description. For recent reviews of the theoretical and experimental situation see [56–58].

2.1.6.2. Probing gluon densities

It is not clear, however, whether this 10% ratio of bound charm to low-mass open charm will extrapolate into the LHC kinematic domain, especially in the very-small-x regime, where novel nonlinear effects are anticipated. If it changes, this in itself is a strong indicator of new phenomena occurring. And if the ratio of hidden to open charm production does not markedly change, then the hidden-charm production should be a faithful indicator, for whatever reason, of the nature of the physics of the more-difficult-to-measure, but more-easy-to-calculate, open charm production. In this regard, it is important to recognize that the J/ψ production process is distinguished by offering the largest reach as far as probing the gluon density at small x is concerned. The kinematic limit, realized in very forward J/ψ production at the LHC, is given by $x \approx 5 \cdot 10^{-8}$. At such small values of x the effect of saturation of the gluon density should manifest itself in terms of a failure of naive extrapolations of total production cross-sections from fixed target and Tevatron energies. It might correspond to an increase of these cross-sections by a factor of ~ 100.

The usefulness of such a measurement to precisely determine the gluon density is probably limited, because the nonperturbative parameters that describe quarkonium formation cannot be completely eliminated by normalizing the cross-section to low-energy data. Nevertheless, the qualitative behavior of the gluon distribution should be clearly visible. The main uncertainties which arise from energy-dependent perturbative QCD effects as well as from nonperturbative effects can be investigated through the x_F dependence of the production cross-section.

The situation could be improved at the expense of losing some of the reach in small x by measuring the p_T distribution at large transverse momentum ($p_T \approx 20\,\mathrm{GeV}$, say), where quarkonium production is for sure dominated by color-octet fragmentation of a virtual gluon as the initiating process. In this case, in the framework of nonrelativistic QCD, the only unknown is a single nonperturbative parameter which can be eliminated by normalizing the rate to Tevatron data.

There is more that can be done to elucidate the detailed mechanism of the quarkonium formation. The comparison of quarkonium and open charm (beauty) production close to threshold over a wide range of transverse and longitudinal momenta, as already indicated above, would be very revealing.

Would this ratio stay the same as simple color evaporation models suggest? Polarization measurements are of special importance, since polarization yields information on the nature of quarkonium binding from a heavy quark-antiquark pair, and, to a lesser extent, also on the underlying heavy quark production mechanism.

Direct J/ψ polarization at large transverse momentum, in particular, can discriminate between the color evaporation model and other ideas, such as the nonrelativistic QCD approach [57], which is diagrammatic, but includes Coulomb-like enhancements due to the low velocity of the heavy quarks. The former mechanism assumes an important role of soft (transverse) gluons being emitted and absorbed during the formation of the quarkonium bound state, such that no information on the spin of the heavy quark pair is preserved. In this case an isotropic angular distribution of decay muons in the J/ψ rest frame is expected. In the nonrelativistic QCD approach a significant fraction of transverse polarization is predicted and it should increase with increasing p_T. As soft gluons should couple to bottomonium more weakly than to charmonium, a comparison of the angular distributions in direct Υ and J/ψ production would be especially interesting.

With good photon identification and energy resolution, a polarization measurement of P-wave χ_{cJ} states, something which has not been done to date, may become feasible via their radiative decays. The χ_{c2} polarization is of special interest here, because at leading order (integrated over all p_T) χ_{c2} is produced with helicity 2, provided color-singlet production dominates the rate. The polarization measurement will clarify the relative importance of alternative production mechanisms, such as color-octet production.

Such measurements are certainly difficult. But for sure the best chance is to search for these states when they are produced at large energies, where the radiative γ at least has a relatively high energy. For a χ_{c2} produced with 700 GeV laboratory momentum, the γ will have a typical energy of 90 GeV.

The bottomonium system has not been explored very well in hadron-hadron collisions so far, mainly because of either lack of statistics or lack of photon identification. For example, it has not been possible so far to separate the indirect contribution to $\Upsilon(nS)$ production through χ_b production and their subsequent radiative decays. Again, such a measurement, while difficult, would add another important piece to our understanding of quarkonium production mechanisms, and in particular to their scaling with the heavy quark mass. For example, the observed ratio of χ_{c1} to χ_{c2} production cross-sections can only be explained by invoking a large contribution from color-octet production to both states. Observation of this ratio for bottomonium states would not only test this explanation, but also probe the coupling of soft gluons to $b\bar{b}$ pairs. If these couplings are described by the nonrelativistic QCD formalism, then the χ_1/χ_2-ratio is predicted to decrease significantly as compared to charmonium. In the color-evaporation model, the ratio would stay constant. Again, in the forward kinematics, the photons from the χ decays carry relatively large momenta and the energy and angular resolutions of the calorimeters may be sufficient for such measurements.

A measurement of the energy dependence of the ratio of the yields of Υ and J/ψ production at large fixed x_F would be of special interest. This ratio is expected to increase with incident energy due to a more rapid increase of gluon density with x at larger virtualities. This effect may be amplified due to nonlinear effects for gluon densities (saturation effects) which should be much more important for smaller virtualities relevant for J/ψ production.

The observation of $\Upsilon(3S)$ at a rate comparable to $\Upsilon(2S)$ at fixed-target and the Tevatron is a difficulty for the nonrelativistic QCD picture, which suggests the existence of an as yet unobserved $\chi_b(3P)$ state. Verifying or excluding this state by direct observation would yield another constraint on the nonrelativistic QCD description of quarkonium production. Besides P-wave states, potential models predict many bottomonium states below threshold that have not been observed so far. Of particular interest would be the observation of D wave states and the observation of η_b in its $\gamma\gamma$ decay.

2.1.7. Searching for BFKL effects in hard processes

As already discussed in Section 2.1.1.2, page 9, a strong growth of the scattering amplitudes is expected in the high-energy limit for the interaction of small color dipoles such as onia. In the BFKL model for the interaction of two dipoles of the size of the J/ψ one expects the total cross-section to increase $\approx s^{0.5}$, see Eq.(2.1). In other models a somewhat smaller increase is expected [4,59].

2.1.7.1. Mueller-Navelet jets

For FELIX, a basic measurement is that proposed by Mueller and Navelet, namely the inclusive measurements of two jets with as large a rapidity interval between them as possible (Mueller-Navelet jets [60]).

This is essentially the quark-quark process already discussed in Section 2.1.1.3, page 10. At present the attempts to find BFKL effects are rather ambiguous. At HERA, extra jet activity in the proton direction is a possible signal, as well as the behavior of F_2 itself. At Fermilab, the evidence from hard double diffraction (rapidity-gap between jets) and small-angle dijet production remains inconclusive.

Mueller and Navelet emphasize the importance of comparing the production cross-sections of the 2 jets at different energies, but the same x_i and p_T. The ratio of the yields is then simply

$$\frac{\sigma_1}{\sigma_2} \sim \left(\frac{s_1}{s_2}\right)^{\omega}, \tag{2.21}$$

where ω is given by Eq.(2.2). This is one of the most important reasons, from the point of view of the FELIX program, for running the LHC at a reduced energy. If this is done, the analysis of data becomes much less theory dependent. In this respect the planned studies at the Tevatron will benefit the proposed program, although the limited rapidity coverage of CDF and D0 remains a limitation. But, in general, reduced-energy running at the LHC is desirable for most any new physics and/or standard physics for which there is a substantial application of perturbative QCD phenomenology.

Other important distinguishing features of the BFKL mechanism for the production of two jets with a large rapidity separation would be the dependence of the transverse momenta of particles produced between the jets, because characteristic virtualities in the BFKL ladder are $\sim p^2_{T\ jet}$ and a different pattern of azimuthal decorrelations of the jets will occur. As mentioned above, attempts to study these effects were recently performed at the Tevatron. The results for the rapidity dependence of the cross-section are not yet compelling [61]. A more refined test is the azimuthal correlation of the two jets [45,62], and this looks more promising.

2.1.7.2. High multiplicities in events with Mueller-Navelet jets

In the two-jet production with Mueller-Navelet kinematics, multiple interactions of the two colliding partons are possible. Mueller and Salam [1] have recently estimated these in a simple analytic model, as well as numerically. Their expansion is in the "number of cut BFKL Pomerons", k, which is in rough proportion to the number of associated jets produced. The results are shown in Fig. 2.16.

The number of jets produced per unit rapidity is $(\alpha_{I\!P} - 1) \cdot k \approx \frac{1}{2}k$. Such events would be quite striking. Over a few units of rapidity there would be, for $k = 10$, about 5 jets per unit rapidity. For jets having $k_\perp$ on the order of 5 GeV this should be right around the saturation regime where one can expect the jets to interact strongly. It is also where our present ability to calculate in perturbation theory breaks down so that one should regard this at best as a rough estimate when k is as large as 10. It must be emphasized that this mechanism of multiple minijet production is distinct from that to be discussed in the next subsection.

2.1.7.3. Elastic (or diffractive) proton-proton scattering at large momentum transfer $|t|$

Another place where the BFKL calculation might be used is the pp large-$|t|$ elastic or diffractive scattering : $pp \to X + p$ [39,63,64]. Here the large scale which justifies the use of perturbative QCD is given by the momentum transfer t to the final proton, and the hadronic scales at the two ends of the ladder do not spoil the BFKL prediction. The main signatures of the BFKL calculation are the BFKL-like energy dependence of the cross-section at fixed t and the slope of the t-dependence which is predicted to be smaller than in typical soft hadronic processes. For detailed discussion of elastic pp scattering see Section 2.2.2, page 35.

2.1.8. Multiple minijets at the LHC

Everyone knows that, for the purposes of hard-collision phenomenology, a high-energy proton may be regarded as a beam of (temporarily) non-interacting partons with a phase-space distribution depending upon the hard-collision scale. Enormous effort has been invested in learning about the distribution in longitudinal momentum of these partons. However, the relevant phase space is not one-dimensional, but three-dimensional. The other two coordinates are most conveniently taken to be the transverse impact plane coordinates.

Very little is known about the transverse distribution of partons, or how they are correlated transversely or longitudinally. For example, in a constituent quark picture we are not yet able to tell whether the infinitely many wee partons associated with an infinite-momentum proton are correlated with the valence system (Fig. 2.17a), whether they are correlated with the distribution of the vacuum chiral condensate, i.e. "pion cloud" (Fig. 2.17b), or whether they are correlated at all. The reason for this profound level of ignorance is that in most processes which are studied experimentally the transverse information is integrated out. One of the most promising sources of impact-plane infor-

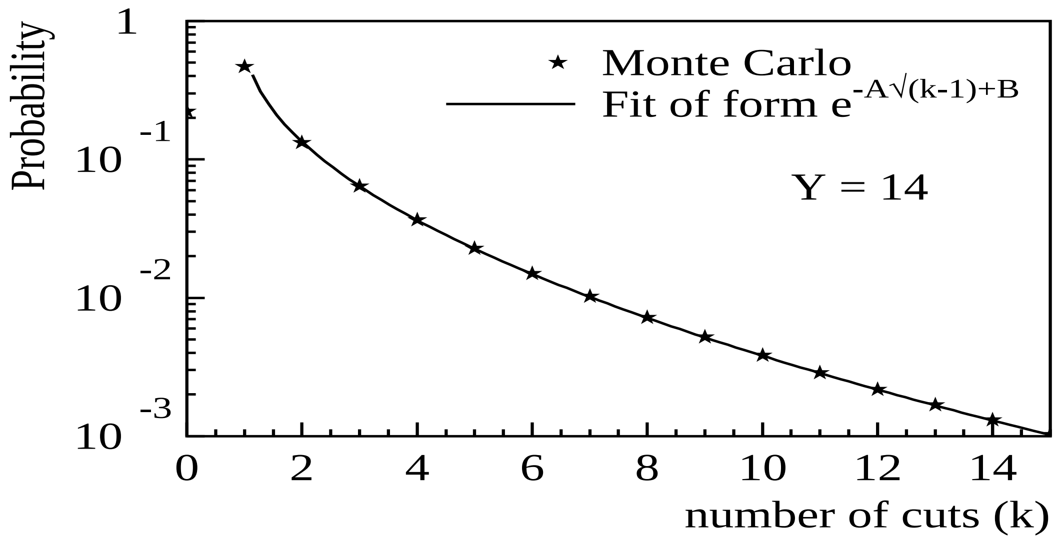

Figure 2.16. Probability of the "number of cut Pomerons", roughly one half the jet multiplicity per unit rapidity, according to the calculations of Mueller and Salam.

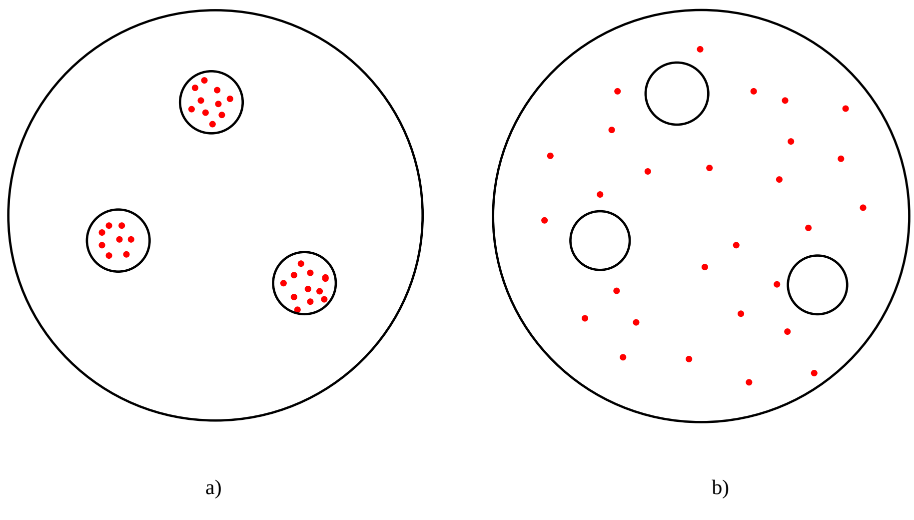

Figure 2.17. Where are the infinite number of primordial "sea"partons in the infinite-momentum state of the proton: inside the constituent quarks (a)—or outside (b)?

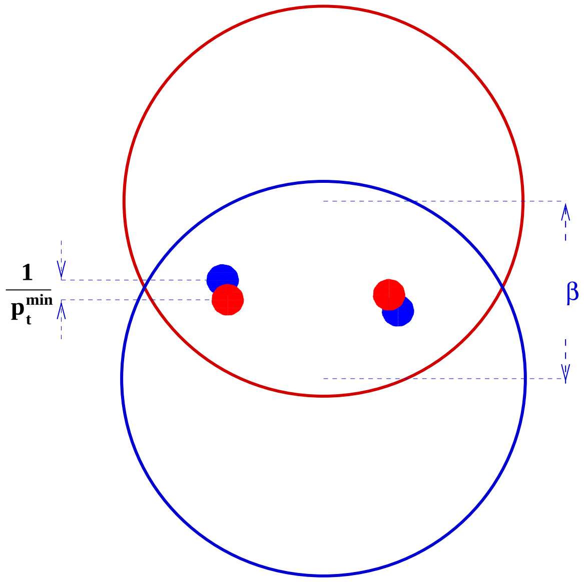

Figure 2.18. A view of double scattering in the transverse plane.

mation is in double- or multiple-parton interactions. Double-parton scattering [65], the simplest example, consists of two different pairs of partons interacting independently in the same inelastic hadronic event, with a momentum transfer larger than some lower cutoff which establishes the onset of a semi-hard regime. The scale in p_T of the semi-hard interaction should correspond to a much smaller distance in coordinate space than the hadronic radius. In the case of a double-parton collision the two interaction regions are therefore well separated in transverse space and, as a consequence, the two-parton processes add incoherently in the cross-section (Fig. 2.18).

The nonperturbative input to the theoretical estimations is the joint parton distribution D_2, which is a function both of the fractional momenta and of the transverse distance b between the two partons: $D_2 = D_2(x, x'; b)$. It is a well-defined convolution of parton densities of projectiles, the simplest measure available for the study of impact-plane structure. Evidently the simplest possibility is one where all multiparton distributions are uncorrelated. In that case $D_2(x, x'; b) = f_{eff}(x) f_{eff}(x') F(b)$ with $f_{eff}(x)$ being the effective parton distribution (namely the gluon plus 4/9 of the quark and anti-quark parton distributions) and $F(b)$, the convolution in the transverse plane of the matter distribution of the two hadrons, is normalized to one. In this case the double scattering process measures σ_{eff} which is defined as

$$\frac{1}{\sigma_{eff}} = \int d^2b\, F^2(b). \tag{2.22}$$

Until recently, the measurements of σ_{eff} have been sparse and not very consistent. But recently quite a large number of double-parton collisions have been observed by CDF [66]; their measurement gives $\sigma_{eff} = 14.5 \pm 1.7^{+1.7}_{-2.3}$ mb. This number is small enough to indicate in fact that some nontrivial transverse-plane correlation structure does exist. On the other hand, by looking at the dependence of σ_{eff} on x, CDF has found no correlation in x in the limited range of values of x available.

In any case, the measurement of multiparton distributions via triple, quadruple etc. scattering processes would test the noncorrelation hypothesis. If valid these processes measure the integral in transverse space of corresponding powers of $F(b)$. The measure of all multiparton scattering cross-sections would therefore allow one to take literally the picture of the projection in transverse space of the matter distribution of the two colliding hadrons. If the noncorrelation hypothesis is invalid, one will learn about nontrivial impact-plane substructure of the projectiles.

From this hypothesis of uncorrelated multiparton distributions, one may estimate the rate of multiparton collisions and extrapolate to LHC energies. The extrapolation suggests that at least 50% of all inelastic events should be characterized by the presence of minijets with transverse momenta larger than 7 GeV. In an inelastic event with minijets, the semi-hard component of the interaction corresponds to the presence of several partonic collisions localized at different points in the transverse plane. Given the noncorrelation hypothesis the distribution in the number of collisions is Poissonian with the average number depending on the impact parameter [67]. One expects therefore that the number distribution of minijets will be characterized by a very large dispersion, corresponding to the differing impact parameters for the reaction. Indeed the number of produced minijets can be used to give an estimate, event by event, of the impact parameter of the hadronic interaction. One expects in fact that the main source of the large event-by-event variation in the number of minijets expected at the LHC is the variation of the number of partonic collisions as a function of the impact parameter.

The rising importance of multiple parton semi-hard collisions with increasing hadron c.m. energy is in fact related to the larger parton densities which are accessible at higher energies. Larger parton densities give larger parton fluxes and growing probabilities for having multiple parton collisions. At the

LHC, the parton distributions at small x are very large. At the p_T scale of $8-10$ GeV, the number of candidate pair interactions is between five and ten thousand per pp collision. It is therefore reasonable that multiple parton collisions, leading to visible minijets, should become a common feature of most of the inelastic events and therefore affect substantially many global characteristics of typical events.

At the LHC energy scale, if one represents the partonic interaction by the exchange of a BFKL Pomeron, one may obtain for the average number of partonic collisions in each hadronic interaction with minijets a number as big as 8 for $p_T^{min}=7$ GeV and 3 for $p_T^{min}=9$ GeV. The actual normalized distribution in the number of partonic collisions is shown in Fig. 2.19 for two different values of the lower threshold for the production of minijets: $p_T^{min}=7$ GeV and $p_T^{min}=9$ GeV. The large number of parton-parton collisions is not strongly dependent on the enhancement of the partonic cross-section at large rapidity distances, which characterizes the BFKL approach. The average rapidity difference between two minijets resulting from the same partonic interaction is, in fact, not too large. It depends slightly on the value of p_T^{min} and typically it is between five and six units. A different approach to the partonic interaction, which is normalized to the UA1 data on the minijet cross section [68], does not change the qualitative features. The actual distribution shown in the figure is obtained by assuming a Gaussian shape for the parton structure in the transverse plane. Although the distribution depends on the specific form of $F(b)$, different functional forms of $F(b)$ do not induce major changes. So far only uncorrelated multiparton distributions have been considered. The main reason of interest in multiple parton collisions is however in the actual measurement of the multiparton correlations. The noncorrelation hypothesis is surely untenable when x is large. To measure the multiparton correlations of the hadron structure one has to look for multiparton processes at large values of x, which corresponds to large rapidities [5]. Combining such measurements with corresponding pA data, the inclusive cross-section to produce minijets at large rapidities would allow one to probe the transverse separation of valence quarks in the proton.

An interesting quantity to study is the long-range rapidity correlation in events with multiple minijet production. One can expect significant deviations from the minimum bias events. The reason is that the multijet trigger predominantly selects central pp collisions with a higher density of soft partons. In such events the long-range correlations are likely to change. In this case the transverse energy and entropy densities are so high that it is even possible that a qualitatively different class of final states is attained, with a new, distinct correlation structure.

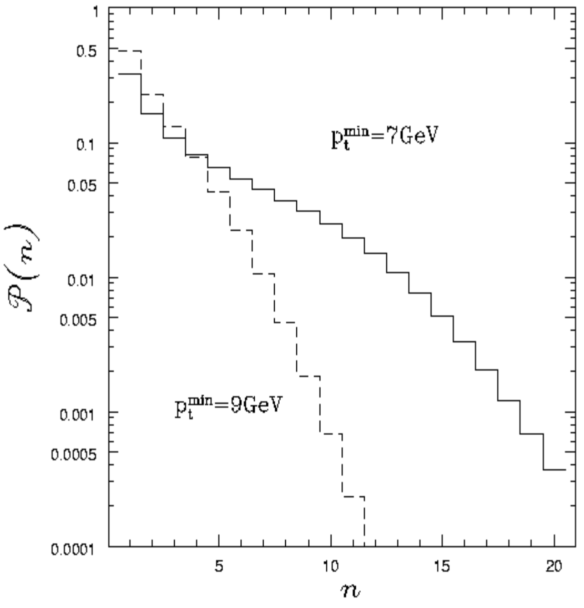

Figure 2.19. A normalized distribution of the number of partonic collisions per hadronic pp interaction at the LHC for two different p_T^{min} thresholds.

2.1.9. QCD structure of jets

Studying the detailed structure of final hadronic states produced in high energy hard collisions is of primary importance for QCD. Not only will this allow one to verify well established perturbative QCD predictions concerning the gross features of hadron jets, but also to study the impact of the color structure of underlying parton processes on the distributions of final hadrons, that is to shed light on the dynamics of confinement. A central feature of the final hadron states in hard processes which follows from QCD is the fractal structure of jets. This means that a large jet consists of smaller jets, which after rescaling have the same partonic substructure [69]. Although the fractal structure of jets is a well-known consequence of QCD evolution, it requires rather large energies to clearly reveal itself. So this is an example of a hard phenomenon where the LHC has evident advantages. The main strength of FELIX for such studies is that it can study the interior structure of jets of laboratory momentum ≥ 3 TeV as a function of p_T over a very broad range of production angles.

2.1.9.1. Mean jet characteristics

Measuring the momenta of all (or all charged) hadrons with transverse momenta $p_T > Q_0$ in an event, allows one to apply the so-called p_T (Durham) jet finding algorithm to unambiguously select hard processes producing parton jets at a given hardness scale p_T and then to study the internal structure of preselected jets, with a variable resolution $Q_0 \ll p_T$. This includes studying

- Mean subjet multiplicities as a function of the resolution scale Q_0, for a given overall hardness p_T,
- Subjet multiplicity fluctuations (KNO distributions),
- Energy spectra of subjets within a given primary jet,
- Angular profiles of relatively soft particles and subjets around the main jet direction.

The latter should reveal (yet unobserved) coherent effects which are sensitive to an overall color structure of the primary parton ensemble, $AB \to CD$, and cause azimuthal asymmetries of the final jets C, D (lopsided jets).

For these gross features of intrajet structure, well elaborated theoretical predictions are available, derived at the perturbative QCD level [69,70]. Decreasing Q_0 down to the hadronic scale may allow one to probe intimate details of the hadronization (confinement) mechanism. Along the way, in particular, one could hope to resolve a long standing problem of the comparative properties of quark *vs.* gluon jets.

The above program should also be carried out imposing an additional angular cone restriction on the particles (subjets) within a given jet. By doing so, one suppresses the contamination from interjet particles and assures a cleaner environment for testing the details of the coherent QCD parton branching picture, hump-backed energy plateau etc.

2.1.9.2. Interjet particle flows

Of importance is a series of studies of the pattern of *interjet* flows of (relatively) soft accompanying particles/subjets. Soft particle flows are driven by the color structure of the hard parton system ("antenna") and exhibit the so-called string/drag effects, see review in [69]. They can be used, in principle, on an event-by-event basis, as an additional trigger for new physics searches.

At least two major open questions can be raised here:

- Studying the ratios of averaged particle flows in different interjet valleys for different colliding partons (qq, qg, gg);
- Visualizing two distinctive patterns of final particle flows accompanying gluon-gluon fusion, $gg \to gg$, a process in which two different color antennae contribute.

Such "color antenna" effects are seen at CDF and D0 already, on a statistical basis [71]. An event-by-event capability for analyzing the pattern of color flow would be especially important to attain. It would have implications, not only for QCD itself, but possibly also for new-particle searches. This challenging goal may become more practical at the LHC because of the higher yields of minijets via BFKL effects, and because of the larger phase-space region into which they can go. On the other hand, there will have to be, at the very least, application of sophisticated techniques of pattern analysis, along with a detailed understanding of underlying-event structure, especially with respect to the role of spectator minijets, to be able to succeed. The subclass of events which have large impact parameter, hence low global multiplicity, and which contain one and only one hard-collision "hot spot" will be important to isolate. If the hard process has a large subenergy, the search for the color flows across the lego plot should be optimal for such an event class.

It should be clear that a close interplay of theory, of good simulation, and of comprehensive experimental data is a necessary condition in exploring this potentially very important topic. The large acceptance of FELIX and its dedicated QCD mission will be extremely valuable assets [72].

2.2. Soft QCD at the LHC

2.2.1. General issues

2.2.1.1. The need to understand soft QCD

The study of generic soft strong interaction processes is sometimes carelessly considered as "not even QCD." This is nothing but denial. Soft QCD is, almost by definition, the part of the theory not readily calculable by perturbative means. However this does not mean that it is uninteresting or unimportant. If for no other reasons than to certify and/or optimize the Monte-Carlo simulations which underlie all of the LHC detector design and physics agenda, it is important to pay attention to the input physics at the most fundamental level possible. In particular, to model reliably the responses of detectors to several simultaneous inelastic pp interactions during single collisions between proton bunches (at LHC ≈ 20 simultaneous interactions for high luminosity operation), it is necessary to measure not only the average characteristics of hadronic collisions but also the event-to-event fluctuations.

At present the physics of hadroproduction in hadron-hadron collisions is much less understood than in electron-positron or even electron-proton collisions. Even the most fundamental question, the choice of suitable degrees of freedom for a sensible description, is uncertain. At intrinsic energy scales smaller than 500–1000 MeV, a description utilizing the chiral effective action is widely used. In such a picture the basic degrees of freedom are constituent quarks and pions, while gluons are of secondary importance. All other hadrons are treated as composite objects, built out of these basic degrees of freedom. On the other hand, a considerable number of theorists aggressively extrapolate the calculational methods and ideology of partonic QCD far into the realm of soft physics. There have been many successful results from this approach. Nevertheless, one still must seriously question their meaningfulness.

The difference between hadron-hadron and, say, electron-positron collisions is evident already upon looking at the initial conditions. In the latter, one begins with only a pair of point-like quarks in a state of $J = 1$ which evolves into the final system of hadrons. But two LHC protons have a typical initial-state J (the product of beam momentum and impact parameter) of about 30,000. At the arrival at the collision point, they are structured objects with internal motions frozen, but with internal configurations which can vary greatly from event-to-event. Are the three valence quarks of an incident projectile close together or far apart? Does the meson field around a nucleon depend on the distance between valence quarks? What happens when quarks shadow each other? The nature of the final state certainly depends upon such parameters, but it has not been easy to isolate them experimentally. Theoretical ideas for doing so exist, but they are inhibited by lack of data, and by the generally gloomy prospects for acquiring such data at collider energies.

2.2.1.2. Event classes: soft Pomerons vs. perturbative gluons

We have already identified some of the most important event classes in the preceding sections.

They include

- Very large impact parameter: peripheral collisions.
- Small impact parameter: central collisions.
- Unusual configurations of the internal states of the protons on arrival at the collision point, especially small-size or even point-like configurations.
- Diffractive final states.
- Final states containing leading-particle tags.

This variety of event classes will, as argued already in the overview, become more extreme at LHC energies. Therefore, it will become less and less relevant to consider final-state properties which have been averaged over these—and probably other—event classes. This feature has implications for theory as well as for experiment.

At low energies, with the distinctions between event classes less prominent, and with less than complete absorption of incident beam protons occurring even for central impact parameters, it did make sense for theorists to do the average, and thereby create a global description of soft processes. A variety of theoretical approaches of this sort exist and are in use. One important class is nonperturbative, based on the string picture of QCD confinement, especially as developed by the Lund group [73]. Others introduce the concept of the soft Pomeron, a pure Regge-pole with intercept near unity [74]. It is an appropriate tool, in principle, for the description of elastic scattering, soft diffraction, and multiparticle production—provided short-range correlations in rapidity dominate the final-state structure. However, corrections, hopefully small and controllable at moderate energies, are anticipated within this framework itself to grow with energy. They must be treated via "multiple Pomeron exchange" contributions, for which there is an elaborate formalism involving Reggeon calculus, AGK cutting rules, etc. [75] This soft-Pomeron formalism by itself generates at sufficiently high energies long range rapidity correlations in multiparticle production, as well as shadowing (absorption) effects in elastic and diffractive scattering.

On the other hand, we have seen that there is another very strong source of such effects from the perturbative, semi-hard interactions of the many small-x gluons, as seen at HERA. It is possible, but less than convincing, to relate this rise in F_2 seen at HERA directly to multiple-soft-Pomeron-exchange effects. The simpler alternative is to recognize the wee perturbative gluons as an independent source of this rapid rise in F_2, with the appropriate implications for $\bar{p}p$ and pp collisions at Tevatron and LHC energies. As we discuss in Section 2.2.3.1, page 39, there are already indications in existing data that the partonic contribution is a distinct component of soft-QCD phenomenology.

Consequently, at the LHC it is likely that there will be applied a hybrid description of the soft collisions. Descriptions of central collisions probably must include a formalism emergent from perturbative-QCD considerations, in addition to the nonperturbative mechanisms extrapolated from lower energies. Very peripheral collisions may be more aptly described by something closer to the stringy or soft-Pomeron methodology used at lower energies, although perturbative-QCD "hot spots" may still occur. The boundary separating the two extremes will probably need to be determined in good part by experiment and phenomenology. And to do this, the separation of the phenomenology into distinct event classes will be vital. Furthermore, it should be clear that the full-acceptance capability of FELIX will be a very strong asset in accomplishing this quite nontrivial task.

In the next subsections we briefly discuss some of the soft-physics topics which can be strongly identified with the aforementioned event classes, and conclude with some brief comments on more generic processes which have been extensively studied and which are of interest.

2.2.1.3. Monte-Carlo codes and soft QCD at the LHC.

One indicator of the theoretical status of soft-collision phenomenology, perhaps the most important from a practical point of view, is how well existing Monte-Carlo codes for soft hadron-hadron collisions identify the above event classes and anticipate the problems which must be faced at the LHC energy scale.

The Monte Carlo models for high-energy proton-proton collisions may be roughly divided into the two broad categories identified above. The first category is based on perturbative QCD, involving the parton densities of the colliding protons, which are convoluted with the hard cross-section of two partons, and supplemented with associated initial-state and final-state parton shower evolution. It is most appropriate for central collisions and extremely high energies.

The second category is built on the Regge theory, viewing the colliding protons in terms of constituent valence quarks and diquarks which interact via soft Pomeron exchange. It is most appropriate for peripheral collisions and relatively low energies. For both categories, the nonperturbative hadronization dynamics of converting the final-state color charges into white hadrons is modelled phenomenologically. Again two models are mainly used; either some version of *string fragmentation* (e.g., Lund, Feynman-Field), or of *cluster formation and decay* (e.g., Marchesini-Webber).

Some event generators of the first, partonic category are:

(i) PYTHIA, probably the most versatile generator, includes high-p_T jet production, low-p_T Pomeron-type gg interactions, a model for multiple parton interactions, and options to trigger on elastic, single-diffractive and double-diffractive events according to the corresponding cross-sections parametrized from data. Hadronization is effected via the Lund string model.

(ii) HERWIG, the most refined and accurate event generator on the perturbative-QCD level, includes high-p_T jet production, resummation of soft, small-x gluon evolution, and next-to-leading order contributions. Hadronization is implemented via the Marchesini-Webber cluster model.

(iii) ISAJET is similar to PYTHIA in its overall structure. But it is much more limited on the QCD sector, since its emphasis lies on new-particle searches and supersymmetry. It incorporates high-p_T jet production, as well as options for triggering on elastic, single-diffractive and double-diffractive events. Hadronization is implemented via independent string fragmentation.

(iv) VNI also utilizes, in addition to the commonly employed momentum-space description, the space-time structure of events. It includes high-p_T jet production, low-p_T soft parton interactions, multiple parton collisions and mini-jet production, as well as the possibility to study spatial fluctuations (e.g. color transparency), and to extract impact-parameter dependence. The Ellis-Geiger cluster model (a space-time extension of the Marchesini-Webber approach) is used for hadronization.

Omitted from all these event generators is the only-recently-observed phenomenon of hard diffraction. This is now being remedied via the introduction of POMPYT, a variant of PYTHIA, based upon a pure Regge-pole interpretation of the soft Pomeron. Only PYTHIA includes soft diffraction.

Only VNI, and to some extent PYTHIA, has the ability to classify events in terms of impact parameter or initial-state configuration, and only PYTHIA and VNI include multiple minijet production.

Examples of event generators of the second, Reggeonic category are:

(v) DPM describes soft interactions among the protons by single and double-Pomeron-exchange, and incorporates a (relatively) simple hard component in terms of quark-quark Born scattering. It includes diffractive and elastic scattering. Hadronization is implemented via string fragmentation.

(vi) FRITIOF is another Lund product, essentially PYTHIA with none of the perturbative-QCD ingredients, and is based solely on string excitation and fragmentation.

(vii) VENUS is a hybrid of FRITIOF and PYTHIA using string degrees of freedom and soft-Pomeron exchange for soft interactions. But it does include a hard component by means of hard-Pomeron exchange, via a perturbative-gluon ladder. This code employs space-time variables in addition to the momentum-space description. For hadronization, Lund string fragmentation is used.

None of these "soft" codes incorporates hard diffraction, minijet production, or parton evolution. At present, none, except VENUS, can address the impact-parameter or initial-state-configuration dependence of the phenomenology.

These quite sophisticated codes incorporate many required features of high energy collisions and are absolutely invaluable practical tools. But it is fair to say that not one of them encompasses the full range of phenomena discussed in this LOI, and that none of them can be expected to describe, for example, the leading-particle behavior and its correlation with phenomena in the central rapidity region. This has to be the case for no other reason than that a proper data base does not exist at collider energy scales.

Likewise, for the description of diffractive phenomena and of correlations induced by impact-parameter and initial-state-configuration dependence, there is again every reason to suspect that these codes will be deficient. There is simply an insufficient data base to provide a reliable calibration.

2.2.2. Large impact parameters

2.2.2.1. Small-t elastic scattering and the soft Pomeron

Much of the interest in large-impact parameter collisions centers on elastic scattering and soft inelastic diffraction. Small-t elastic scattering in fact serves to define the impact-parameter region (via the Fourier transform of the elastic amplitude) for which inelastic diffraction occurs. This is the "gray" impact-parameter region, where absorption is neither complete nor absent. These events, containing rapidity gaps, are customarily described in terms of the exchange of a Reggeon, the soft Pomeron. The problem of the structure of the soft Pomeron, and indeed even the question of whether it is the most appropriate descriptive language, is central to the problem of understanding high energy soft interactions.

A very appealing, and in many respects very successful, picture of the soft Pomeron has been proposed by Donnachie and Landshoff [74]. Their soft Pomeron is a pure Regge pole, implying that the energy dependence of the total cross-section is a pure power, s^ϵ. Their predictions of elastic scattering, in terms of Pomeron-pole exchange between constituent quarks with Regge-intercept $\epsilon = 0.07 - 0.11$, give an excellent description of the data [74].

Most fits to the existing data predict a cross-section at the LHC energy not far from $110 - 120$ mb. For example, the recent fit of Ref. [76] leads to

$$\sigma_{\rm tot}(pp)(\sqrt{s} = 14\,\mathrm{TeV}) = 113.9 \begin{array}{c} +8.3 \\ -7.4 \end{array} \mathrm{mb}.$$

This value agrees with a cosmic-ray measurement [77]. Note that the conflict between the two Tevatron data points [78] leads to substantial uncertainty in these fits.

At the LHC, the nucleon will look more like a black disk and less like the Gaussian density seen thus far. Thus competing viewpoints, which do not assume Regge-pole dominance even at low energy, may be more favorable at the LHC energy scale. Existing data can be fitted either in terms of the above Pomeron Regge-pole exchange [74], which corresponds to small shadowing corrections, or in terms of exchange of a Pomeron with $\alpha_P(0)$ much higher, $\epsilon \approx 0.2$, implying large shadowing corrections described by multiple Pomeron exchanges [75].

Fits [74] to elastic scattering data suggest that the effective Pomeron trajectory is linear in t for moderate t:

$$\alpha(t) = 1 + \epsilon + \alpha' t \ .$$

The value $\alpha' = 0.25$ GeV^2 was extracted from data more than 20 years ago [79]. It has a direct effect on the forward exponential slope $B(s)$ in elastic scattering: if single-Pomeron exchange alone is included then

$$B(s) = B_0(s_0) + 2\alpha' \; \ell n \left(\frac{s}{s_0}\right) \; .$$

On the contrary, in the Froissart limit where the proton behaves as a black disc, $B(s) \propto \ell n^2 s$.

The increase of $B(s)$ with energy implies that the mean impact parameters in pp scattering also increase with energy, i.e. that at sufficiently large energies the total cross-section is dominated by peripheral collisions, instead of central collisions, as is the case at medium energies. The value of the slope B found at the FNAL collider implies mean impact parameters in pp scattering $< b^2 >\approx 1.4$ Fm^2. Extrapolation to LHC energies leads to $< b^2 >\approx 1.6$ Fm^2. These impact parameters become comparable with average internucleon distances in nuclei. So a description of pA and AA collisions at LHC energies in terms of multiple Pomeron exchanges becomes doubtful.

The universality of the slope of this effective Pomeron trajectory on the choice of the projectile has not been checked experimentally thus far above $\sqrt{s} = 25$ GeV. As discussed in Sections 1.2.9, page 6, and 2.2.4.2, page 42, the FELIX program includes the measurement of the absolute value and the energy dependence of the slope $B(s)$ in the elastic, diffractive pp scattering, in meson(photon)-proton, and meson-meson scattering.

2.2.2.2. Elastic scattering—medium t

Even if the exchange of two Pomerons is a small contribution to the total cross-section, and therefore also to elastic scattering at very small t, this will not be so at larger $|t|$; the distribution is flatter than for single-Pomeron exchange. As s increases, the double-Pomeron contribution increases only half as rapidly with energy. On the other hand, at $t = 0$ it rises more rapidly than single-Pomeron exchange.

Therefore, as s increases, the value of t for which the two contributions are equal moves downward.

One consequence of this is that the shape of the differential cross-section, as a function of t, changes with increasing energy. It happens that, at the Tevatron energy, the two contributions combine in such a way that an exponential fit $e^{-b|t|}$, with b independent of t, is quite good [74], although this is not true for either lower or higher energies. At lower energies $d\sigma/dt$ is concave up in a log/linear plot, while at very high energies it should be concave down. This behavior is also what is expected from the optical-model picture. The interplay of single and double scattering allows one to explain the presence of the dip in the elastic cross-section at ISR energies at $|t| = 1.4$ GeV^2, and its conversion to a shoulder at the CERN $p\bar{p}$ collider. Estimates [74] suggest that at the LHC the minimum may reappear at $|t| \sim 0.5$ GeV^2.

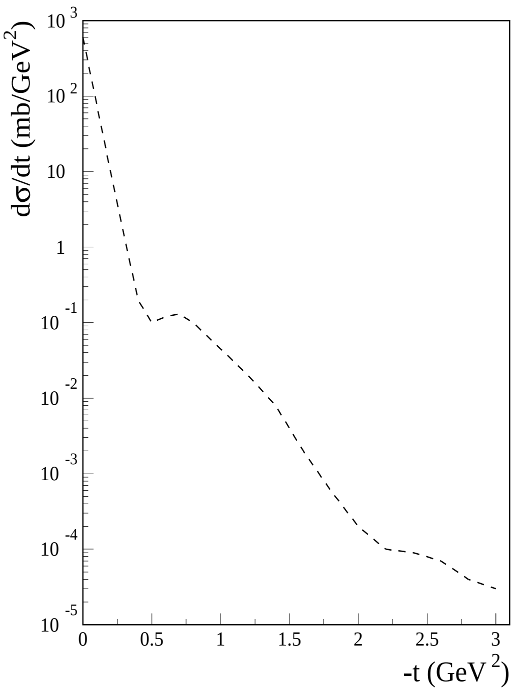

Figure 2.20. Elastic scattering differential cross-section at $\sqrt{s} = 14$ TeV in an impact-picture calculation [80].

2.2.2.3. Elastic scattering—high t

At ISR energies, the pp elastic differential cross-section has a strikingly simple behavior for $|t|$ greater than about 3 GeV^2: it is energy independent and behaves as $|t|^{-8}$ (Fig. 2.21). This is consistent with the three valence quarks from one nucleon scattering independently and simultaneously from the three valence quarks from the other nucleon. It may be a simple one-gluon exchange [20], or a color-singlet exchange mechanism [81], between the quarks. It will be interesting to see whether this energy-independence at large $|t|$ survives at the LHC.

In particular, the regime of large spacelike $|t|$ is associated with small interquark transverse

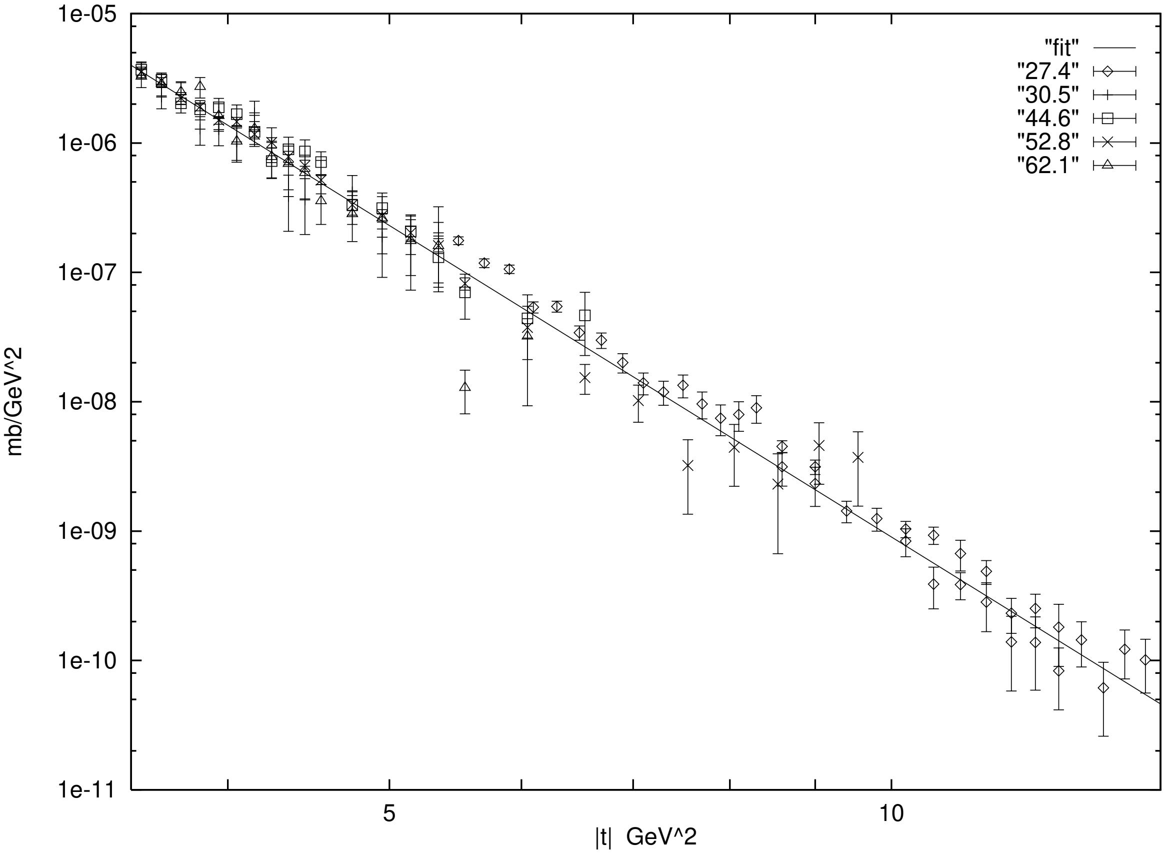

Figure 2.21. The differential cross-section for pp elastic scattering, with the fit $0.09|t|^{-8}$.

distances within a proton, and may be linked with perturbative-QCD phenomena, in particular the BFKL energy dependence discussed in Section 2.1.1.2, page 9. If the energy dependence of the elastic cross-section is parametrized by an effective Regge trajectory $\alpha_{eff}(t)$, then this approach predicts a minimum value for this trajectory in the spacelike region. At small $|t|$, $\alpha_{eff}(t) \geq 1$, it is known to decrease with increasing $|t|$, becoming significantly smaller than 1. But at sufficiently large energies and large $|t|$, according to the BFKL approximation [82], the differential cross-section would *rise* rapidly with $\sqrt{s}$, again implying an effective Regge trajectory above unity.

It is intriguing that UA8 has observed some nonlinearity of the effective Pomeron trajectory, as suggested by perturbative-QCD [39], in the differential cross-section for single soft diffraction: $pp \to Xp$. They find

$$\alpha(t) = 1.08 - 0.25|t| + 0.07|t|^2 \tag{2.23}$$

with $|t|$ measured in GeV^2. This form of the effective trajectory suggests that $|t| \geq 3\ GeV^2$ is necessary for the onset of such a new perturbative-QCD regime.

On the other hand, it may be that the cross-section at large $|t|$ is smaller at FELIX than at lower energies. This is anticipated in the impact-picture approach [80], as a consequence of a purely absorptive energy-dependent interaction. A variety of other predictions exist, and are summarized by Islam in his FELIX Note [83]. This includes a survey of interpretations of the structure of the differential cross-section in the "dip" region, containing a minimum and secondary maximum of the t-distribution (at ISR energies), which separates the regions of intermediate and large $|t|$. This interference region is different for pp and $p\bar{p}$ interactions, so the extrapolation of expectations to the LHC energy scale is difficult.

In summary, the estimates of cross-sections in the large-$|t|$ region, a region which some theorists insist is controlled in principle by short-distance, perturbative-QCD dynamics, are in practice uncertain, and vary over orders of magnitude.

2.2.2.4. Flavor dependence of hadron elastic collisions

If single-Pomeron exchange dominates two-body processes, there will be factorization relations between total and differential cross-sections for interactions of different beam particles [84]. FELIX should provide measurements of total cross-sections of pp, γp and $\gamma\gamma$ collisions, as well as a variety of others ($\pi p, \pi\pi, Kp, K\pi$, ...) using forward tags. There should also be measurements of various exclusive channels like $\gamma\gamma \to V_1 V_2$ where $V_i \equiv \rho, \omega, \phi, J/\psi$-meson (cf. Section 2.4.4, page 59. The ability to measure a broad range of processes will provide a good probe of the interaction of large size hadrons, where the s and $|t|$ dependences are nearly universal, to the perturbative-QCD regime of scattering of a small object on a large object (e.g. $\gamma\gamma \to \rho + J/\psi$), where one expects a much faster energy dependence, similar to that observed in the $\gamma p \to J/\psi + p$ reaction at HERA. In general, a weak energy dependence of the $|t|$-slope of the cross-section is expected. But there may be BFKL effects in onium-onium interactions, such as the two J/ψ mesons in $\gamma\gamma$ collisions. This process, in the BFKL approximation, would increase with energy, approximately proportional to s. Processes involving elastic photoproduction of one or two ϕ's may provide especially valuable interpolation points.

2.2.2.5. Soft single diffraction

From elastic scattering information, the impact-parameter region where absorption goes from 90% to 10% is roughly 1.5 ± 0.7 fm. It is here where most inelastic diffraction should occur. Larger impact parameters may of course contribute as well, with reduced yields. And because the nucleons will look more like black disks at LHC energies and less like the Gaussian density distributions seen so far, the sum of elastic, single diffractive, and double-diffractive cross-sections should saturate at nearly 50% of the total cross-section, with the elastic portion taking a larger share than at Tevatron energies. Thus the ratio of diffractive to elastic scattering should decrease with energy. This is because inelastic diffraction, an edge effect, should disappear in the black disc limit.

On the other hand, a pure single-Regge-pole exchange predicts that the ratio of inelastic diffraction (to a given, fixed range of final states) to elastic scattering should be independent of energy. Experimentally, a measure of this is the ratio of inelastic diffraction to the elastic pp cross-sections at $t = 0$:

$$R(s) \equiv \left[\frac{d\sigma_{\text{inel. diff.}}/dt}{d\sigma_{\text{el}}/dt}\right]_{|t=0}.$$

At $\sqrt{s} \geq 100$ GeV this ratio decreases with increasing energy, from about $0.3 - 0.35$ at $\sqrt{s} \sim 60$ GeV, to 0.15 at the Tevatron. Extrapolation to the LHC [85] gives $R(\sqrt{s} = 14\text{TeV}) = 0.06 - 0.07$. On the other hand, in the Pomeron-pole picture this ratio is expected to *increase* with energy, because of the increasing range of diffractive masses available with increasing energy.

2.2.2.6. Double diffractive dissociation and double-Pomeron exchange

From both the theoretical and experimental sides, there is more uncertainty for the expected LHC rate of double inelastic diffraction (both protons dissociated; one central rapidity gap) and soft double-Pomeron exchange (neither proton dissociated; central hadron production only). Double diffraction dissociation can occur via scattering of subsystems of the proton projectiles (e.g. single scattering of constituent quarks), so a much broader t-distribution is anticipated. Consequently, an estimate of the cross-section for double diffraction is rather large, about 5 mb for the LHC [86]. Shadowing effects should manifest themselves in long-range rapidity correlations between the two diffractive states for large diffracted mass.

This distinctive experimental feature, the slow decrease of cross-section with momentum transfer, is seemingly in variance with the fact that diffractive processes are more peripheral than elastic scattering. It has been suggested [87] that the amplitudes of diffractive processes should contain significant contributions of amplitudes with spin flip, which become zero at zero scattering angle. With FELIX, it should be possible to study spin alignment effects for selected channels.

Final states in soft double-Pomeron exchange may help to distinguish different pictures of soft diffraction. If the Pomeron is a Regge pole, then it is arguable that the $J = 2$ "recurrence" on its trajectory ought to be preferentially produced: is this state a glueball? Or is soft-diffraction simply the collisions of pion clouds, i.e. soft excitation of the chiral vacuum? If so, the coherent production of pion clusters, especially at low p_T and relative p_T, may be a possible alternative.

Hints of the latter behavior may exist in UA1 correlation data. As mentioned in the overview, strong Bose-Einstein effects seem to be present under these conditions, and are strongest when the associated multiplicity is *low*, suggesting it originates in the periphery of the colliding systems. Therefore it is appropriate that extensions of such correlation studies be done on nondiffractive and diffractive subsystems having relatively low rapidity density dN/dy.

The phase-space region $3 < \eta < 6$ (5–100 mrad) can be used as an alternative to a "barrel" detector to see (boosted) products of Pomeron-Pomeron collisions. For low-mass quasi-isotropic systems, this rapidity acceptance is already reasonably good for seeing all the secondaries, and "endcap" information (100–200 mrad; 2–5 mrad) is available too. The photon and charged particle coverage is on endwalls in this region, and granularity and resolution is excellent. This comment of course also applies to the study of $\gamma\gamma$ collisions. Double-Pomeron-exchange processes leading to low mass final states are, as is also the case for $\gamma\gamma$ collisions, a rich source of spectroscopic information. The implications are discussed in Section 2.4.6. The cross-section for double-Pomeron production of states of large mass M can be estimated roughly from factorization

$$M^2 \frac{d\sigma_{DPE}}{dM^2 d\eta} \sim \frac{1}{\sigma_{\rm inel}} \left(\frac{d\sigma_{SDD}}{d\eta_{\rm gap}} \right)^2 \approx 5\ \mu{\rm b}$$

where η is the central rapidity of the diffractively produced state. This suffices to produce an enormous, high-quality sample in FELIX.

2.2.2.7. Bose-Einstein correlations and very large impact parameters

Meson radiation by any source should obey Bose-Einstein statistics. How this occurs in detail is a much more complex problem, not completely explored to this day [88]. The interest in Bose-Einstein correlations is due to their sensitivity to the hadron formation region and to the possible formation of new forms of hadron matter. The unmistakable signal that the Bose-Einstein effect is at work is the observation of like-sign two-pion correlations (known as the Hanbury Brown-Twiss effect), namely the strong enhancement of the correlation function at low four-momentum differences, Q; for recent reviews see [89]. This correlation function is defined as the ratio of the double inclusive cross-section to the product of single inclusive cross-sections, with proper normalization.

At LHC energies, several new phenomena may lead to a substantial change of the picture of the Bose-Einstein correlations. These include

1. The increase with energy of the effective transverse size of the area where hadrons are produced.
2. The large increase of hadron densities at the central rapidities resulting in an increase of the radius of the last collision.
3. The change of composition of primary particles (increase of the fraction of heavy resonances) due to the high entropy densities at early times in the collision process.
4. The presence of large long-range rapidity correlations, and of fluctuations of multiplicity in minimum bias events.
5. the possible formation of large, long lived objects such as disoriented chiral condensates or related phenomena.

As a result one can expect a relatively strong dependence of the radius and the coherence parameter of the Bose-Einstein correlations on rapidity, on the associated hadron multiplicity, on the presence of leading particles in the events, etc.

2.2.3. Central collisions

2.2.3.1. Hidden minijet phenomena

It is in soft and semi-soft central collisions that there is the greatest potential for real surprises. In Sections 2.1.1, page 9, and 2.1.8, page 28, it was emphasized that the gluon densities become so large that visible minijet activity, at a p_T scale of 5 to 10 GeV, is expected to become a feature of the generic central collision. While all the nonperturbative phenomena present at lower energy will still be present, this new mechanism at the very least will greatly enrich the phenomenology. In addition, for the p_T scale of 1 to 5 GeV, the microscopic dynamics probably still originates within the perturbative quark-gluon QCD regime, and the gluon-gluon luminosities will be even higher. However, the difference is that real minijets cannot be manifestly seen in the final state. At best, only clusters of low-p_t hadrons will mark the approximate locale of an underlying parent gluon.

Nevertheless, high multiplicity in the final state should characterize this class of events, and they may already be a significant component of existing event samples from the $Sp\bar{p}S$ and Tevatron. In particular, the shape of the multiplicity distributions has an appearance suggesting a two-component structure. This feature has been modelled [97] in terms of a sum of two independent negative-binomial contributions, with energy-dependent normalizations, means, and dispersions (see Fig. 2.22). What is found is a rapid growth with energy of the high-multiplicity component, presumably to be

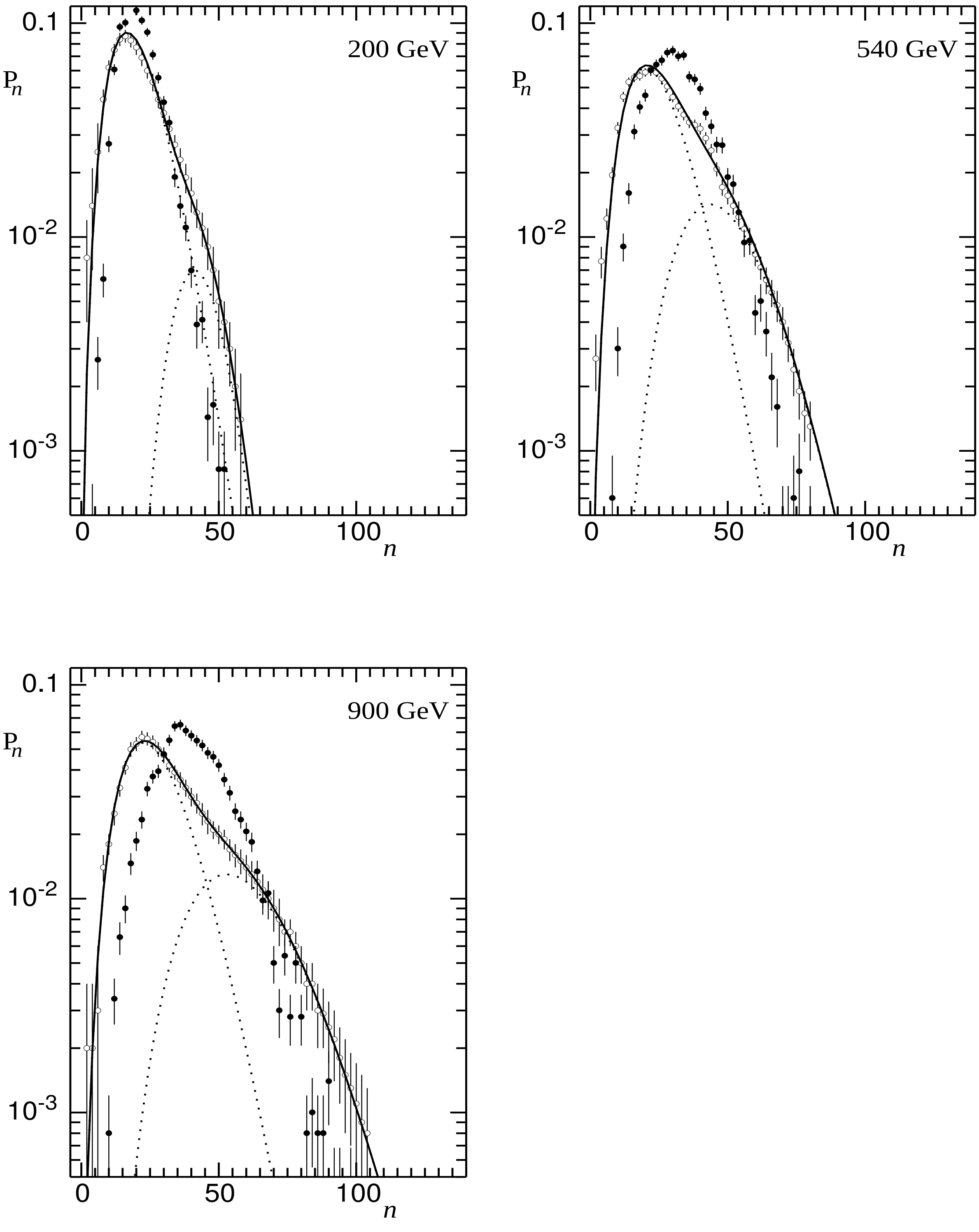

Figure 2.22. Charged particle multiplicity distributions at c.m. energies 200 GeV, 546 GeV and 900 GeV. Data (open dots) are from the UA5 Collaboration; the solid line is the fit in terms of two negative-binomial distributions whose components are given by the dashed lines. The solid dots show the result of Monte Carlo calculations (PYTHIA).

identified with the perturbative-QCD minijets. How to extrapolate in detail this model to the much higher LHC energy scale is fraught with great uncertainties. But the conclusion that this "minijet" contribution will dominate the global multiplicity distribution is robust.

2.2.3.2. Can thermalization occur?

At a more speculative level, it may be that the gluon densities at this lower scale, say $p_T = 1 - 2$ GeV, may be so large as to create a class of novel final states, characterized by a partial or complete thermalization of first-generation produced partons. If so, the initial energy densities and temperatures could be extraordinarily high, especially for shadowed, small-size initial-state configurations colliding at small impact parameter. There is here a clear link to the similar speculations for A-A collisions. We again note that it is in central pA collisions, in the (large) rapidity region free of ion fragmentation products, that the relevant gluon-gluon luminosity per collision is maximized.

The search for such "thermalized" final states can follow the leads suggested by the heavy-ion community: enhanced p_T, existence of transverse flow, enhancement of strangeness and heavy-flavor production, enhancements in soft dilepton production, unusual event texture, etc. One would look for such novel transitions as function of associated multiplicity, or perhaps of minijet activity.

2.2.3.3. Are there novel leading-particle effects?

The nature of the leading fragment distribution may also be dramatically modified under these circumstances. Imagine boosting the LHC process to a frame of reference where one has a 7 PeV beam colliding with a 7 GeV beam. There may be such a dense wall of gluons in the 7 PeV beam that all partons in the 7 GeV beam are swept forward via gluon-Compton scattering. If that happens, the secondaries, moving forward in this reference frame at nearly the speed of light, will be stuck to the Lorentz-contracted 7-PeV gluon wall, and leave behind a piece of "vacuum" with no memory of the initial valence quanta of the 7 GeV beam. The large-angle decay products of this space-time region (as viewed in this reference frame) may therefore be novel and interesting, and approach a new limiting distribution obeying approximate Feynman scaling. This may also be a good region for a disoriented-chiral-condensate search, as described in the next subsection. The pseudorapidity region of interest is roughly 5-7, and a detailed examination of it, as well as the even more forward region, is best done by the FELIX detector.

2.2.3.4. Is disoriented chiral condensate produced?

In the overview it was already mentioned that the decay products of a disoriented chiral vacuum (DCC) might be a component of the final state hadron distribution, perhaps seen best at low p_T or in low-mass clusters of pions. The main signature for this behavior is an unusually large dispersion in the distribution of the fraction f of pions, appropriately sampled, which are neutral. In the ideal case, instead of a binomial distribution peaked at 1/3, one finds an inverse-square-root distribution.

This subject is still a young one, and a quite speculative one. There is no compelling argument that DCC must exist, but there is no compelling argument that it does not exist. There have been two experimental searches, one at the Fermilab collider, and the other in heavy ion beams at CERN. No evidence in favor of the presence of DCC has been found. These experimental initiatives are stimulating the theoretical development, which is still in too primitive a condition to deliver realistic simulations of DCC production.

Nevertheless, the search phenomenology and strategy has been refined. Useful tools, the factorial moments of multiplicity distributions, well known in the multiparticle-dynamics community, appear to allow a sensitive search strategy for DCC in small phase-space intervals. From the joint multiplicity distribution of pions and gammas, one constructs robust measures [90] for detecting the presence of DCC. At present there is activity, especially with regard to exploiting wavelet analysis techniques [91], in generalizing these methods to large phase space regions, in order to search for unusual pattern structure created by this mechanism. It is not understood what the correlation structure (in lego phase space) of the disoriented chiral order parameter is likely to be, although a correlation length of order 1 - 2 lego units is the natural expectation.

This subject is related closely to that of Bose-Einstein correlations and to other possible mechanisms of producing hadrons coherently. It is becoming integrated into the general phenomenology of multiparticle dynamics, and can be expected to develop considerably between now and the commissioning of the LHC.

The specifications for good experimental searches are mainly the ability to count gammas and charged pions event by event with momentum analysis, especially at low p_T (below 100 MeV in particular), and with the inclusion of the forward region of phase-space, where cosmic-ray evidence for DCC-like phenomena occurs. In these respects, FELIX is an especially good detector.

2.2.4. Special initial-state configurations

2.2.4.1. Small-size colorless configurations

In Section 2.1.5, page 24, we have already considered the diffractive excitation of point-like configurations into final states containing jets. These processes should have analogues at lower p_T scales, which however may be consequences of more non-perturbative features of hadron structure. For example, such fluctuations arise naturally for constituent quark models of a hadron. For string models, the interaction cross-section is minimal for an initial state string configuration oriented along the momentum vector of the projectile and is maximal for strings oriented in the transverse plane. Thus color-coherent phenomena (color transparency in the perturbative domain, and color-opacity effects in the nonperturbative domain) can lead to large fluctuations of the average characteristics of high energy processes, which go well beyond the optical-model approximation. The cross-section of small configurations increases rapidly with energy, and thus the role of color-transparency effects in the average characteristics of pp collisions may decrease with the increase of the energy. However important effects should persist for the special hard processes already discussed in Section 2.1.5, page 24.

2.2.4.2. Leading particle tags

Another set of special initial-state configurations are those associated with the leading-particle tags mentioned in the overview, Section 1.2.9, page 6. For example, the one-pion exchange tag using a leading neutron ($x \gtrsim 0.8$), neglecting absorption corrections, is

$$\frac{d\sigma_{pp}}{d\Gamma\, dx_\pi dp_T^2} = \frac{1}{2\pi}\left(\frac{g^2}{4\pi}\right)\frac{x_\pi}{x_N}\frac{p_T^2}{(p_T^2+m_\pi^2)^2}\frac{d\sigma_{\pi p}}{d\Gamma}$$

with $x_\pi = 1 - x_N$ and p_T the transverse momentum of the neutron. The system Γ detected by FELIX can be any final state of the πp system.

At low impact parameters this formula is likely to be wrong. Absorption corrections can be applied; they will modify the p_T^2 distribution and lower the rate somewhat. However the fraction of pp triggers into the system Γ that can be ascribed to the one-pion exchange πp process, after appropriate cuts on neutron energy and p_T in the zero-degree, forward calorimeter, should be greater than 10^{-3}.

Similar calculations can be set up for Δ and Λ tags. In all cases, if the subprocess cross-sections are at all reasonable, the estimated rates will be comfortably high. The real problem will be separating the desired signal from the continuum background. The physics of that background, hence its importance, is quite uncertain, due to the nearly nonexistent leading-particle-production data base.

2.2.5. Generic collisions

The average behavior of particle production is also, of course, important. This is too broad and too mature a field to properly summarize here. The best way of surveying those issues of current interest which have not been covered here is to refer to the sequence of recent conferences on multiparticle dynamics [92,93] and hadron-collision phenomenology. What one finds there, first, is the search for a suitable description able to encompass what is known about generic multiparticle-production phenomenology. In addition, of course, there is the search for interesting correlation structures in the data.

In e^+e^- annihilation, some correlations are seen and are largely understood in terms of jet production, parton-level branching processes, and a reasonable phenomenology of hadronization and resonance production. This is expressed in terms of event-generators that reproduce well the observed correlations, as well as analytic techniques expressing the event-generator physics reasonably faithfully.

But, as repeatedly emphasized already, this happy state of affairs does not exist in hadron-hadron collisions. Correlation structures appear which are much less understood. Important tools used for the study of correlations and fluctuations are the factorial moments and cumulant moments of multiplicity distributions, measured usually in limited regions of phase-space, of variable size. It is found that the dependence of the factorial moments on the phase-space size is that of a power law, over a remarkably large range of sizes [94]. This dependence, known as intermittency, is evocative of self-similarity and fractality, as found in branching processes. It is not at all clear whether this is the correct interpretation, and further study and more data are for sure needed.

As already mentioned in Section 2.2.2.7, page 39, there are also strong Bose-Einstein-like correlations seen at low p_T and low cluster masses [96]. They also are not well understood, and may be related to the intermittency phenomenon. There are also persistent reports of anomalous bremsstrahlung at very low p_T, and this deserves being followed up.

The factorial and cumulant moments of multiplicity distributions, central objects of interest for the study of intermittency, Bose-Einstein effects, and DCC searches, are phase-space integrals over the correlation functions. The correlation functions themselves show rich structure and energy dependence. Of particular importance are the strong long-range rapidity correlations which emerge at collider energies [98], but are largely absent at fixed-target energies. In all models of multiparticle production, soft or hard, it is anticipated that these correlations will on average further strengthen at the LHC energy scale. In the soft, Reggeon picture, it is multiple-Pomeron-exchange (or, more simply, multiple sources per event in the transverse impact plane for secondary particle production [99–102]). In the hard, perturbative-QCD picture, the long-range rapidity correlations are simply induced by the gluon-exchange itself. However, as the particle and/or minijet density gets extremely high, there may appear a new regime with *less* correlation structure. This, for example, happens in central ion-ion collisions, where only short range correlations survive.

Therefore the continuation of all these studies of correlations and fluctuations may lead to evidence of a new distinct regime of conditions to be faced by multihadron production phenomenology. It should be especially interesting to study long-range correlations between *four* distinct phase-space regions: the two beam fragmentation regions ($x \geq 0.03$; $|\eta| \geq 7$) and the left-moving and right-moving "central" regions (e.g. $2 \leq \eta \leq 5$).

We have already emphasized the importance of inclusive-distribution measurements in all these phase-space regions, in particular with respect to flavor and baryon-number composition. Without supplementary particle-identification capability, this is nontrivial to do with FELIX. However a variety of species, such as K_S, Λ, ϕ, ω, η, π^0,...will be accessible.

Complementary to all these "local" samplings of the multiparticle final states will be the "global" methods which search for event-by-event textures or patterns in complete phase space. In addition to the well-established textures created by jets, resonance clusters, and rapidity gaps, there have been hints in data of the existence of other structures in the phase-space. There have been sightings of narrow spikes in the rapidity distribution [103], and of highly coplanar multijet final states [104]. The systematic search for such effects is at present hampered by limited statistics. Serious pattern-analysis methodologies are also a necessity, and the introduction of wavelet techniques may be a useful tool in the future.

In summary, a large array of techniques and body of experience is available for the analysis and interpretation of new data from the LHC. It must be kept in mind that this expertise, and the present description of multiparticle production, has in large part been built upon experiments done in full acceptance at fixed target energies, along with some collider data from the ISR, and from UA5 and UA1, with event samples no larger than 10^6 per experiment. The first round of data from FELIX would immediately improve that situation hundredfold, in an entirely new energy regime.

2.3. Hard and soft QCD in pA collisions

2.3.1. Physics motivations

2.3.1.1. Ions are really black at the LHC energy scale

There are many motivations for the study of proton-ion collisions at the LHC, but the most basic is that it simply has not been done at all at modern collider energies. Use of nuclear targets at fixed target energies has been commonplace and of great use in elucidating production dynamics. And, as argued repeatedly in the preceding material, the conditions at LHC collider energies will be quite different even for pp collisions. So big surprises in pA collisions are to be expected. For most of the topics we have already considered, having the capability of studying their A-dependence is, as we discuss in more detail below, an important asset. But in still more general terms, there are major differences to be expected from what is seen at fixed-target energies. The mean free path of the proton projectile in nuclear matter is diminished by a factor of about 3, and thus there are many more obstacles placed in the way of the incident proton. At fixed-target energies the mean number of "wounded" nucleons in a central pPb collision is about 6, while at the LHC this is replaced by about 20. The impact parameters typical for pp scattering increase by a factor ≈ 1.5 between 100 GeV and LHC kinematics. So the proton will often interact simultaneously with nucleons which have essentially the same longitudinal coordinate but which have large transverse separations.

Obviously this corresponds to a dramatic departure from the space-time picture of pA interactions at intermediate energies. Consequently the proton may be more easily excited into exotic high-mass or high-rapidity-density final states than in a collision with a single nucleon. The changes are so great that the conventional Gribov-Glauber picture of nuclear cascading may require fundamental modifications.

2.3.1.2. Gluon densities of heavy ions are definitely saturated, and the possibility for novel phenomena is maximized

Given that the gluon densities of the projectile and ion are both so high, there may well be new classes of strong-interaction phenomena which occur within the short-distance, near-the-light-cone space-time region one associates with perturbative QCD. It is even more probable in pA collisions than in pp collisions that, as discussed in Sections 2.1.1, page 9 and 2.1.8, page 28, the densities of partons, and of energy-momentum, may be high enough to "burn away" the nonperturbative QCD vacuum structure in these "hot spots", leaving behind only a dense partonic fluid in principle governed by perturbative dynamics but in practice involving short-distance strong couplings. If there is a large enhancement of hard-collision, gluon-induced processes, then there could be an enhancement of heavy-flavor production as well. The study of the x and A-dependence of forward J/ψ and Υ production (in the direction of the fragmenting proton) should be especially accessible and incisive.

Conventional hard-collision phenomenology such as dilepton production, direct photon production, and dijet production allow by definition the introduction of a distribution of partons in the ion. However, the relation between this parton distribution, the nucleon's parton distribution and the distribution of the nucleons within the ion is not at all straightforward. Even for single nucleons the gluon densities rise with x so strongly that saturation effects are anticipated. The gluon densities for ions are much, much higher and the perturbative saturation phenomena should be manifest.

In general, the A-dependence of DGLAP-BFKL type hard-collision phenomenology will shed much light on the nature of the dynamics. And in all cases, it will be important to compare the A-dependence of the yield of hard-collision products in the direction of the fragmenting proton with the particle production in the direction of the fragmenting ion: the A-dependences in the two regions may be expected to differ significantly.

With regard to soft, nonperturbative physics, even what to expect for the A-dependence of the generic, minimum-bias particle production is very uncertain. Will there be "Feynman scaling" of the leading fragments of the nucleon, especially when the collision is a central one? Existing data are very sparse. What do exist indicate that leading-particle production is suppressed quite strongly in central proton-nucleus collisions already at fixed target energies. If so, does this trend continue with energy? And if the trend does continue rather strongly, so that no leading particles are seen, what does this imply for the multiplicity distribution, $dN/d\eta$, at large rapidities in the proton hemisphere? Just energy conservation would suggest that it must grow rapidly for central as opposed to peripheral collisions. Indeed can the amount of absorption be so large that "thermalization" occurs?

2.3.1.3. What happens to soft and hard diffraction in pA collisions?

Soft rapidity-gap processes are not very well understood, and A-dependence studies will be of considerable value. What is the A-dependence of inelastic diffraction and double-Pomeron exchange processes? The nucleus is nearly black at the LHC for all but the fringe impact parameters. Soft inelastic diffraction is believed to be determined by fluctuations in the amplitude for absorption of the projectile wave packet, and is expected to be strongly suppressed at the LHC, in comparison to lower energies. As a result, at LHC energies the nucleus may serve as a very effective filter, enhancing the contributions of semi-hard diffraction originating from the scattering of protons in weakly interacting configurations, as discussed in Section 2.1.5, page 24.

However, it is not out of the question that even in central pA collisions, high-mass inelastic soft diffraction might occur at some level. The time at which a diffractive rapidity-gap "edge" is formed is in general quite large: it can be many tens or hundreds of fermi later than the collision time (in typical reference frames). In the intervening time interval, there is a lot of particle emission from the candidate diffractive system moving down the beam axis, and it may be that this system "forgets" its past as it evolves. If so, there could be the possibility that it evolves into a state which is not orthogonal to a single nucleon, and therefore some of the time will produce the diffractive final system, no matter what its condition at early times. While this scenario may seem unlikely, it would not seem so were the data to show that such a phenomenon exists. It will be important to look.

Such gaps if present would most likely lie completely within the phase-space region of the fragmenting proton (the "coherent" phase-space region (b) discussed below in Section 2.3.2.1, page 46), and would provide extremely important information on the nature of the "soft" Pomeron.

Hard diffraction, even more than soft, is expected theoretically to be peripheral. The number of multiple interactions with the nucleons at the edge of the nucleus should be small, and consequently the Glauber-Gribov picture should be the standard of reference. Nevertheless, as discussed in Section 2.1.4.1, page 19, it appears that even hard diffraction has important nonperturbative features, with perhaps a relatively close relationship to the poorly-understood mechanisms of soft diffraction. Therefore, it again will be important to look for central hard diffraction in pA collisions.

2.3.1.4. Impact-parameter dependence is accessible and important

As is already apparent from the preceding discussion, the proton-ion processes emphasize the importance of thinking in terms of the transverse structure of the process, especially on the impact-parameter dependence of the phenomenology. This way of thinking is commonplace in the heavy-ion community already; the determination event-by-event of the impact-parameter (angular momentum), and even the orientation of the collision plane, of the colliding ions is an essential tool [105]. It is implemented for example via measurement of leading fragments, as well as via the distribution of transverse energy and entropy. On the other hand, in hadron-hadron or lepton-hadron collisions the dependence of the phenomenology on transverse coordinates has been almost completely neglected, although as discussed in Sections 2.1.5, page 24 and 2.2.4.1, page 42, the opportunities for doing this at LHC energies with FELIX are more promising.

Proton-ion collisions interpolate between the extremes. We have already mentioned that the impact-parameter dependence of generic particle production provides vital information. This is also the case for ion parton distributions, and for the frequency of occurrence of diffraction or rapidity-gap processes.

It should be possible to determine the impact parameter event-by-event. The technique differs from what we have discussed for pp collisions. As discussed in Section 2.3.2.2, page 46, the nuclear fragment distribution should be a good discriminant.

2.3.1.5. Proton-ion collisions probe transverse nucleon structure

As already discussed in Sections 1.2.6, page 5, 2.1.5, page 24, and 2.2.4.1, page 42, one supposes that in some subclass of events the distribution of constituents in the initial proton may be unusually local in the transverse, impact plane when the proton collides with the ion. If this is so, its effective cross-section per nucleon will be greatly reduced, perhaps all the way to the perturbative-QCD level. If the effective cross-section of such a point-like configuration goes below 20 mb, there will be an appreciable probability that it can penetrate through the center of a Pb ion and survive. This would lead to a highly enhanced yield of diffractive production of the products of the point-like configuration in collisions with heavy ions.

Not only might the properties of the final-state collision products depend upon the nature of the transverse structure of the proton primary at arrival at the collision point, but even the conventional parton distributions may also be affected. For example, again consider, as in Section 2.2.4.1, page 42, a nucleon as a small quark and small diquark connected by a narrow QCD flux-tube. It should be clear that if the flux-tube is at right angles to the collision axis at arrival, then the valence partons will have comparable longitudinal momentum or x. On the other hand, if the flux tube is parallel to the direction of motion, then one of the valence systems will have very large x, and the other very small. This happens because in this case the internal longitudinal momenta of the valence systems, in the rest frame of the projectile proton, are in opposite directions. Therefore the smallness of the configuration is correlated with the joint x-distribution of its constituents. This kind of nonfactorization may be determined by the study of the perturbative-QCD processes of dilepton, direct-photon, or dijet production as a function of the centrality of the collision.

2.3.1.6. Proton-ion collisions "calibrate" ion and cosmic-ray phenomenology

An extremely important reason for the study of proton-ion collisions is that it provides fundamental input information necessary for the interpretation of ion-ion collisions. Especially with respect to the hard-collision processes, determination of the ion parton distributions experimentally in pA collisions appears to be an absolute prerequisite. In addition, the study of energy losses for secondary partons propagating through nuclear matter, of the energy and baryon-number flow from the proton projectile into the central rapidity region, and of the presence already in pA collisions of unusual forms of the produced hadron system, would have a strong influence on the phenomenology of ion-ion collisions.

As discussed in Section 2.5, page 70, the measurement of the basic parameters of proton-ion collisions for $A = 14 - 16$ is very relevant for the interpretation of ultra-high-energy cosmic-ray extensive-air-shower data. In addition, data from heavier ions will be important in comparing LHC data with cosmic-ray data from emulsion-chamber experiments such as JACEE or Chacaltaya-Pamir.

2.3.1.7. The FELIX detector has special advantages

While many of the above topics will be accessible to all detectors at the LHC, and while it is hoped that all collaborations take the above physics issues seriously, it is clear that the FELIX detector has special advantages. Not only is the study of leading proton fragments paramount for many of the above issues, but also the study of ion-fragments for the impact-parameter tagging. Indeed in all of the items above, it is easy to see that the capabilities provided by FELIX are extremely advantageous. In particular, as emphasized already in the context of pp collisions, the capability of FELIX to study in detail the parton distributions at extremely small x, down to values smaller than 10^{-6}, together with the impact-parameter-tagging feature, makes many of the above studies unique to FELIX.

2.3.2. Generic features of pA collisions

2.3.2.1. Basic subregions of final-state phase space

In terms of the phase space of produced hadrons, we may divide the particle production mechanisms into at least three distinct regions:

a) The soft fragments, mainly pions, nucleons, and spallation products, produced more or less isotropically in the rest frame of the ion, are an important indicator of the centrality of the proton-ion collision, as discussed in more detail in the next subsection. In the collider frame, these fragments will typically carry transverse momenta of hundreds of MeV at most, and longitudinal momenta in the TeV range; hence their pseudorapidities will be in excess of 8-9.

b) Produced hadrons, as seen in the ion rest frame, which are so energetic that their production angles are small compared to 1 fm divided by the nuclear diameter (60 mrad in Pb), will have formation lengths large compared to the nuclear diameter. Taking a factor 10 for safety (6 mrad instead of 60), this defines roughly the boundary of what may be called, somewhat inaccurately, the "coherent" phase-space region in the collider reference frame. This boundary is roughly at a pseudorapidity of 3-4 in the ion direction, and this phase-space region then extends through central pseudorapidities all the way to the leading-proton fragments. In this phase-space region the production amplitude for those produced particles depends on the interaction of the projectile with all the "wounded" nucleons in the ion, via a nontrivial quantum cascade mechanism.

c) The remaining phase-space region, which is in the ion-hemisphere and extends from pseudorapidities of about 3-4 to 8-9, should have enhanced secondary-particle multiplicity due to fairly conventional, classical cascading mechanisms within the nuclear matter. However, as we discuss in Section 2.3.4.2, page 53, even in this phase-space region what to expect is quite uncertain. But the features of this part of the final state may again be of much use in tagging the impact parameter of the incident proton.

It is the phenomenology in the "coherent" phase space region (b) which impacts most directly upon both perturbative hard-QCD phenomenology and the soft-QCD nonperturbative processes. The phenomenologies of the remaining regions are essential, however, especially in their potential for providing tags of impact-parameter and of the initial-state configuration of the proton.

2.3.2.2. Triggers for centrality of pA collisions

Studies of interactions with nuclei at energies $\sqrt{s} \leq 40$ GeV have established a correlation between the centrality of the collisions and the multiplicity of nucleons produced in the nucleus fragmentation region. This correlation has been observed in fixed target experiments [106] both for the production of slow fragments with momenta ≤ 300 MeV/c, and for the production of protons with momenta $700 > p_N > 300$ MeV/c emitted backward and forward in the nucleus rest frame (black and grey particles in the terminology of emulsion studies). The black particles are predominantly produced in pre-evaporation and in evaporation of the residual nuclear system.(This category should include soft neutrons, which are not detected in the emulsion experiments and which for heavy nuclei are the major channel of evaporation.) The gray particles are predominantly produced via two mechanisms. The first is emission of short-range-correlated nucleon pairs hit by the projectile, together with their secondary hadrons.(These contribute to both forward and backward hemispheres in the nucleus rest frame.) The second mechanism is the production of secondaries into the forward direction (in the nucleus rest frame) by "wounded" nucleons [107]. The number of gray particles grows approximately linearly with the number of wounded nucleons. FELIX will be able to observe these fragments and hence distinguish central from peripheral collisions. Note that all these fragments to good approximation move with the same velocity as the incident ion, and are therefore found in the far-forward phase-space region (a) discussed in the previous subsection.

Similarly the total multiplicity of fast hadrons (shower particles) was found to depend linearly on the number of wounded nucleons. The dependence of the number of black, gray, and shower particles on centrality is likely to be different, due to the larger elementary cross-section of the pN interaction at LHC energies. Nevertheless the qualitative pattern is likely to be preserved.[3] Another option to select more central collisions (especially for heavy nuclei), easily available for collider experiments, is the study of event structure as a function of the multiplicity of the neutrons with very small energies in the nucleus rest frame. In collider kinematics these neutrons are emitted at very small laboratory angles and are absorbed by the forward zero-degree calorimeter. Since all these neutrons have energies close to E_A/A the energy detected in the calorimeter measures the soft neutron multiplicity. Thus we conclude that FELIX will have several handles for determining the centrality of collisions. To calibrate these " gauges" a systematic study of soft processes with a variety of nuclei will be necessary.

2.3.3. Hard QCD phenomena in pA scattering

2.3.3.1. Parton densities of nuclei

Nuclear parton distributions at small x: nuclear shadowing phenomena

We discussed in Sections 2.1.1, page 9, and 2.1.2, page 12, that in the small x region one can probe nonlinear QCD effects and explore the fundamental question of what kind of dynamics slows down and eventually stops the rapid growth of the cross-section (or the structure functions $F_2(x)$ and $xG(x)$) at small x. The use of nuclei allows one to enhance these effects. Indeed, in the small x regime a hard collision of a parton of the projectile nucleon with a parton of the nucleus occurs coherently with all the nucleons at a given impact parameter. The coherence length by far exceeds the nuclear size: in the kinematic regime accessible for FELIX it can reach up to 10^5 fm (in the nucleus rest frame). In the rest frame of the nucleus this can be visualized in terms of the propagation of a parton in high density gluon fields over much larger distances than is possible with free nucleons. In the Breit frame it corresponds to the fact that small x partons cannot be localized longitudinally to anything close to the Lorentz-contracted thickness of the nucleus. Thus low x partons from different nucleons overlap spatially, creating much larger parton densities than in the free nucleon case. This leads to a large amplification of the nonlinear effects expected in QCD at small x; see e.g. [108,109].

Constraints from unitarity [110] indicate that nonlinear effects (i.e. effects not accounted for by the standard evolution equations) should become significant at much larger values of x for the nuclear parton densities than for the nucleon parton densities. It has been estimated [108–112] that the x-range where nonlinear effects become significant differs for a heavy nucleus and for a nucleon by more than one to two orders of magnitude, assuming its gluon density $xG(x,Q^2)$ is proportional to x^{-n} with $n \sim (0.2-0.4)$.

The analysis of Section 2.1.2, page 12, has shown that in the case of pp scattering FELIX is able to probe gluon as well as quark structure functions at very small x, see Figs. 2.6, 2.9. In the case of nuclei a very similar range can be probed: $x_{min}(A) = \sqrt{\frac{A}{Z}} x_{min}(pp)$[4].

It is worth emphasizing that for these measurements it is again necessary to study the jets, leptons and photons at rapidities close to the nucleon rapidity. In this y-range, the accompanying soft hadron multiplicities are relatively small, leading to a soft particle background comparable to that in pp scattering. In fact, for $|y_{max} - y| \leq (2-3)$ the background level may even be smaller than in pp collisions.

Thus the arguments presented in Section 2.1, page 9, for using a relatively low minimum-p_T cutoff for the jets should hold in this case as well. Since the cross-sections for hard processes increase roughly linearly with A, even short runs with nuclear beams will produce data samples sufficient to measure parton distributions with *statistical* accuracy better than 1% practically down to the smallest x which is kinematically allowed. The systematic errors for the ratios of nuclear and nucleon structure functions are also expected to be small since most of these errors cancel in the ratios of the cross-sections, cf [109].

[3] One example of a possible change is a significant reduction of the probability for a spectator to survive in the interaction with the projectile nucleon, leading to a reduction of the ratio $E\frac{d\sigma^{p+A\to p+X}}{d^3p}/\sigma_{inel}(NN)$ with an increase of $\sigma_{inel}(NN)$. Here the nucleon is in the nucleus fragmentation region, carrying a fraction of the nucleus momentum $\geq 1/A$.

[4] The factor $\sqrt{\frac{A}{Z}}$ is due to the difference of maximal energy per nucleon for the acceleration of a nucleon as compared to a proton.

Nuclear parton distributions at large x

FELIX will have sufficient luminosity to measure production of W and Z bosons at $0.4 > x_A > 0.1$, in the ion hemisphere. Even for such forward production, their decay products typically emerge at angles $\geq 20 - 100$ mrad, and can be reliably distinguished from ion-fragmentation debris. In this kinematic regime, the A-dependence of the ion's structure function $F_2(x, Q^2)$, as measured in Z^0 production and charge-averaged $W^{\pm}$ production, should be independent of A with an accuracy of 1-2%. Hence, these distributions can be used to measure nuclear shadowing effects with an accuracy better than $\sim 5\%$ down to $x \sim 3 \cdot 10^{-7}$ for quarks, and to $x \sim 4 \cdot 10^{-6}$ for gluons.

Centrality dependence for parton distributions

A simple but very important application of centrality triggers would be a study of the dependence of the shape of the parton distribution on the impact parameter. As described above, it should be possible to normalize the parton distributions at small x to the values of the quark distributions at $x_A \sim 0.1 - 0.2$, where nuclear effects on quark distributions are small, for all nuclear densities.

Naturally one expects larger gluon shadowing for central impact parameters. It is expected to be accompanied by an enhancement of the gluon densities ("anti-shadowing") at $x \sim 0.1 - 0.2$ (up to 20% for the case of Pb) [113] which could be probed by comparing gluon-dominated to quark-dominated cross-sections. This enhancement follows from the necessity to satisfy momentum and baryon charge sum rules and from the lack of nuclear enhancement in the data on the antiquark distribution in nuclei [114]. Note that it is just these effective gluon distributions which one needs for the calculation of the minijet production in the central AA collisions at the LHC.

2.3.3.2. Multi-jet production

Multiparton distributions

As already pointed out in Section 2.1.8, page 28, the large number of gluon-pairs available for semihard scattering at the LHC energy scale may saturate the unitarity limit already at the level of perturbative interactions. This interesting feature allows the possibility of describing, within the perturbative approach, global features of the typical inelastic event. If this is possible, the domain of understanding of strong interactions would be greatly extended. But this achievement would not come without a price. One is in fact forced to introduce into the perturbative picture of the interaction new nonperturbative quantities. They are the multiparton distributions, which in fact represent our present lack of knowledge of the nonperturbative structure of the hadron.

But the experimental opportunity at the LHC energy is in fact the actual measurement of these multiparton distributions. In this respect the use of nuclear targets is of great help. The interesting feature of semihard interactions with a nuclear target is represented by the large number of partons of the target as compared with the proton case and by the combined possibility of varying the number of partons both by choosing different values for the minimum jet p_T, and also by varying the nuclear atomic mass number. These two possibilities allow one to use the interaction on a nucleus as a very efficient tool to investigate the nonperturbative structure of the proton.

Nuclear enhancements

The advantage with the nuclear target is that the large enhancement in the number of parton collisions allows one to have sizeable rates of interactions at significantly larger values of transverse momenta. Indeed the problem with the unitarity limit is twofold. One faces it at the hadronic (or nuclear) level and one faces it also at the partonic level. When the unitarity problem is present at the hadronic level one is in the regime where the presence of many scattering centers has to be taken into account. When the problem appears at the level of parton-parton interactions, the structure of the single interaction itself shows up in a non-trivial way. Although this represents a rather interesting possibility for the understanding of perturbative QCD, it is very important to be able to have a clear distinction between the two different regimes. One has a much cleaner access to the information on multiparton distributions in the regime where the partonic interaction is elementary. The larger the momentum transfer, the simpler and better understood is the structure of the partonic interaction.

The relevant quantity is the dependence with A of the probability for multiple parton interactions. The cross-section for production of two pairs of coplanar jets due to the interaction of two partons of each projectile is [115]:

$$\sigma = \sigma_1 \cdot A + \sigma_2 \tag{2.24}$$

where the first term is due to interactions where two partons of the nucleus belong to the same nucleon and the second term is due to interactions with partons of two different nucleons.

In contrast to σ_1, which we discussed in Section 2.1.8, page 28, the term σ_2 in Eq.2.24 does not depend on the transverse separation between partons "1" and "2" in the proton. Hence it *directly measures* the correlated parton density in the nucleon: $f(x_1, x_2)$. Using information from the CDF double scattering experiment[116] on the mean transverse separation of partons in a nucleon, one expects that the contribution of the second term is dominant for heavy nuclei:

$$\begin{aligned}\frac{\sigma_2}{\sigma_1 \cdot A} &\approx \frac{(A-1)}{A^2 \cdot 1.4\ fm^2} \int T^2(b)\ d^2b \approx \\ &\approx 0.45 \cdot \left(\frac{A}{10}\right)^{0.5}_{A \geq 10}. \end{aligned} \tag{2.25}$$

Here the quantity

$$T(b) = \int_{-\infty}^{\infty} dz\ \rho(z, b) \tag{2.26}$$

is the nucleon density per unit area, the so-called optical thickness, with $\rho(\vec{r})$ the nuclear density, normalized so that $\int d^3\vec{r}\ \rho(\vec{r}) = A$.

In Eq.(2.25) nuclear shadowing effects are approximately taken into account if the momentum fraction x_A of at least one of the partons belonging to the nucleus is large enough ($x_A \geq 0.02$).

Other opportunities with multi-jets include

- Probing correlations between partons in the nucleus at high densities, i.e. for $x_{1\ A}, x_{2\ A} \ll 10^{-3}$, which would provide qualitatively new information about the dynamics of nuclear shadowing.
- Studying the accompanying soft hadron production (cf. the discussion in Section 2.3.4.1, page 52), which would allow measurement of the transverse size of a proton configuration containing partons x_1, x_2. In particular, the production of 4 jets with two jets at large x in the proton fragmentation region $x_1 + x_2 \geq 0.5$ may provide another way to look for point-like configurations in nucleons; see Section 2.1.5, page 24.
- Investigating three- and four-parton correlations in protons and nuclei.

2.3.3.3. Propagation of partons through nuclear matter

Studies at fixed-target energies have established an interesting pattern of nuclear effects for high-p_T inclusive particle production. The ratio of inclusive production on nuclei to the same process on a nucleon, $A^{f(x,p_t)}$, shows an effective exponent $f(x, p_t)$ exceeding 1 at $p_T \geq 1.5$ GeV, the so-called Cronin effect [117]. Analogous studies of the A-dependence of jet production have been inconclusive, to large extent because the transverse momenta of the jets are small.

Recent work [118–121] on the energy loss of high energy partons in a finite QCD medium, including cold nuclear matter, leads to the expectation that the energy losses of partons propagating through nuclear media should depend relatively weakly on their energy, and in fact may be quite small. They also indicate that energy losses in hot matter should be much larger than in cold matter, making jet quenching a probe of the state of the matter produced at early times in AA collisions. This adds importance to the experimental studies of parton propagation effects.

The medium-induced gluon radiation of a very energetic incident quark or gluon propagating through matter is found to be independent of energy provided the initial jet energy is large enough, typically ≥ 30 GeV (for quarks) in the rest frame of the medium. For a quark jet [119,120], the medium-induced energy loss increases *quadratically* with the length L and is independent of E for $E \to \infty$. For $L = 5$ fm, the asymptotic ΔE is estimated to be less than 1 GeV in a cold nuclear medium, making it difficult to check experimentally this remarkable dependence on the length L.

However, the smallness itself has implications. If leading partons suffer no significant energy degradation in traversing the center of a Pb nucleus, then the inclusive distribution of the leading secondaries can be expected to obey approximate Feynman scaling. This goes against the trend seen in fixed-target experiments, as well as against some of the arguments made in preceding sections of this document. But even if the scaling is there, the inclusive distributions and particle ratios may be quite distinct from what is found at low energies, because there is no suppression of short-distance multiple scattering effects.

The QCD prediction for transverse-momentum broadening due to multiple scattering is similar to the ordinary multiple-scattering result: a quark (gluon) from a projectile proton collides with the various target nucleons exchanging transverse momentum $\vec{p}_\perp$ at each collision before forming e.g. a Drell-Yan pair (J/ψ). The expression is

$$\langle p_\perp^2 \rangle = \frac{\alpha_s C_F \pi^2}{2} (xG)\, \rho L \simeq 0.5\, \alpha_s \left(\frac{L}{5\text{fm}}\right) \text{GeV}^2 \tag{2.27}$$

This effect of the transverse-momentum broadening of jets due to initial-state multiple scattering is easier to measure. Recent analysis of Drell-Yan data [122] and of J/ψ data [123] in pA collisions, agrees with the estimate in Eq.(2.27) with $\alpha_s \simeq 1/3$, when it is assumed that the broadening is entirely due to initial state interactions.

There are several options for probing parton propagation with FELIX:

- The A dependence of p_T broadening in the production of Drell-Yan pairs as a function of the energy of the parton (x_F), its virtuality ($M^2_{l^+l^-}$) can be studied at FELIX in a extremely wide kinematic range from $E_q \sim 20$ GeV to $E_q \sim 5 \cdot 10^7$ GeV in the nucleus rest frame. This would allow one to check the expectation of [119] that p_T broadening is energy independent.

- The A dependence of dijet acoplanarity and of individual jet shapes can be studied for high p_T jets which are moving relatively slowly in the ion rest frame, something which can be seen only in a FELIX type detector, as well as for jets with very high energies in the ion rest frame. The γ-jet sample would allow an especially clean interpretation.

- The ability of FELIX to detect both quarkonium production and open heavy quark production in similar kinematics would provide unique opportunities for the comparison of propagation of color singlet and color octet systems through nuclear media. For example, would the production of $J/\psi, \psi', D\bar{D}, \Upsilon, B\bar{B}$ at $x_A \sim 0.5$ have the same A-dependence? Would the rate of production of charm particles with $x_A \sim 1$ increase with A faster than A due to slowing down of c-quarks and/or reinteractions of charmed hadrons in nuclear media? Such measurements would be a challenging task for FELIX, due to the larger multiplicities of hadrons produced in the nucleus fragmentation region. However at least some of the channels like $J/\psi, \Upsilon$, and $e\mu$ pairs from open-charm decays may be accessible.

2.3.3.4. Search for color transparency effects

Interaction of point-like configurations with nuclei

We discussed in Sections 1.2.6, page 5, and 2.1.5, page 24, that hadrons are thought to occasionally fluctuate to small size, point-like configurations, within which color is localized in a small transverse area. In case of the scattering off nuclei, this physics leads to many coherent phenomena. Some of them have been observed in fixed target experiments; for a review, see references [48]. Because the gluon densities are high at the ultra-high energies of the LHC, many formerly point-like configurations may interact with rather larger cross-sections. Nevertheless these cross-sections are likely to be substantially smaller than the average cross-section, as discussed in Section 2.1.5, page 24.

Transverse mapping of the nucleon

As mentioned in Section 2.3.1.5, page 45, the use of nuclear targets with a hard trigger allows one to address the question of correlations between the longitudinal distribution of partons in a nucleon and the strength of the interaction of such configurations with the target (roughly speaking with the transverse size of the configuration). Since the presence of a parton with large $x \geq 0.6$ requires three quarks to exchange rather large momenta, one may expect that these configurations have a smaller transverse size and hence interact with the target with a smaller effective cross-section $\sigma_{eff}(x)$. Suggestions for such a dependence of the size on x are widely discussed in the literature; see e.g. [124]. Using as a guide a geometric (eikonal type) picture of pA interactions and neglecting (for simplicity) shadowing effects for nuclear parton densities one can estimate the number of wounded nucleons $\nu(x, A)$ in events with a hard trigger (Drell-Yan pair, γ-jet, dijet,...) as a function of σ_{eff} [125]:

$$\nu(x, A) = 1 + \sigma_{eff}(x)\frac{A-1}{A^2}\int T^2(b)\, d^2b, \tag{2.28}$$

where the nuclear density per unit area $T(b)$ is defined in Eq.(2.26), Section 2.3.3.2, page 48. For average inelastic pPb collisions, $\sigma_{eff} \sim \sigma_{inel}(pp)$, and $\nu \approx 10$ at the LHC. This is somewhat larger than the average number of wounded nucleons in pA collisions, due to the selection of more central impact parameters in events with a hard trigger.

A decrease of the effective cross-section for large x, say, by a factor of 2, would result in a comparable drop of the number of "shower" particles, and perhaps "gray" and "black"particles (cf. Section 2.3.2.2, page 46) as well, produced in the collision along with a significant drop of the total multiplicity.

Another interesting quantity to study in coincidence with the hard trigger is the number of leading particles in the nucleon fragmentation region. If the fragmentation process does not remember the removal of one fast parton one may expect a stronger drop of the forward ($z_h \geq 0.3$) multiplicity with A than in the inclusive processes $p+A \to h+X$, where scattering off the edge of the nucleus gives a significant contribution (see the discussion in Section 2.3.4.2, page 53). On the other hand, if a large x_p trigger selects a small size configuration, the pattern could be reversed, leading to a nearly A-independent multiplicity of accompanying forward particles.

Semihard coherent diffraction.

Ultimately for the processes dominated by the scattering of a proton in a point-like configurations the A-dependence of the total coherent diffractive cross-section would be proportional to $A^{4/3}$ (modulo nuclear shadowing effects for parton densities which may reduce the A-dependence to about $A^{(1-1.1)}$). This should be compared to the $A^{0.25}$ dependence, which is expected for soft processes at the LHC energies. Thus the observation of a rapid increase with A of a particular channel of diffraction would provide a clear signature of the importance of point-like configurations in the process.

Theoretically the cleanest process is the diffraction of a proton into three high p_T jets, which was discussed for the pp case in Section 2.1.5, page 24. The expected rapid growth of this cross-section with A leads to sufficient rates even for short pA runs. Other possible channels include production of two high p_T jets carrying a large fraction of the nucleon momentum. This may originate from the scattering of a proton in a configuration where two quarks came close together, leading to a reduction of the size of the projectile. Another suggested channel is diffraction to $B_c + D_{\bar{c}}$ originating from small configurations in a nucleon containing a $c\bar{c}$ pair [126].

Survival probability in rapidity-gap events

In the geometric, Gribov-Glauber picture of nucleon propagation through the nucleus the gap survival probability decreases with A as

$$R_A = \frac{\sigma_{in}(pp)}{\sigma_{in}(pA)} \int d^2b\, T(b)(1-\sigma_{in}(pp)T(b))^{A-1}, \quad (2.29)$$

where again $T(b)$ is the optical thickness defined in Eq.(2.26). Eq.(2.29) predicts a very strong suppression of the gap events for scattering off nuclei: for example by a factor of $\sim 4(12)$ for scattering from $^{16}O(Pb)$. Obviously if the parton of the nucleon belongs to a point-like configuration, the survival probability will be much larger. Ultimately, if one would be able to select scattering off configurations interacting with $\sigma_{eff} \leq 15$ mb, the probability would start to increase with A.

Hard diffraction dissociation of the Pomeron by the nuclear medium

To get a better understanding of the parton structure of the Pomeron it would be interesting to measure large $|t|$ diffraction of the projectile proton into an exclusive state (p, N^*), together with high p_T dijets in the nucleus fragmentation region. An especially interesting case is for "superhard" Pomeron kinematics, when the jets carry practically all the momentum of the Pomeron (see discussion in Section 2.1.3.2, page 19). If such a process is due to the scattering of the proton in a point-like configuration, the cross-section should be approximately proportional to A. To understand the role of soft rescatterings in such a process it would be instructive to compare this process with large $|t|$ diffraction, with the jets carrying a smaller fraction of the Pomeron momentum, and also with the case where no jets are produced.

Color transparency in quasielastic processes

We discussed in Section 2.2.2.3, page 36, that at sufficiently large $|t|$ elastic pp scattering also may be dominated by the scattering of smaller than average-size configurations. Thus it is natural to ask whether these configurations are absorbed by the target with the same cross-section as a generic proton. The study of the quasielastic reaction $p+A \to p+p(N^*)+(A-1)'$ at $t \sim$ few GeV^2 would allow addressing this question. Measurements for $|t| \leq 10$ GeV^2 would require only a few days of FELIX running in a pA mode. The triggering would be similar to what is done for elastic pp scattering. In addition, it would be possible to use the forward acceptance of FELIX to suppress background processes containing pion production.

Such large $|t|$ color transparency experiments have been carried out at $E_{inc} \sim 6-15$ GeV, with complicated results. But most of those complexities of interpretation should be absent at the much higher FELIX energy.

It should be possible to detect a relatively small decrease of the effective cross-section σ_{eff} from $\sigma_{tot} \approx 120$ mb; see Fig. 2.23. Note also that it should be possible to study the change of the A dependence from rather small $|t|$, where a geometric approximation is likely to work, up to quite large $|t|$. Since the cross-section for absorption of a low-momentum nucleon which is formed close to the interaction point (in the nucleus rest frame) weakly depends on this momentum the only significant source of the change of the A dependence as a function of t would be a change in the transparency of the projectile.

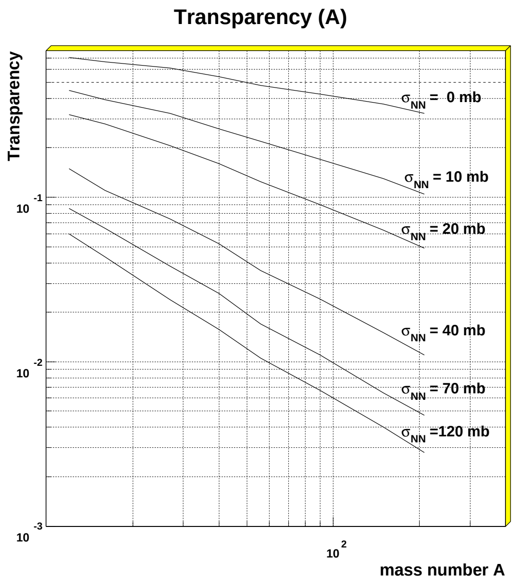

Figure 2.23. A dependence of the nuclear transparency in the $pA \to pp(A-1)$ reaction at large $|t|$, as a function of the effective interaction cross-section of the projectile proton.

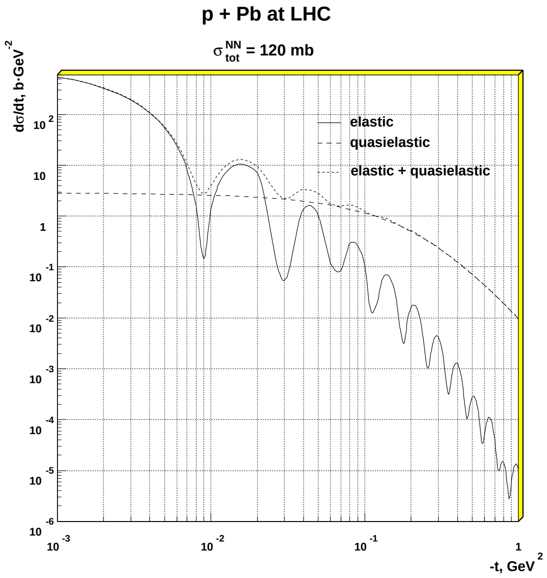

Figure 2.24. cross-section of elastic and quasielastic $p\ Pb$ scattering

2.3.4. Basic characteristics of soft pA collisions

We already discussed in Section 2.3.1.1, page 43, that soft pA physics at LHC energies may dramatically differ from low energies, $\sqrt{s} \leq 40$ GeV, where most available data exist, if for no other reason than that the effective radius of a proton becomes comparable to the internucleon distances in nuclei and that the mean free path becomes smaller than the average internucleon distance. Consequently, although a black disc model will still reasonably describe total and perhaps elastic cross-sections of pA interactions as for pre-LHC energies, the underlying dynamics may be quite different. This is especially the case, given in addition the emergence of minijet phenomena at the LHC energy scale.

2.3.4.1. Total and elastic cross-sections

Due to the large value of the cross-section of the elementary pp interaction, the proton-nucleus interaction at all impact parameters except near the edge is practically black. As a result the total cross-sections for pA scattering depend very weakly on the nucleon-nucleon total cross-section, the ratio of real to imaginary part of the forward nucleon-nucleon scattering amplitude, and on inelastic shadowing effects. For example, variation of $\sigma_{tot}(pN)$ between 100 and 120 mb and Re/Im between 0.00 and 0.15 leads to an increase of the cross-section of pA scattering by 4-8%, while inelastic shadowing effects reduce the cross-section by only 1-2%.

The study of elastic scattering, which constitutes nearly half the total cross-section, may provide a somewhat more sensitive test of the dynamics of the soft interaction. In particular, the study of the diffraction pattern of the minima and maxima of elastic scattering may allow one to probe in detail the picture of multiple interactions of the projectile with nuclei.

FELIX will be able to study elastic scattering off nuclei in two ways. For the lightest nuclei, such as ^4He, the acceptance in the nuclear arm ($t_{min}(pA) = Z^2 t_{min}(pp)$) should be good enough to measure elastic scattering through a direct coincidence measurement.

For heavier nuclei, to avoid backgrounds from beam gas interactions it seems only possible to study processes with nuclear excitations. These have huge cross-sections up to $|t| \gg 1$ GeV^2 (see Fig. 2.24). To select these processes one would use the forward calorimeter to select events for which the nucleus was excited and emitted photons with average energy ~ 5 GeV and $\theta \sim 0.2$ mrad, or for which the nucleus decayed with the emission of neutrons.

2.3.4.2. Inelastic soft diffraction by nuclei

The very strong absorption present at central impact parameters results in the expectation that inelastic diffraction predominantly occurs from scattering of the proton off the nuclear edge. This gives only a very slow increase with A of the inelastic diffractive cross-section $\propto A^{0.25}$. However it is natural to expect that the production of different final states is determined by configurations with different average interaction cross-section - e.g. states with charm, minijets, etc. For these states one expects a much more rapid increase of the cross-section with A (see the discussion in section 2.3.3.4, page 50). Hence the study of the A-dependence of various channels of inelastic diffraction, without nuclear breakup, can again shed new light on the fluctuations of the interaction strength at ultra-high energies. The beam-gas background in this case is a difficulty, but one can hope to suppress it by an accurate determination of vertex position. Alternatively one can analyse incoherent diffractive processes where nuclear decay products are observed in the forward detector.

Again, the standard of reference for the treatment of these processes should be Glauber-Gribov theory, since the number of multiple interactions with nucleons in the nucleus should be small.

2.3.4.3. A-dependence of the particle production

Particle production in the proton fragmentation region

The A-dependence of hadron production in the proton fragmentation region remains one of the least understood aspects of hadron-nucleus interactions. Practically all available data are inclusive. They indicate that the cross-section is dominated by the production of leading particles at large impact parameters, where the projectile interacts with only one or two nucleons of the nucleus. As a result very little information is available about hadron production at the central impact parameters which are most crucial for the study, for example of AA collisions. Theoretical predictions for this region are also rather uncertain.

In eikonal type models, where the energy is split between several soft interactions, one may expect a very strong decrease of the yield of the leading particles. The dependence is expected to be exponential with path length in the nucleus; their mean energy is attenuated exponentially. On the other hand, if the valence partons of the projectile do not lose a significant amount of their initial momentum, as suggested by perturbative QCD [118,119] and already discussed in Section 2.3.3.3, page 49, the spectrum of leading particles may approach a finite limit for large A [127]. However, this limit may differ even qualitatively relative to what is seen in pp collisions at low energy. Another open question is the change of the A-dependence due to the increase of the total pp cross-section by nearly a factor of three from fixed target energies. If the probability of leading particle production is determined by collisions with one or two nucleons, the spectrum of forward particles would be suppressed much more strongly at LHC energies than at fixed target energies.

FELIX will be able to measure the A-dependence of the production of a variety of leading hadrons: neutrons, protons, Δ-isobars, hyperons, K_S's, and π^0's. Use of impact-parameter tags, as discussed in Sections 1.2.9, page 6, and 2.2.4.2, page 42, will be very important in disentangling the dynamics. The very limited data now available do not contradict the idea of a limiting distribution for the hadron fragmentation when averaged over impact parameter; see [127].

Particle production in the central region

The Gribov-Glauber model including inelastic screening effects, but neglecting the final state interactions between the hadrons produced in different Pomeron exchanges, as well as neglecting the interactions of these hadrons with the nuclear target, leads to a prediction that at high energies and rapidities y, such that $|y_p - y| \gg 1$ (the fragmentation region (b) of Section 2.3.2.1, page 46), the inclusive spectrum of produced hadrons should be proportional to that in the inclusive cross-section of hN scattering:

$$\frac{d\sigma^{p+A\to h+X}(y,p_T)}{dy\ d^2p_T} = A\frac{d\sigma^{p+N\to h+X}(y,p_T)}{dy\ d^2p_T}. \quad (2.30)$$

Since $\sigma_{inel}(pA)/\sigma_{inel}(pN) \propto A^{2/3}$, Eq.(2.30) implies that the multiplicity of particles produced in the inelastic pA collisions should increase with A, roughly as $A^{1/3}$. Data at fixed target energies do not contradict this relation, but the energy is too low for an unambiguous interpretation.

The opposite extreme is to assume that the effects of multiple semihard interactions of the projectile hadron are the main mechanism of particle production. Multiple short range scatterings between partons (minijet production) together with associated QCD radiation (gluon bremsstrahlung) then are assumed to produce the major part of the total entropy and transverse energy. Such a model has been developed by Geiger, with an eye to appli-

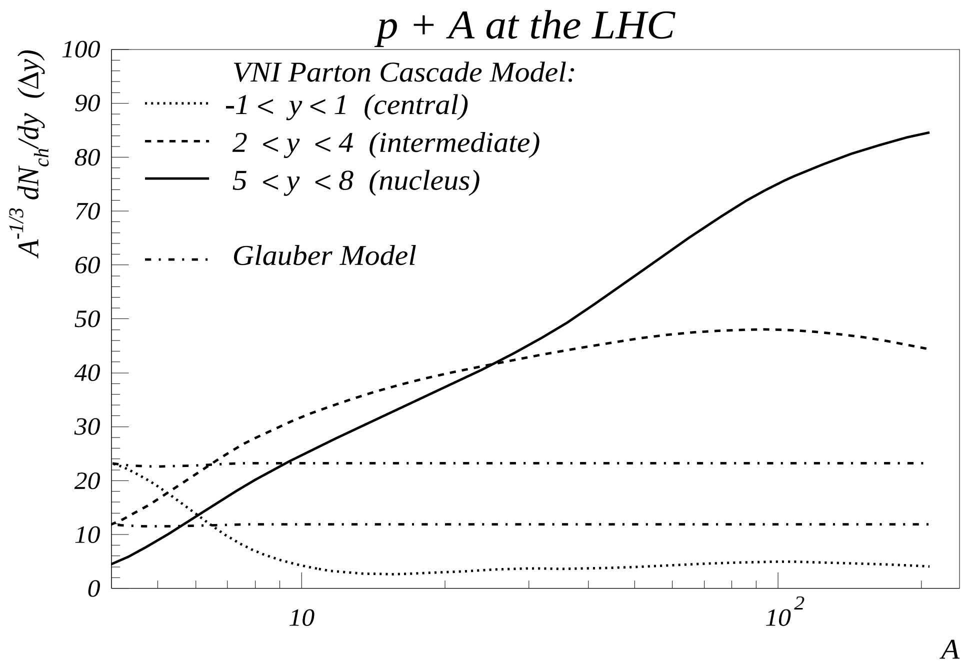

Figure 2.25. Comparison of the prediction of the Glauber-Gribov model with the quark-parton cascade model of [128] for the A-dependence of hadron production.

cation to AA collisions [128]. For pA collisions, this model predicts an A-dependence of hadron production which differs very substantially from the expectations of the Gribov-Glauber model, see Fig. 2.25.

Particle production in the ion fragmentation region

For rapidities close to the nucleus rapidity, (fragmentation region (c) of Section 2.3.2.1, page 46) there are indications of the contribution of slow hadron re-interactions, which lead to an increase of the multiplicity of nucleons with momenta $1.0 \geq p_N \geq 0.3$ GeV, as compared with expectations neglecting final state re-interactions (a factor of ~ 2 for heavy nuclei) [107]. As we have repeatedly discussed, it is doubtful that the Gribov-Glauber picture is correct at LHC energies, so one may expect significant deviations from the expectations based on Eq.(2.30).

This actually is the case in the model of Geiger, mentioned in the previous subsection, as can be seen in Fig. 2.25. It must be emphasized that a quantitative understanding of the physics of particle production in pA collisions in this phase-space region is a prerequisite for understanding the corresponding phenomenology in AA collisions.

2.4. Two photon physics in pp and AA collisions

2.4.1. Overview

The large fluxes of quasi-real photons associated with the Coulomb fields of ultrarelativistic heavy ions at the LHC will lead to $\gamma\gamma$ collisions with cross-sections which scale roughly as Z^4. Effective luminosities in a broad range of $\gamma\gamma$ mass intervals will be orders of magnitude higher than achieved at present e^+e^- colliders.

The physics interest in $\gamma\gamma$ collisions at the LHC is centered on QCD processes at moderate center-of-mass energies, with a primary goal being light and heavy quark spectroscopy. The high luminosity and high quality of the FELIX tracking make this an especially attractive option. Another advantage is that the rapidity range from 2 to 6, which is covered by the UA1 and D0 portions of the FELIX detector, is an especially practical phase-space region for accepting the products of the $\gamma\gamma$ collisions. In particular, the boosted secondary photons will be detected with percentage resolutions in energy and angle comparable, at the same p_T, to what is attained in a good e^+e^- detector such as CLEO.

It may seem strange at first that a collider operating at many TeV in the center of mass should be used for light-quark spectroscopy. Nevertheless, this subject is today and almost certainly will continue to be a serious frontier of QCD research. The nonperturbative sector of QCD remains the greatest challenge to theory. And there are many fundamental unanswered questions still open in light quark spectroscopy.

A central issue is whether states beyond those built from $q\bar{q}$ and qqq exist. Gluon degrees of freedom are endemic in perturbative QCD, but there is no deep understanding of their role in the nonperturbative regime. Glueball spectroscopy is predicted by lattice-QCD and related models. There is some consensus that the lightest state is 0^{++} and has a mass of about 1.5 GeV, while 0^{-+} and 2^{++} are just above 2 GeV. Hybrid states, where gluonic degrees of freedom are excited in the presence of the $q\bar{q}$ "seed", are also predicted to lie around 2 GeV. Here the 0^{-+} and 2^{++} are accessible to the $\gamma\gamma$ process. An additional array of states (with $C = +1$ all accessible to the $\gamma\gamma$ process) up to 4 GeV and beyond are anticipated. Also predicted is an exotic 1^{-+} state, which is not possible for the simple $q\bar{q}$ classification. It is accessible to $\gamma\gamma^*$, but unfortunately not to $\gamma\gamma$. Somewhat less fundamental but nonetheless interesting are possible multiquark $qq\bar{q}\bar{q}$ or meson "molecules" such as $K\bar{K}$.

In addition, at the LHC there is enough luminosity to access, in principle, the spectroscopy of single $C = +1$ heavy quarkonia such as η_c, χ_c, η_b and their radial excitations. Unlike LEP 200, the two photon processes in heavy ion collisions at LHC enable studies of the final states with b-quarks.

One may ask why $\gamma\gamma$ channels are so special for such investigations. The γ couples to the charge and spin of the constituents. Historically it has been the case that γ-induced processes were very important in establishing the quark model itself:

- Deep inelastic γ (and ν) interactions established the u and d charges of partons; recent polarized-γ studies show that the spin structure of partons in hadrons is more profound than hitherto suspected.

- Nonperturbative studies in photoproduction and in $e^+e^- \to \rho : \omega : \phi : \psi$ revealed the $(u\bar{u} \pm d\bar{d}) : s\bar{s} : c\bar{c}$ structure of the vector mesons from the squared charge of the constituents. This "gift" of nature that produced ideally mixed vector mesons in flavor was an essential piece of information that pointed the way toward the quark model in the early 1960's. The $\gamma\gamma$ channels may provide similar impetus in the $C = +1$ channels that these pioneering studies did for the $C = -1$ channels.

The capabilities for $\gamma\gamma$ physics at the LHC are not, however, limited to spectroscopy. Already at present energies a variety of processes have been studied, for which the parton structure of the photon is important [129]. Multijet production is an especially attractive LHC process [130]; the two photon mass region, $M < 150$ GeV, is accessible.

In addition, heavy ion collisions at the LHC provide the possibility to observe a variety of important diffractive processes, both hard and soft. One example of such processes is the diffractive dissociation of one photon into dijets, either light flavors at high p_T, or heavy flavors at any p_T: $\gamma\gamma \to jet + jet + V$. Diffractive production of two vector mesons, $\gamma\gamma \to V + V$, is also important. When the vector mesons are made of the light quarks, a "soft" behavior is expected. When at least one of the vector mesons is built from heavy-flavor quarks, this process is ideal for probing high energy mesononium and onium-onium scattering. As discussed in Sections 2.1.1.2, page 9, and 2.1.1.6, page 11, the cross-sections for such processes are predicted to increase strongly with energy.

Photoproduction physics, similar to what is done at HERA, is also accessible at the LHC at much larger center-of-mass energies. On the one hand, coherent photoproduction processes constitute a potential background for the $\gamma\gamma$ physics, and must be understood. This background problem will be discussed in the next subsection. On the other hand, the photoproduction process is interesting in its own right. As already discussed in Section 2.1.1.6, the study of vector-meson photoproduction, especially in the comparison of energy dependence for light mesons like ρ and ϕ with heavy onia, ψ and Υ, is important for the study of small-size initial-state configurations (color transparency) and of the gluon distributions in the ions. In addition, the spectroscopy of higher mass systems produced in γ-Pomeron collisions is essentially unexplored and will be, like it or not, available for study in FELIX. This is also the case for the products of Pomeron-Pomeron collisions, another potential source of background. However, the physics of double-Pomeron exchange is probably best addressed in pp running, with the AA data constituting a useful supplementary source of information. [5]

[5] In ion-ion collisions, it should be understood that the phrase "Pomeron exchange" must be interpreted broadly; the idea of Regge-pole amplitudes dominating such a complex process is too simplistic. Here we only imply that the process has the same diffractive, rapidity gap structure as the extreme case of simple exchange of a Pomeron Regge-pole.

One aspect of pp double-Pomeron-exchange physics not emphasized in the previous sections is that of spectroscopy. The basic physics issues which are addressed are very similar to those expressed above for $\gamma\gamma$ collisions. But of course the nature of the incident Pomeron "beams" is still very enigmatic: are they to be viewed mainly as pion cloud or mainly as gluon degrees of freedom? If it is the latter, then the Pomeron-induced processes can be expected to be especially rich in glueball spectroscopy. But since the places in the detector that the products of double-Pomeron-exchange go are the same as for the $\gamma\gamma$ process, since the trigger is essentially the same, and since the choice of channels to be studied is the same (essentially everything with $C = +1$), the experimental problems have a very large (but not complete) overlap. We return to this subclass of processes in Subsection 2.4.6.

The very large $\gamma\gamma$ luminosities lead to very large cross-sections for QED processes such as dilepton pair production. Besides being vital for monitoring purposes, the production of τ pairs may be interesting in its own right [131], in particular, in measuring anomalous magnetic and electric dipole moments with good precision.

Finally the $\gamma\gamma$ luminosities are so high that it is not out of the question to search for particles beyond the standard model, especially light Higgs particles, new leptons, or SUSY sleptons [132–134], produced in a relatively clean environment. Higgs decays into $b\bar{b}$ pairs are a candidate for study. Furthermore, the low production rate for non-strongly interacting particles (sleptons, charginos, neutralinos) in Drell-Yan and gg-fusion processes may make the two photon processes preferable to pp for their observation [135].

2.4.2. Isolating $\gamma\gamma$ processes in ion-ion collisions

Even leaving aside for now the pure electromagnetic processes, some of which have truly huge cross-sections, the strong ion-ion cross-sections are orders of magnitude larger than the $\gamma\gamma$ hadroproduction cross-sections of interest. Of course most of these lead to easily distinguishable final states. What is left to consider are essentially strong double-Pomeron-exchange processes at the ion-ion level, as well as diffractive photoproduction, "γ-Pomeron fusion". The primary signature of these backgrounds, as is the case for the $\gamma\gamma$ signal, is large rapidity gaps in both directions along the beams.

The triggering for these channels is the same as discussed for double-Pomeron exchange processes in pp collisions, namely activity (hit density in tracking systems, transverse-energy deposition in calorimetry, pulse-heights in trigger scintillator) in specified regions of the lego plot (where one envisages the products of the gamma-gamma collisions to lie), and no activity in the remainder of the lego plot, except possibly in the zero degree calorimeter. By "no activity" is meant no activity induced by primary particles from the collision. In practice, of course, one will define this in a more operational way as the absence of activity above noise thresholds, and with obvious backgrounds rejected.

Since the basic trigger is identical to a double-Pomeron-exchange trigger for pp collisions, it will evidently accept at this level all the double-Pomeron-exchange processes which occur for AA collisions. As we will discuss in detail below, the estimated total cross-section for the double-Pomeron exchange process is competitive with that of the signal. The estimates are not fully reliable, if for no other reason than that double-Pomeron exchange cross-sections for pp collisions are nearly nonexistent. In addition the question of how to extrapolate from low energies to the LHC energy scale is likewise very uncertain.

However, the situation is much better than this, because the bulk of this background process will be incoherent on the nucleus, unlike the $\gamma\gamma$ signal of interest. The typical recoil transverse momenta of the nucleons participating in the primary double-Pomeron-exchange collision will be hundreds of MeV and will in general lead to nuclear excitation. Thanks to the large Lorentz boost of the ions at the LHC, the decay products of such excitations carry a large amount of energy and will almost always be visible in the forward part of the FELIX detector. Evaporation neutrons will produce a well-defined 3 TeV signal in the zero-degree calorimeter (ZDC). Even a 10 MeV gamma ray will leave a 10 GeV electromagnetic shower in the forward calorimeter. Protons and pions from nuclear breakup will be swept into the forward tracking system of the FELIX detector. These and other such signatures, such as the very low total p_T of fully reconstructed final states, can be used offline to reject the incoherent Pomeron-induced processes. The actual efficiency which can eventually be achieved will depend on the details of the nuclear breakup and the forward geometry, and on performance parameters of the FELIX detector. (Beam-gas backgrounds are also a serious concern, but are beyond the scope of the considerations here.) Given the paucity of primary input data, it is premature to try to estimate the exact level of purity of the $\gamma\gamma$ signal which will be achieved.

Nevertheless, there will be a residual coherent 'background', involving both exchanged photons and Pomerons, that couples to the entire nuclei. This includes two-photon, photon-Pomeron and double-Pomeron interactions that can closely mimic the reactions of interest. These interactions will exhibit similar rapidity gaps and nuclear form-factor-imposed kinematic constraints. Consequently, they can only be separated from the signals of interest by conventional high energy physics analysis cuts, and by their distinctively different A and Z dependences.

In any case, it is undeniably very important to have a good estimate of the fraction of these double-Pomeron-exchange events for which the ion does not break up. Highly detailed estimates do not yet exist. But the probability that the recoil given to the nucleon is small enough that it can be absorbed coherently by the nucleus is arguably proportional to the ratio of the square of the proton size to the nuclear size, namely $\propto A^{-2/3}$ (per ion). In principle this gives nearly two orders of magnitude suppression of this background for the $CaCa$ collisions of greatest interest, and of course an even greater suppression for $PbPb$ collisions.

Further study, especially primary data on the systematics of double-Pomeron-exchange processes at collider energies, is needed to determine how serious these backgrounds will be. One promising source of information may be the program at RHIC, where there is interest in accessing this physics. There are already detailed studies under way by the STAR collaboration. Monte Carlo simulations of most of these background processes have been performed. Detailed numerical estimates of the backgrounds are not yet available. Although these studies correspond to a much lower beam energy, in a considerably less hermetic detector, it is found that selecting on a specific final state, with nothing else in the detector, together with cuts on the p_T of the produced hadron system, is sufficient to yield a good signal to noise ratio for a number of analyses of interest [136]. FELIX, being a full acceptance detector should have a much easier time than STAR, despite the increased beam energy, with correspondingly better signal to noise ratios. However, for the case of poorly defined final states, such as jets, the analysis may be much tougher, and the feasibility remains to be determined.

But no matter how this issue evolves, the full acceptance in the forward direction of FELIX is clearly of critical importance in the discrimination of the $\gamma\gamma$ signal from such strong-interaction diffractive backgrounds, making it a uniquely powerful instrument at the LHC for the investigation of this interesting class of processes. And as mentioned in the previous section, the backgrounds will also be classified and available for study; they contain very interesting physics as well.

The two photon processes themselves are also classified according to the nature of the excitation of the ion, if any, after the collision: incoherent, semi-coherent or coherent. In incoherent processes, the ion, as discussed above, is broken up. The semi-coherent processes are electromagnetic-dissociation processes, where one or both of the ions is excited by the Weizsacker-Williams Coulomb field of the other, for example into the giant dipole resonance. Coherent processes leave the nucleus in the ground state.

At the LHC, the secondary ion in a coherent process cannot be directly detected after the interaction, because its recoil is so small that it remains within the phase-space of the circulating beam. Therefore it is the rejection of generic forward activity which has to be the primary signature of the $\gamma\gamma$ process.

The squared four-momentum of each photon is small, as coherent emission from the whole nucleus limits its value to $q^2 < 1/R^2$, with R the radius of the nucleus. Both photons are therefore quasi-real. In the Weizsacker-Williams approximation the cross-section is expressed in the form [137]:

$$\frac{d\sigma_{AA\to AAX}}{dMdY} = \sigma_{\gamma\gamma\to X}(M^2)\cdot\frac{dL_{\gamma\gamma}}{dMdY}, \qquad (2.31)$$

where $\sigma_{\gamma\gamma\to X}(M^2)$ is the cross-section of X-system production in $\gamma\gamma$-collisions, M is the invariant mass of the $\gamma\gamma$-system, and Y its rapidity. The last factor, $dL_{\gamma\gamma}/dMdY$, is the differential effective $\gamma\gamma$-luminosity. It is proportional to the ion beam luminosity L_{AA} (as the photons are emitted coherently), to the fourth power of the ion charge Z^4 for symmetric collisions, and to $Z_1^2 Z_2^2$ for asymmetric collisions. Due to this coherence factor, heavy ion collisions are clearly more favorable for the study of two-photon processes. However the larger cross-section of electromagnetic processes in a heavy ion beam (for example, $\simeq 300$ barn in the case of Pb beams) reduces the lifetime of the heavy ion beams for very large Z. This favors the use of lighter ions, which yield a beam-luminosity larger than for the heaviest ions. Consequently, the highest two-photon luminosities are achieved with Ca beams [138].

The estimates of luminosity using the Weizsacker-Williams approximation may be questioned when the Z becomes as large as for lead. However the conclusion that $CaCa$ collisions is optimal does not depend upon this feature, and the relatively low value of Z for Ca should not lead to large corrections.

Another important variable is the average running time per year which is anticipated for the different ion species. Because pp collisions have an exposure time larger by an order of magnitude than for ions, they may also be of interest for two-photon physics. The expected ion luminosities, running times and beam energies for different ion species (cf. Section 4.2, page 102) are shown in Table 2.1.

2.4.3. Luminosities for $PbPb$, $CaCa$ and pp collisions

The effective $\gamma\gamma$ luminosity is a complicated function depending on the two-photon invariant mass, the beam energy and the type of ion one uses. When the two ions overlap, the strong interaction leads to a large number of forward-produced particles in the final state, and the two-photon processes in these collision will be totally lost. In the black disc approximation, we therefore have to exclude collisions with impact parameter $b < 2R$ (with R the ion radius).

In addition, if the final state is produced within one of the nuclei they can interact strongly, again making the detection of such an event as a two-photon process impossible. Therefore we must also restrict the individual impact parameters b_1, b_2 of the $\gamma\gamma$ system, relative to the ions, to be larger than R.

These restrictions lead to essential modifications of the effective $\gamma\gamma$ luminosity, compared with what is calculated for e^+e^- collisions [139]. These effects lead to an adiabatic cut-off of the photon energy spectrum, and therefore to a related cut-off of the luminosity at an invariant $\gamma\gamma$ mass

$$M_{\gamma\gamma}^{max} \simeq 2\gamma_A/R, \tag{2.32}$$

where $\gamma_A = \gamma_p Z/A$ is the Lorentz factor of the ions in the laboratory frame and $R \simeq r_0 A^{1/3}$, with $r_0 \simeq$ 1.2 fm. In the case of proton collisions we have taken as proton radius its charge rms value of 0.8 fm. Thus the accessible $\gamma\gamma$ mass range, $M \leq M_{\gamma\gamma}^{max}$, increases for the case of light ions and of protons, due to the favorable γ_A and R factors in comparison to heavy ions.

The effective $\gamma\gamma$-luminosity for different ion species can be expressed in terms of a universal function [140–142] $\xi(x)$:

$$dL_{\gamma\gamma}/dx = \frac{\alpha^2 Z^4}{\pi^2}\frac{16}{3x}\xi(x) \tag{2.33}$$

where x is the normalized $\gamma\gamma$-mass $x = M/M_{\gamma\gamma}^{max}$. Therefore we expect an extension of the accessible $\gamma\gamma$ mass range, for example, in $CaCa$ collisions by about a factor of two (i.e. up to $\sim$ 450 GeV) compared with that in $PbPb$ collisions, mainly due to the smaller radius of Ca ions. For pp collisions this reduction of the luminosity appears only at $M_{\gamma\gamma}^{max} = 4\ TeV$. The differential $\gamma\gamma$-luminosities versus two-photon mass for pp, $CaCa$ and $PbPb$ collisions, as well as for e^+e^- collisions at LEP 200, are shown in Fig. 2.26. These luminosities have been calculated for integrated luminosities of the primary ion collisions as quoted in Table 2.1. For e^+e^- collisions, an integrated luminosity of $\mathcal{L}T = 100$ pb^{-1} was used.

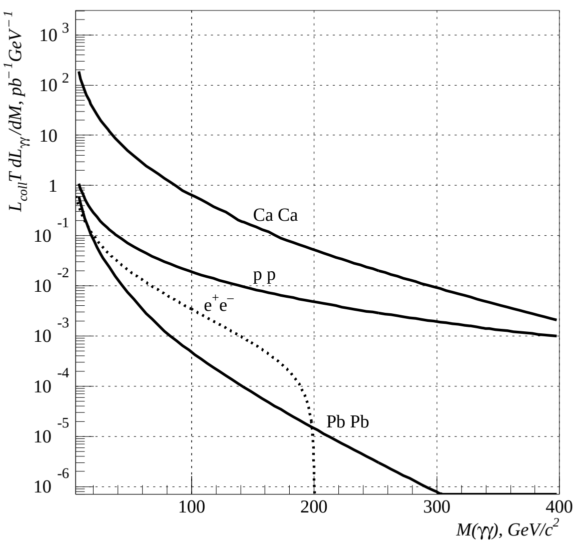

Figure 2.26. The differential $dL_{\gamma\gamma}/dM$ luminosities for different ion species at LHC and for e^+e^- at LEP 200 normalized for integrated luminosities of the primary collisions over the expected run times per year TL_{coll}, which are equal to $10^3\ pb^{-1}$, $4\ pb^{-1}$, $10^{-4}\ pb^{-1}$ and $100\ pb^{-1}$ for pp, CaCa, PbPb and e^+e^- collisions respectively.

It is clearly shown in Fig. 2.26 that $CaCa$ collisions are most favorable for two photon physics in heavy ion collisions. The effective $\gamma\gamma$ luminosity in $PbPb$ collisions is more than two orders of magnitude smaller than in $CaCa$ collisions. For LEP 200 the $\gamma\gamma$-luminosity per year is comparable to the estimated luminosity for $PbPb$ collisions, but extends only up to 200 GeV for the effective $\gamma\gamma$ masses.

At fixed values of the $\gamma\gamma$ mass M, the effective luminosity $dL_{\gamma\gamma}/dMdY$ is a Gaussian like function of the rapidity with mean value $Y_0 = 0$. As an example, in Fig. 2.27 the Y-dependence of the $\gamma\gamma$-luminosity is shown at several values of the $\gamma\gamma$-mass in the case of $PbPb$ collisions. A half-width of the

Table 2.1. Luminosities of ion collisions, for the FELIX run scenario.

Collision	Luminosity ($cm^{-2}s^{-1}$)	Bunch spacing (ns)	Run time ($s/year$)	CM Energy (TeV)
pp	$10^{29} - 10^{31}$	25	10^7	14
$PbPb$	10^{26}	$25, 125$	10^6	1148
$CaCa$	$4\ 10^{30}$	25	$10^5 - 10^6$	280
pPb	10^{30}	$25, 125$	10^5	126
pCa	10^{31}	25	10^5	63

Y-distributions can be roughly characterized by the value

$$Y_{\gamma\gamma}^{max} = \ln \frac{M_{\gamma\gamma}^{max}}{M}, \tag{2.34}$$

where $M_{\gamma\gamma}^{max}$ is defined by Eq. (2.32). Thus the rapidity interval increases with the Lorentz factor of the ions and decreases with the radius of the ions as well as logarithmically with the mass of the $\gamma\gamma$-system. In particular for $\gamma\gamma$-masses comparable with $M_{\gamma\gamma}^{max}$ the rapidity distribution is concentrated around zero values of the rapidity, see Fig. 2.27, and therefore heavy systems are produced in $\gamma\gamma$-collisions almost at rest in the laboratory frame. As

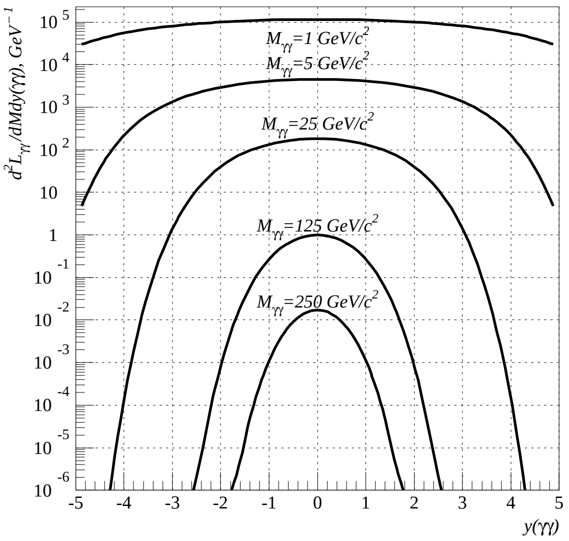

Figure 2.27. The differential $dL^2_{\gamma\gamma}/dMdY$ luminosities at $M = 1, 5, 25, 125, 250$ GeV for $PbPb$ collisions at LHC.

for the transverse momentum of the $\gamma\gamma$ system, its value is limited by the condition of photon virtuality, $q^2 < R^{-2}$. Therefore the maximum transverse momentum of a system produced in a coherent ion-ion collision is $p_T^{max} \approx \sqrt{2}R^{-1}$. But in most events the $\gamma\gamma$ system has a transverse momentum even smaller, of order [137].

$$p_T \ \sim \ M/\gamma_A, \tag{2.35}$$

Hence in a typical mass range, say $M < 100$ GeV, one has $p_T \sim 30$ MeV in $PbPb$-collisions and ~ 25 MeV in $CaCa$ collisions.

2.4.3.1. Luminosity monitoring

In the light of the inherent uncertainties in the luminosity estimates, it is clearly vital to have ways of checking the theoretical calculations of the luminosity by an appropriate $\gamma\gamma$ luminosity monitor. A good process for this purpose is the production of $\mu^+\mu^-$ pairs. The expected rates for $PbPb$, $CaCa$ and pp collisions in the FELIX geometry ($|\eta| > 2.25$) are shown in Fig. 2.28. From the figure one can see that during a standard one-month run the statistical accuracy which can be reached for this dimuon monitoring process is of the order of 1% in the mass range up to 10 GeV in $PbPb$ collisions and up to 50 GeV in $CaCa$ collisions.

The use of e^+e^- pair production for $\gamma\gamma$ luminosity monitoring does not substantially improve the statistical precision. There is also greater uncertainty in the accuracy of the theoretical calculations than in the dimuon case. Nevertheless the 5% statistical level in the precision of the $\gamma\gamma$ luminosity monitoring can be extended up to 130 GeV in $CaCa$ and up to 30 GeV in $PbPb$ collisions.

2.4.4. Cross-sections, rates, and triggers

2.4.4.1. Cross-sections

Events in ion collisions are classified according to the value of the impact parameter and the nature of the ion interaction:

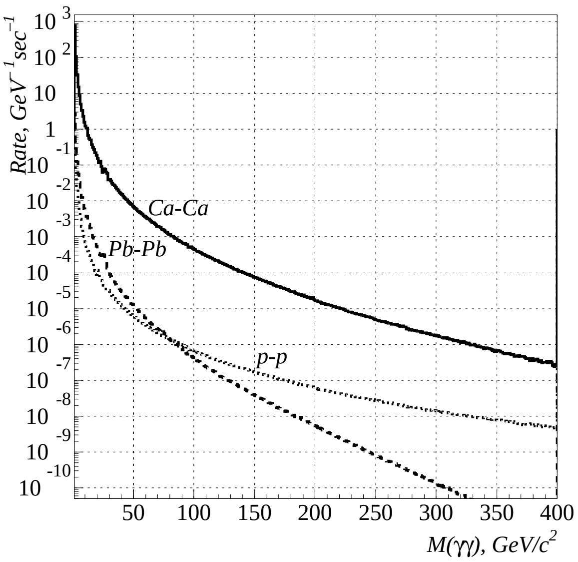

Figure 2.28. Detection rates of $\mu^+\mu^-$ pairs in $PbPb$, $CaCa$ and pp collisions at the LHC in the forward-backward geometry of FELIX.

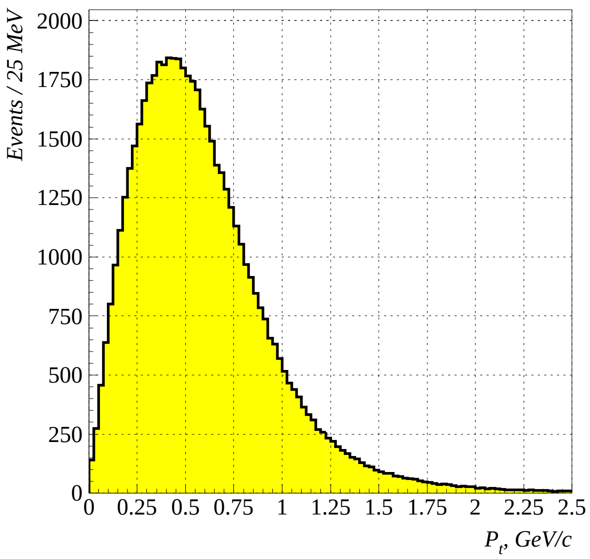

Figure 2.29. The P_t distribution of the system produced in central diffraction processes obtained with the PHOJET event generator [148].

- Strongly inelastic ion-ion interactions, occurring when the impact parameter of the ions b is less than the sum of ion radii, $b < R_1 + R_2$.
- Diffractive interactions in "grazing" ion collisions, when $b \sim R_1 + R_2$. The strong interactions between the ions are in this case mainly caused by single and double Pomeron exchange at the LHC energy scale.
- Peripheral interaction of the ions, when $b > R_1 + R_2$.

The first class can be excluded by FELIX by requiring both ions to remain (almost) intact. The processes of interest are two-photon, photon-Pomeron and double Pomeron processes. As already discussed above, the momentum transfer in the Pomeron interactions is much larger than in the photon interactions. Therefore the requirement that the ions not break up strongly suppresses the double Pomeron contribution in coherent collisions of heavy ions. Nevertheless, as already emphasized above, this contribution is not demonstrably negligible, and is not under good theoretical control.

The cross-section of the strong, inelastic interaction of ions is reasonably described in the framework of a hard-sphere overlapping model [143]. For collisions of identical ions

$$\sigma_{nucl} = \sigma_0 \; (2A^{1/3} - \Delta R)^2, \tag{2.36}$$

where $\sigma_0 \simeq 70\ mb$, A is the ion mass number and $\Delta R = 1.3$. For more accurate cross-section calculations, the semiclassical optical model [144] or the Gribov-Glauber model [145] can be used.

For the cross-sections for double-Pomeron processes, which are actually peripheral nuclear interactions, simple geometrical considerations suggest a scaling with the ion radius $\sim A^{1/3}$. In the context of simple single-Pomeron-exchange phenomenology [146], the differential cross-section of hadron production in the double Pomeron processes can be roughly estimated:

$$\frac{d\sigma_{DP}}{dm_X^2} = \frac{\sigma_{DP}}{m_X^2}\;(A^{1/3} + \delta) ln \frac{s_{NN}}{(m_X m_N R)^2} \tag{2.37}$$

where $\sigma_{DP} = 1.3\ \mu b$, m_X is the effective mass of the hadron system in the central rapidity region, $\sqrt{s_{NN}}$ is the CM energy in the corresponding nucleon collisions, m_N is the nucleon mass, $R = r_0 A^{1/3}$ is the ion radius, and $\delta = 1.5a/r_0$ is connected with the width of the nuclear surface. After integration of Eq. (2.37) over dm_X in a range up to $m_X^{max} = \sqrt{s_{NN}}/m_N R$, the total cross-section of the double Pomeron processes can be estimated. The results are shown in Table 2.2 as the cross-section of the reaction $AA \to AAX(DP)$. A more refined description of the double-Pomeron as well as Pomeron-photon processes can be performed in the framework of the two-component Dual Parton

Model (DPM), cf. for example [147]. The corresponding cross-sections of central diffractive (mainly double Pomeron) processes obtained with the PHOJET event generator [148] are shown in Table 2.2, reaction $AA \rightarrow \tilde{A}\tilde{A}\ X(CD)$. But the PHOJET generator does not distinguish the final states of the colliding ions. Therefore the generated processes combine the coherent diffractive interactions of the ions (i.e. when the ions after interaction are intact) with excitation and even full disintegration of the ions. Note again that the average transverse momentum of the hadron system in the central rapidity region is of the order of 450 MeV (cf. Fig. 2.29), which is an order of magnitude higher than that in two photon processes(Eq. 2.35). This feature can help to distinguish the two processes whenever the final state produced by the photons is fully reconstructed. The cross-sections for the coherent two photon processes can be obtained by folding the effective $\gamma\gamma$ luminosities in the Weizsacker-Williams approximation with the corresponding cross-sections for the two photon interactions, as expressed in Eq. (2.31). In particular, for an estimation of the total cross-section of $\gamma\gamma$ processes we have used the parametrization of Schuler and Sjostrand:

$$\sigma_{\gamma\gamma}^{tot}(s) \ \simeq \ 211\ (s/s_0)^{\epsilon} + 297\ (s/s_0)^{-\eta}\ \ nb, \qquad (2.38)$$

where, $\epsilon \simeq 0.0808$, $\eta \simeq 0.4525$ and $s_0 = 1\ GeV^2$ [149].

The pure electromagnetic processes of e^+e^- and $\mu^+\mu^-$ pair production are needed for luminosity monitoring. The cross-section for low-mass e^+e^- pair production can be estimated according to the approximate formula [150]:

$$\sigma_{e^+e^-} = \frac{28}{27\pi}\frac{(Z\alpha)^4}{m_e^2} ln^3\gamma_A, \qquad (2.39)$$

where m_e is the electron mass and γ_A is the Lorentz factor of the ions in the laboratory frame. A highly accurate determination will take a lot of work, due to nontrivial coherent effects in nuclei, which are sensitive to the multiple scattering of the pair as it traverses the nuclear matter. However, these effects are far less important for the $\mu^+\mu^-$ process.

The probability of ion excitation in two-photon processes has been studied recently in a semiclassical impact parameter approach [139]. Particularly important is the excitation of the Giant Dipole Resonance (GDR). The probability of ion excitation as a function of the impact parameter of the collision can be approximately expressed in the form [139]:

$$P_{GDR}(b) = 1 - exp\ (-\frac{3\alpha Z^2}{16\pi^2 b^2}\frac{(A-Z)Z}{A^{2/3}}\ mb). \qquad (2.40)$$

Similarly the total probability for the electromagnetic dissociation of the ion, including the GDR, has been given for $PbPb$ collisions as [151]

$$P_{Dis}(b) = 1 - \exp\ (-\frac{303\ fm^2}{b^2}) \qquad (2.41)$$

The probability of the GDR excitation is about 40% per Pb ion, and about 1% per Ca ion, at an impact parameter of $b = 2R$. As each of the ions can be excited, the excitation probability for at least one ion is about 65% and about 2% for $PbPb$ and $CaCa$ collisions respectively.

The electromagnetic dissociation of ions in the one photon processes are also subdivided into excitation into the GDR and into electromagnetic dissociation above the GDR excitation. The cross-section for ion dissociation at the GDR can be estimated [138,139] as:

$$\sigma_{GDR} \simeq 67.5\frac{(A-Z)Z^3}{A^{2/3}}\ \mu b, \qquad (2.42)$$

The cross-section of the ion electromagnetic dissociation above the GDR can be approximated by the formula [138,139]:

$$\sigma_{ED} \simeq 108\ A^{0.9}\ Z^2\ \mu b. \qquad (2.43)$$

The cross-sections of all these processes as well as the expected event rates are shown in Table 2.2 for $PbPb$, $CaCa$ and pp collisions.

2.4.4.2. Rates

We have already noted that the cross-section for hadroproduction by two photons is only a small fraction of the inelastic ion-ion hadroproduction cross-section; cf. Table 2.2. In the case of $PbPb$ collisions the cross-section ratio of $\gamma\gamma$ to nuclear interactions is of the order of 2%, whereas this ratio falls to 5×10^{-3} in $CaCa$ and to 2×10^{-7} in pp collisions ($W_{\gamma\gamma} > 1$ GeV). Most of this background is easily rejected, the remaining double-Pomeron-exchange piece being the most serious remnant.

The semicoherent, electromagnetic-dissociation processes lead to excitation of ions. Especially important is the Giant Dipole Resonance excitation, which leads to the emission of a soft neutron in the ion rest frame [141]. In the laboratory frame the emitted neutron will have an energy of about 3 TeV (due to the Lorentz factor of the excited ion) and will strike the zero degree calorimeter, providing a very clean signature of the GDR excitation. In $PbPb$ collisions the electromagnetic-dissociation cross-section is large, $\sigma_\gamma = 230$ barn, even compared with that of the nuclear ion interaction ($\sigma_{nucl} = 7.8$ barn). In the case of $CaCa$ collisions this cross-section, $\simeq$2 barn, is almost the same as the nuclear

Table 2.2. Cross-sections ($M_X > M_{cut}$) and event rates of the main processes in $PbPb$, $CaCa$ and pp collisions with luminosities 10^{26}, 4×10^{30} and 10^{32} cm^{-2}sec^{-1} respectively.

Reaction	$M_{\rm cut}$ GeV	PbPb-collision σ, b	PbPb-collision rate, Hz	CaCa-collision σ, b	CaCa-collision rate, Hz	pp-collision σ, b	pp-collision rate, Hz
$AA \to X$ (Nuclear)	–	7.8	7.8 10^2	2.1	8.4 10^6	0.1	1.0 10^7
$AA \to AA\ X$ (DP)	–	1.0 10^{-3}	0.1	0.8 10^{-3}	3.2 10^3	0.5 10^{-3}	5.0 10^4
$AA \to \tilde{A}\tilde{A}\ X$ (CD)	2.0	7.3 10^{-3}	0.7	5.1 10^{-3}	2.0 10^4	1.0 10^{-3}	1.0 10^5
$AA \to AA\ X$ (CD)[1)]	2.0	4.7 10^{-5}	4.7 10^{-3}	3.3 10^{-5}	1.3 10^2	6.5 10^{-6}	6.5 10^2
$AA \to AA^*_{GDR}$	–	130	1.3 10^4	0.9	3.6 10^6	–	–
$AA \to AA^*_{ED}$	–	90	0.9 10^4	1.2	4.8 10^6	–	–
$AA \to AA\ e^+e^-$	–	2.3 10^5	2.3 10^7	800	3.2 10^9	6.3 10^{-3}	6.3 10^5
$AA \to AA\ e^+e^-$	1.0	0.5	0.5 10^2	2.8 10^{-3}	1.1 10^4	5.0 10^{-8}	5
$AA \to AA\ \mu^+\mu^-$	–	2.2	2.2 10^2	1.2 10^{-2}	4.8 10^4	1.3 10^{-7}	13
$AA \to AA\ \mu^+\mu^-$	1.0	0.15	15	8.0 10^{-4}	3.2 10^3	1.4 10^{-8}	1.4
$AA \to AA\ \gamma\gamma \to X$	2.0	0.03	3	6.0 10^{-4}	2.4 10^3	1.3 10^{-8}	1.3
$AA \to AA^*_{GDR}\gamma\gamma \to X$	2.0	0.05	5	1.2 10^{-5}	4.8 10^2	–	–

[1)] $p_T(X) < 50$ MeV/c

cross-section, see Table 2.2. Thus we can expect important contributions from these processes in the zero degree calorimeters. The corresponding event rates are shown in Table 2.2.

As shown in Table 2.2, the inclusive cross-section for e^+e^- pair production in heavy ion collisions is huge ($2.3\cdot10^5$ barn in $PbPb$ and 800 barn in $CaCa$). It is so large that for central collisions the probability of pair emission per event is large compared to unity. A significant fraction of the electrons and positrons are emitted in the forward and backward directions. Although most of the produced pairs have very small mass, $m_{e^+e^-} \sim 3m_e$, and very small energies, the cross-section for production of energetic electrons, say greater than several GeV, is not small. Direct calculations [152] give the numbers shown in Table 2.3. These events produce an intense background mainly for the UA1 electromagnetic calorimeters. However, because the pairs are swept overwhelmingly into the bending plane of the detector (actually a bending surface), they will occupy at worst only a very small portion of the acceptance.

Table 2.3. Cross-sections and event rates for e^+e^- pair production when both electron and positron, have energy higher than a given threshold, E_{thr}, for $PbPb$ and $CaCa$ collisions with luminosities 10^{26} and 4×10^{30} $cm^{-2}sec^{-1}$ respectively.

E_{thr} GeV	$\sigma(AA \to AA + e^+e^-)$ $PbPb$	$\sigma(AA \to AA + e^+e^-)$ $CaCa$	Event rate, MHz $PbPb$	Event rate, MHz $CaCa$
0.25	3.5 kb	12 b	.35	48.
0.50	1.5 kb	5.5 b	.15	22.
1.0	0.5 kb	1.8 b	.05	7.2
2.5	0.08 kb	0.3 b	.008	1.2
5.0	0.03 kb	0.1 b	.003	0.4

2.4.4.3. Triggers

As mentioned in Section 2.4.2, the basic triggers for the $\gamma\gamma$ processes are essentially the same as for the double-Pomeron-exchange processes in pp collisions, and are based on the pattern of activity in all of phase space seen by FELIX. It is anticipated that the detailed trigger thresholds in the various phase-space regions and the correlations between them for an effective $\gamma\gamma$ trigger is "programmable", so that no separate discussion is needed here; cf. Chapter 9. The development of these detailed trigger strategies will be mostly driven by the program of diffractive, rapidity-gap physics in pp collisions, likely to precede in time high-luminosity $CaCa$ running.

Examination of Table 2.3 shows that the rate of double-Pomeron plus $\gamma\gamma$ events in $CaCa$ collisions approaches 10 kHz at design luminosity. This is probably one to two orders of magnitude higher than what will be written to tape, so additional rejection will be needed. For spectroscopy, one can tighten the pattern requirements, so that the produced low mass system is directed toward the rapidity region of interest for the detailed analysis, say $2 < \eta < 6$, with rapidity gaps required elsewhere in the phase space. For the diffractive photoproduction channels there will be an extra rapidity gap which can be put into the pattern trigger. And of course the design run would be preceded by an early "minimum bias" run at lower luminosity, where these refinements need not even be considered. In all cases it will be in offline analysis, not in the trigger, where the problems of separating the double-Pomeron, diffractive-photoproduction, and true $\gamma\gamma$ processes must be faced.

2.4.5. Basic QCD phenomena

2.4.5.1. The $\gamma\gamma$ total cross-section and event structure

Minimum-bias event rates in two photon processes are high enough to study soft and semihard interactions of photons at $\gamma\gamma$ cms energies up to 450 (200) GeV in $CaCa$ ($PbPb$) collisions. This is 4 (2) times larger than the energy range accessible at LEP 200 (cf. Table 2.2).

The energy dependence of the $\gamma\gamma$ total cross-section is of special interest, inasmuch as the hadronic composition of a real, energetic photon contains, in addition to a soft "vector-dominant" hadronic portion (60%-80%), a more-or-less point-like $q\bar{q}$ piece which acts as a relatively small color dipole. Therefore the energy dependence may contain a component which has the rapid rise characteristic of the BFKL dynamics discussed in Section 2.1.1.2. In photoproduction there is no evidence of such a rise, but there could be an enhancement in $\gamma\gamma$ collisions due to the occasional presence, with $\sim 10\%$ probability, of two small dipoles in the initial-state configuration.

To measure the total cross-section, it is very advantageous to have large enough acceptance to see the entire final state and the rapidity gaps beyond. The final state structure in $\gamma\gamma$ collisions is like generic hadron-hadron collisions at comparable cms energy W; the energy flow in the final state is mainly in the forward and backward directions. In the experiments at LEP 200, much information about two photon events disappears down the beam directions [154]; 30% to 50% of the hadronic energy is lost in the forward-backward directions.

The measurement accuracy of the total hadron cross-section in two photon processes at LEP is not so much limited by event statistics as by the need for a precise description of competing reactions such as beam-gas or beam-wall scattering, annihilation reactions etc. [154]. This is probably not the problem for FELIX, nor is statistical accuracy or efficiency in detection of the $\gamma\gamma$ processes. Instead, the accurate determination of coherent-photoproduction and double-Pomeron-exchange contaminations may be the most important limitation. As discussed in previous subsections, this limitation is very difficult to assess at present.

2.4.5.2. Exclusive vector-meson pair production

The study of exclusive vector-meson pair production in two photon processes allows the study of Pomeron-exchange factorization relations at high energies, and to study various color-coherent phenomena. Given the assumption that single Pomeron exchange dominates these two-body processes, factorization relations [84] among total cross-sections for pp, γp and $\gamma\gamma$ collisions are predicted

$$\sigma_{tot}(\gamma p)^2 = \sigma_{tot}(pp)\ \sigma_{tot}(\gamma\gamma), \tag{2.44}$$

as well as among the differential cross-sections:

$$\frac{d\sigma(\gamma\ p \to V_1\ p)}{dt}\frac{d\sigma(\gamma\ p \to V_2\ p)}{dt} = \frac{d\sigma(\gamma\gamma \to V_1\ V_2)}{dt}\frac{d\sigma(pp \to pp)}{dt}, \tag{2.45}$$

$$\frac{d\sigma(\gamma\gamma \to V_1\ V_1)}{dt}\frac{d\sigma(\gamma\gamma \to V_2\ V_2)}{dt} = \frac{d\sigma(\gamma\gamma \to V_1\ V_2)}{dt}^2. \tag{2.46}$$

Perturbative-QCD predicts that the energy dependence of the cross-sections for vector mesons built of light quarks: $V_1, V_2 = \rho, \omega, \phi$ should be close to that for soft QCD two-body processes, while the energy dependence of the cross-sections for the combined production of V_1 and hidden heavy-flavor V_2 like J/ψ or Υ (and their excited states) should be proportional to the square of the gluon distribution in V_1, i.e. to be as strong as what is observed at HERA for the photoproduction of J/ψ. The cross-section for the production of two hidden charm or beauty vector mesons would resemble onium-onium scattering. As discussed in Sections 2.1.1.2, page 9, and 2.1.1.6, page 11, the BFKL dynamics may well apply in this case, leading to a large enhancement for production of such onium states compared to the expectations of Eqs. (2.44-2.46). In particular, estimates [155] indicate that Eq.(2.45) may underestimate the cross-section for the of $J/\psi + J/\psi$ channel by a factor $\sim 10^2$ for $W \sim 100$ GeV. In addition, it is not evident that the shrinking with energy of the diffraction peak will be the same for photoproduction of J/ψ and Υ than, say, for the ρ meson, since in the BFKL limit very little shrinkage is expected.

The $\gamma\gamma \to V_1V_2$ cross-sections have been calculated from Eq. (2.46) on the basis of data for vector meson photoproduction at HERA and for pp elastic scattering. The differential cross-sections $d\sigma(\gamma\gamma \to V_1V_2)/dt$ can be parameterized in the form:

$$\frac{d\sigma}{dt}(\gamma\gamma \to V_1V_2) = A_{V_1V_2} \left(\frac{W}{W_0}\right)^{C_{V_1V_2}} \exp\left(tB_{V_1V_2} + 4t\alpha'_{V_1V_2} \ln\frac{W}{W_0}\right), \tag{2.47}$$

where t is the squared transfer momentum in the reaction $\gamma\gamma \to V_1V_2$, W is the effective mass of the vector pair, and $W_0 = 50$ GeV. Other cross-section parameters and cross-sections, at a 2-photon mass $W > 20$ GeV, are shown in Table 2.4.

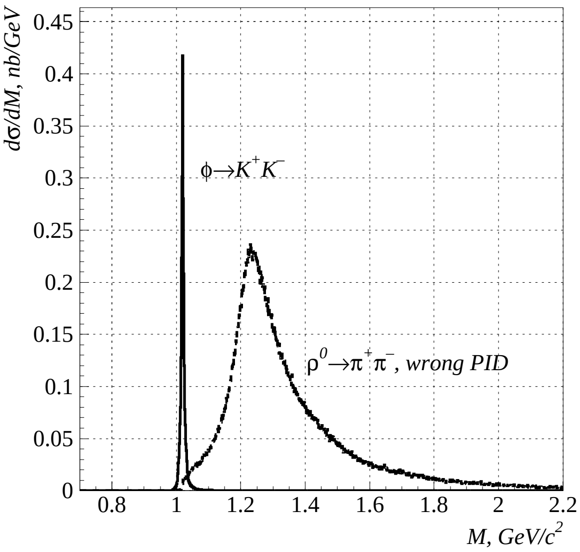

Figure 2.30. Mass spectrum of K^+K^- systems of detected process $\gamma\gamma \to \omega\phi \to 3\gamma K^+K^-$ and $\pi^+\pi^-$ system of detected process $\gamma\gamma \to \omega\rho^0 \to 3\gamma\pi^+\pi^-$, if pions are misidentified as kaons.

As typical examples we consider below the detection of several specific V_1V_2 channels, including ω and J/ψ production in combination with ρ, ω and ϕ mesons detected in the forward and backward portions of the FELIX detector. For the ω identification we use its 3γ decay, i.e. $\omega \to \pi^0\gamma \to 3\gamma$, which can be effectively detected and triggered by the electromagnetic calorimeters. For detection of the J/ψ we use its decays into lepton pairs: e^+e^- and $\mu^+\mu^-$. Both decay channels can be triggered by the electromagnetic calorimeters or muon chambers. The

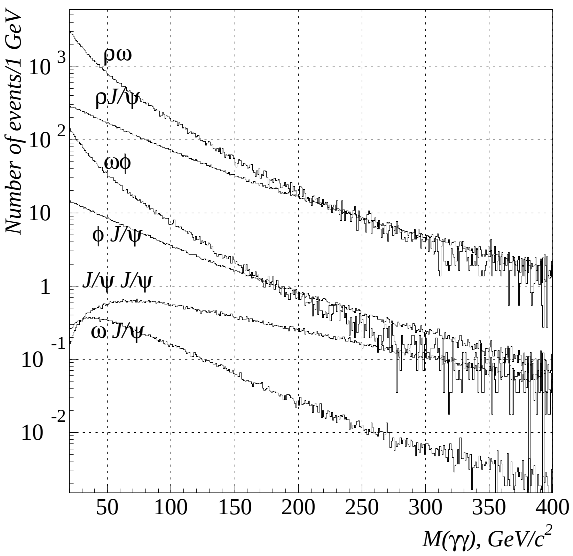

Figure 2.31. Mass spectrum of the detected $\gamma\gamma \to V_1V_2$ events during 10^6 *sec* run with $CaCa$ in the FELIX geometry. The branching ratios of the decays, $\omega \to \pi^0\gamma$, $\phi \to K^+K^-$, $J/\Psi \to e^+e^-$ are taken into account.

$\phi \to K^+K^-$ decay may be detected without identification of charged kaons if there is only one unidentified hadron pair in an event (Fig.2.30). In Fig.2.31 the V_1V_2 mass distributions expected for the $\gamma\gamma \to V_1V_2$ events are shown for $CaCa$ collisions, for several choices for the produced vector mesons. The detection efficiencies in the forward/backward geometry, as well as branching ratios of the vector meson decays ($\omega \to \pi^0\gamma$, $\phi \to K^+K^-$, $J/\psi \to e^+e^-$), have been taken into account.

The number of events expected in $PbPb$ collisions is marginal for studies of the $\rho\omega$, $\omega\phi$, ρ J/ψ (and therefore $\rho\rho$ and $\rho\phi$) systems. As one can see from Fig. 2.31, in $CaCa$ collisions the mass range for these processes up to 150 GeV is attainable, due to the higher $\gamma\gamma$-luminosity. The detection efficiency for the ω J/ψ and $\omega\omega$ systems can probably be improved by using the 3π decay of the ω. A study of the $\phi\phi$ system in its $2K^+2K^-$ decay mode may be performed if identification of charged kaons exists in the FELIX detector. But a study of ϕ J/ψ and say J/ψ J/ψ is not possible with FELIX if the above factorization estimates hold. However, if the BFKL dynamics is valid, there will be a chance to observe these processes.

Table 2.4. Parametrization of $\gamma\gamma \to V_1V_2$ cross-sections and corresponding cross-sections of the meson pair production in two photon processes of ion collisions at $M_{\gamma\gamma} > 20$ GeV.

Meson pair	$A_{V_1V_2}$ nb	$B_{V_1V_2}$ $(GeV/c)^{-2}$	$C_{V_1V_2}$	$\alpha'_{V_1V_2}$ $(GeV/c)^{-2}$	$\sigma_{tot}(AA \to AA_{\gamma\gamma\to V_1V_2})$	
					$PbPb$, μb	$CaCa$, nb
$\rho\rho$	150	6	0.22	0.25	230	3.2 10^3
$\rho\omega$	33	6	0.22	0.25	51	700
$\rho\phi$	17	4	0.22	0.25	41	560
$\omega\phi$	1.9	4	0.22	0.25	4.5	62
$\phi\phi$	0.5	2	0.22	0.25	2.1	30
$\rho\ J/\psi$	1.1	2.5	0.80	0.0	3.0	47
$\omega\ J/\psi$	1.3 10^{-1}	2.5	0.80	0.0	0.35	5.6
$\phi\ J/\psi$	6.8 10^{-2}	1.5	0.80	0.0	0.3	4.9
$J/\psi\ J/\psi$	3.1 10^{-4}	1.5	1.38	0.0	1.2 10^{-3}	0.02
$J/\psi\ J/\psi^{*)}$	$0.16/\ln(W/M_\psi)$	1.5	2.00	0.0	0.2	4.6

$^{*)}$ BFKL approximation

2.4.5.3. Diffractive photoproduction of heavy quarkonia

Diffractive vector meson photoproduction is a valuable window on the interface between perturbative QCD and hadronic physics. While elastic processes are commonly described through non-perturbative, phenomenological methods, hard exclusive photoproduction of heavy mesons is calculable in perturbative QCD. It has been shown [156] that the cross-sections of hard diffractive processes off a hadronic target are proportional to the square of the gluon distribution in the nucleon. The x at which the gluon density is probed is given by $x \approx m_V^2/W^2$ where m_V is the mass of the vector meson and W denotes the invariant mass of the photon-nucleon system. Initial HERA data on photoproduction of J/ψ mesons [157] confirms the rapid increase of the cross-section with energy W, predicted by perturbative QCD.

At FELIX, hard diffractive vector meson photoproduction can be investigated especially well in AA collisions. In comparison to previous experiments, the very large photon luminosity should allow observation of processes with quite small γp cross-sections, such as Υ photoproduction. Measurements to much higher energies than available up to now will also be possible. At HERA, for example, diffractive J/ψ photoproduction has been measured up to $W \sim 160$ GeV), while with FELIX this should be possible up to $W \sim 1$ TeV. The cross-section for diffractive J/ψ and Υ production has been estimated using the color dipole formalism [158]. The cross-sections for diffractive photon-nucleon scattering are folded with the photon flux calculated in the quasi-classical approximation, and the shadowing effects are calculated within the Gribov-Glauber approximation [145]. In Figs. 2.32, 2.33 the expected differential cross-sections $d\sigma/dW$ for exclusive production of J/ψ and Υ mesons are shown. The calculations have been done for $W > 20$ GeV, and a pseudorapidity of the mesons of $|\eta| < 4$. This ensures that the beam remnants are well separated from the diffractively produced mesons. In Table 2.5 the integrated cross-sections are given for several W-cuts.

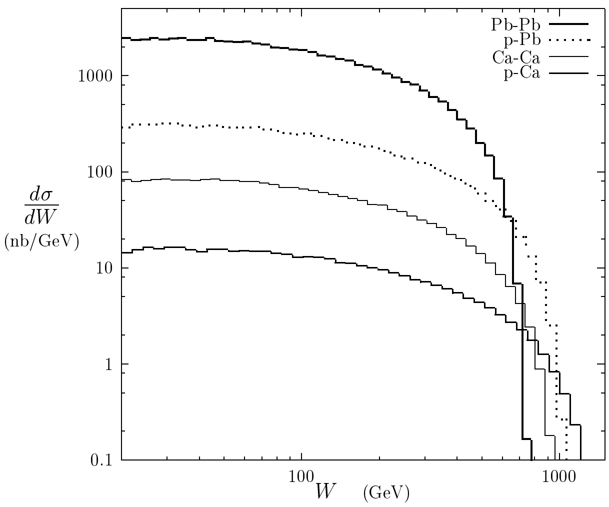

Figure 2.32. Differential cross-section for exclusive diffractive J/Ψ production in photon-pomeron collisions.

The efficiencies of J/ψ and Υ detection in the

Table 2.5. Cross-sections for exclusive diffractive photoproduction of vector mesons in various pA and AA collisions at the LHC.

Meson / Energy	σ_{pCa}, nb	σ_{CaCa}, nb	σ_{pPb}, nb	σ_{PbPb}, nb
J/ψ ($W >$ 20 GeV)	5400	21 10^3	67 10^3	400 10^3
J/ψ ($W >$ 200 GeV)	3100	10 10^3	33 10^3	150 10^3
J/ψ ($W >$ 500 GeV)	1100	2.2 10^3	9 10^3	16 10^3
Υ ($W >$ 20 GeV)	4.9	17	55	280
Υ ($W >$ 200 GeV)	3.8	11	37	150
Υ ($W >$ 500 GeV)	1.7	3.3	12	20

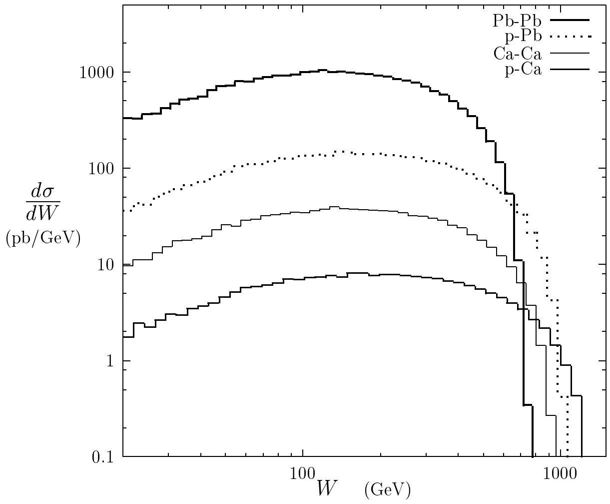

Figure 2.33. Differential cross-section for exclusive diffractive Υ production in photon-Pomeron collisions.

e^+e^- and $\mu^+\mu^-$ decay modes are almost zero in the rapidity interval $|Y| < 1.5$. Beyond this range the efficiencies become large. During a 10^6 sec run we expect the detection of 3×10^6 and 800 J/ψ in the e^+e^- decay mode for $CaCa$ and $PbPb$ runs respectively. For Υ we expect the detection of 600 events in $CaCa$ collisions in the same decay channel, while the event number in the $PbPb$ run is negligible. The differential cross-section of the J/ψ photoproduction can be measured up to $W = 1000$ GeV with a statistical accuracy better than 3%, whereas the cross-section of the Υ production can be measured up to $W = 800$ GeV with a 20% accuracy if the two leptonic decay modes (e^+e^- and $\mu^+\mu^-$) are combined.

2.4.6. Hadron spectroscopy

2.4.6.1. Light quark spectroscopy

In the overview it was stressed that photon-photon collisions provide an independent view of the QCD world of meson and baryon spectroscopy. The states which are produced resonantly in the s-channel will have $C = +1$, opposite to what is obtained from e^+e^- annihilation reactions. This in turn leads to quite distinctive features of the systematics. In particular,

- There will be a characteristic flavor dependence for the production of the various states comprising a $q\bar{q}$ nonet with ideal mixing:

$$\Gamma_{\gamma\gamma}(\frac{(u\bar{u} + d\bar{d})}{\sqrt{2}} : \frac{(u\bar{u} - d\bar{d})}{\sqrt{2}} : s\bar{s}) = 25 : 9 : 2$$

  So the relative widths, as given above, establish the pattern of flavor mixing. The question of which J^{PC} nonets are ideally flavor-mixed (like ρ, ω, and ϕ, or a_2, f_2, f_2' for the 2^{++} nonet), and which are not (like the 0^{-+} nonet), is critical to the understanding of the nature of the dynamics of flavor mixing. A systematics is needed, but at present little is known. The $\gamma\gamma$ reaction provides unique information.

- The J^{PC} dependence of the production ratios is also an important characteristic. Within a ^3L_J multiplet, one has in a nonrelativistic approximation

$$\Gamma(^3P_2 :^3 P_1 :^3 P_0) = 1 : 0 : 15/4 \qquad (2.48)$$

  whereas as $m_q \to 0$, $\Gamma(^3P_0) \to 0$. The $\Gamma_{\gamma\gamma}(^3P_2)$ width is known; determining the remaining $\Gamma(^3P_J))$ will provide new insight on the enigma of how to relate the small, partonic current-quark masses to the constituent-quark masses of spectroscopy. For example, is $\Gamma(^3P_0) > \Gamma(^3P_2)$, as the constituent-mass limit implies, or is it the other way around, as implied in the current-quark limit?

Relations similar to Eq. 2.48 exist for the higher multiplets, and enable, for example, separation of the 2^{++} radial excitation of the $^3P_2(1270)$, expected at ~ 1800 MeV, from the $^3F_2$ state expected to lie in the same mass region [159]. The $^3P_2$ is predicted to be entirely produced in $\gamma\gamma$ collisions in the $J_z = 2$ substate . This is an exact selection rule nonrelativistically, and should be tested in $\gamma\gamma \to \chi_c$ or χ_b; it is still robust when relativistic corrections are included [160]. It is also good empirically for $f_2(1270) \to \gamma\gamma$. In contrast, a $^3F_2$ is predicted to have a $\gamma\gamma$ width from $J_z = 0$ roughly 1/3 to 1/2 of that from $J_z = 2$. So observation of a significant $J_z = 0$ contribution for a 2^{++} around 1800 MeV, say, can help to distinguish the $^3F_2$ from the radial excitation of $f_2(1270)$, $^3P_2$. (These remarks are also true for the $b\bar{b}$ system, where the radial $^3P(\chi_2)$ and the $^1F(\chi_2)$ are possibly below $B\bar{B}$ threshold.)

The general conclusion from this particular example is that the $\gamma\gamma$ process provides powerful information on both the flavor *and* the spin/angular-momentum internal structure of hadrons.

The $^3P_0$ states are pivotal also, because the lightest glueball is predicted to be $\cong 1.6$ GeV, which is in the vicinity of the $^3P_0$ nonet. Hence mixing will occur [161,162], with the $f_0(1370)$, $f_0(1500)$, and $f_{(J=0?)}(1710)$ as the physical states of interest. The couplings to the $\gamma\gamma$ system can disentangle the pattern of the 0^{++} states and clarify the role of $f_0(1500)$ and $f_{(J=0?)}(1710)$ in the glueball-$q\bar{q}$ mixing. There is much attention paid to this question at present, because lattice QCD predicts $M \cong 1.6 \pm 0.1$ GeV for the 0^{++} glueball mass in the quenched approximation. The implications for $\gamma\gamma$ processes [163] is that $\gamma\gamma \to \pi^+\pi^-$ or $\pi^0\pi^0$ should give $f_0(1370)$ with $\Gamma(\gamma\gamma) \cong 3 - 5$ KeV, while $f_0(1500)$ is predicted to have $\Gamma(\gamma\gamma) \cong 0.05 - 0.3$ KeV [160]. The Aleph collaboration is searching for this state, and they are already at an interesting level of sensitivity [164].

The $f_J(1710)$ may be accessed best in $\gamma\gamma \to K\bar{K}$, or in $\eta\eta$, as its $q\bar{q}$ content is expected to be dominantly $s\bar{s}$. The 4π state in $\gamma\gamma$ collisions is also good for accessing the $f_0(1370)$ and $f_0(1500)$. The $\eta\eta$, $\eta\eta'$, and $\eta'\eta'$ states are also very nice "strategic" channels and, with good endwall calorimetry in FELIX, may well be very accessible. The $\gamma\gamma$ system obviously couples preferentially to charged constituents, while it is believed that the η and η' couple strongly to glueballs. It would therefore be interesting to see what the spectrum of states looks like in these channels; it would sensitively probe the mixing structure between $q\bar{q}$ channels and gg channels.

The $f_0(980)$ and $a_0(980)$ states remain enigmatic. These states couple strongly to $K\bar{K}$, even though they are near or even below $K\bar{K}$ threshold. Are they $K\bar{K}$ bound states [165] or $q\bar{q}$ states shifted by couplings to hadronic channels [166], or multiquark states? If they are $K\bar{K}$ "molecules", one expects [167]

$$\Gamma(f_0, a_0 \to \gamma\gamma) \cong 0.6\ KeV \tag{2.49}$$

In contrast, $q\bar{q}$ states at this mass would be expected to have widths (computed by using $f_2 \to \gamma\gamma$ as input)

$$\begin{aligned} \Gamma(f_0 \to \gamma\gamma) &\cong 2.5\ KeV \\ \Gamma(a_0 \to \gamma\gamma) &\cong 1.0\ KeV. \end{aligned} \tag{2.50}$$

These numbers are driven by the 25:9 ratio for $(u\bar{u} + d\bar{d})$:$(u\bar{u} - d\bar{d})$ in relative size–assuming this flavor content by the similarity in the f_0:a_0 masses.

Experimental widths appear quite small for these channels; they each have a central value of 0.25 KeV with 30 -40% error ranges. This suggests that the $\gamma\gamma$ coupling is driven by $K\bar{K}$, although with the large errors, one cannot yet rule out a 25:9 ratio favoring the f_0 over the a_0.

2.4.6.2. Double Pomeron exchange in *pp* collisions: opportunities for spectroscopy

Double-Pomeron-exchange processes in *pp* collisions, leading to low to moderate masses, are an important potential resource for spectroscopy. These processes have been considered in this subsection as a possibly annoying background for the $\gamma\gamma$ physics. And it is certainly the case that they are best studied in *pp* collisions, where one has the information on the momentum transferred to the leading protons, positively detected in the FELIX Roman-pot system.

The discussion in Section 2.2.2.6 of spectroscopy issues for the double-Pomeron-exchange processes was deferred to this subsection, in order that the direct comparison with the corresponding $\gamma\gamma$ physics, both experimentally and theoretically, could be made. It should be abundantly clear that in terms of physics goals and experimental technique, there is a great overlap. But there is an extra dimension present in the case of double-Pomeron exchange. As always, one would like to search for as many resonant states as possible and determine masses, widths, branching ratios, etc. However, the physics of the production mechanism has not the relative simplicity possessed by the $\gamma\gamma$ initial state. Understanding the dynamics associated with Pomeron exchange is a very important goal in itself, and the spectroscopic information on Pomeron structure complements the information coming from the systematics of hard and soft diffraction at the much higher p_T and mass scales which were discussed at length in Sections 2.1.3, page 16, 2.1.4, page 19, 2.2.2.5, page 38, 2.2.2.6, page 38. As an example of the importance of the detailed Roman-pot information, it should be noted that a strong dependence of the produced resonant systems on the magnitude of the *difference* of the recoil transverse-momenta imparted to the two leading protons has been recently observed [168]. Empirically it appears that well-established P and D wave $q\bar{q}$ states (such as $f_1(1285)$), $f_1(1420)$, $f_2(1525)$, and $\eta_2(1700)$) are strongly suppressed when this transverse-momentum difference dp_T is small. On the other hand, they become prominent when dp_T is large [169]. At small dp_T the remaining states include the glueball candidates $f_0(1500)$ and $f_J(1710)$. There also appears in this limit a broad tensor state $f_2(1900)$ that has a mass consistent with the a 2^{++} state on the Pomeron trajectory. The implications of these results for the nature of these mesons and/or diffractive scattering phenomenology are not yet understood. A detailed comparison of their production in Pomeron-Pomeron *versus* $\gamma\gamma$ collisions, especially when done with the same detector and under very similar conditions, offers intriguing prospects.

2.4.6.3. Heavy quark spectroscopy

The C-even states of heavy quarkonium cannot be produced in e^+e^- collisions directly, but only through the subsequent radiative decays of the C-odd vector states. Two photon processes provide the opportunity to produce these states *directly*. In the narrow width approximation, the production cross-section of a resonant state in $\gamma\gamma$ collisions is given by the formula [170]:

$$\sigma_{\gamma\gamma\to R}(M^2_{\gamma\gamma}) = 8\pi^2(2J+1)\,\Gamma_{\gamma\gamma}\,\delta(m^2_{\gamma\gamma}-M^2_R)/M_R, \qquad (2.51)$$

where J is the spin of the state and $\Gamma_{\gamma\gamma}$ is its two-photon width.

For charmonium production, the $\Gamma_{\gamma\gamma}(\eta_c)$ is known from experiment [171]. But the two photon widths of P-wave charmonium states have been measured with only moderate accuracy. Here for the cross-section calculations we use theoretical estimates of these widths based on perturbative QCD [172]. Similar predictions of two photon widths for bottonium states can be found elsewhere [173,174].

In Table 2.6 the cross-sections for quarkonium production in the rapidity range $|Y| < 7$ for the two-photon processes, as well as the expected numbers of events, are presented for the 10^6 sec runs with ion luminosities as shown in Table 2.1. As background processes, marked in the Table as $\gamma\gamma \to X$, we consider minimum-bias two photon processes in the mass range $M \pm \Delta M$, where ΔM is the expected mass resolution for the hadron system produced in $\gamma\gamma$ collisions. In the FELIX forward-backward geometry, $\Delta M \approx 40$ MeV. The minimum-bias cross-section has been calculated according to equations (2.31) and (2.38).

As one sees from Table 2.6, millions of C-even charmonium states will be produced in coherent two photon processes during a standard 10^6 sec heavy ion run at the LHC. The detection efficiency of charmonium events has been estimated as 5% for the forward-backward FELIX geometry. On this basis, we expect detection of about 5×10^3 charmonium events in $PbPb$ and about 10^6 events in $CaCa$ collisions. This is two to three orders of magnitude higher than what is expected during 5 years of LEP 200 operation [154]. The ratio of the minimum-bias background to the charmonium events is of the order of 2-9 if no specific decay modes are taken into account. By selecting distinctive charmonium decays, we expect to reduce the background level by a large factor, as already achieved at LEP experiments [175].

In Fig. 2.34 the expected mass spectrum of charmonium states is shown for a 10^6 sec $CaCa$ run, in the mass range up to 4.5 GeV for the forward/backward geometry of FELIX and with the assumption of charged-kaon identification. The minimum-bias background was generated with the TPHIC generator [176]. For all events the cut $P_t < 30\ MeV/c$ was applied to select the exclusive final states. The same spectrum without charged kaon identification is shown in Fig.2.35. As one sees from these figures, if no special η_c decay channels are taken into account, the signal to background ratio for the η_c is expected to be at the level of about 1/3. But if no particle identification for charged kaons exists in the forward/backward regions of the FELIX detector, the relative background level is 4 times worse.

The study of C-even bottonium states in two photon processes in the forward/backward FELIX geometry is rather doubtful due the small detection efficiency (of order of 0.2%) and a high value, ~ 300,

Table 2.6. Production cross-sections and event numbers for heavy quarkonia produced in 10^6 sec run in $PbPb$ and $CaCa$ collisions with luminosities 10^{26} and 4×10^{30} cm^{-2}sec^{-1}.

State	Mass, MeV	$\Gamma_{\gamma\gamma}$ keV	$\sigma(AA \to AA+X)$		Events for 10^6 sec	
			$PbPb$	$CaCa$	$PbPb$	$CaCa$
η'	958	4.2	22 mb	125 μb	2.2 10^6	5.0 10^8
η_c	2981	7.5	590 μb	3.8 μb	5.9 10^4	1.5 10^7
χ_{0c}	3415	3.3	160 μb	1.0 μb	1.6 10^4	4.0 10^6
χ_{2c}	3556	0.8	160 μb	1.0 μb	1.6 10^4	4.0 10^6
$\gamma\gamma \to X$	2950	–	1.4 mb	9.0 μb	1.4 10^5	3.6 10^7
η_b	9366	0.43	370 nb	3.0 nb	37	12000
χ_{0b}	9860	2.5 10^{-2}	18 nb	0.14 nb	2	560
χ_{2b}	9913	6.7 10^{-3}	23 nb	0.19 nb	2	760
$\gamma\gamma \to X$	9400	–	140 μb	1.0 μb	1.4 10^4	4.0 10^6

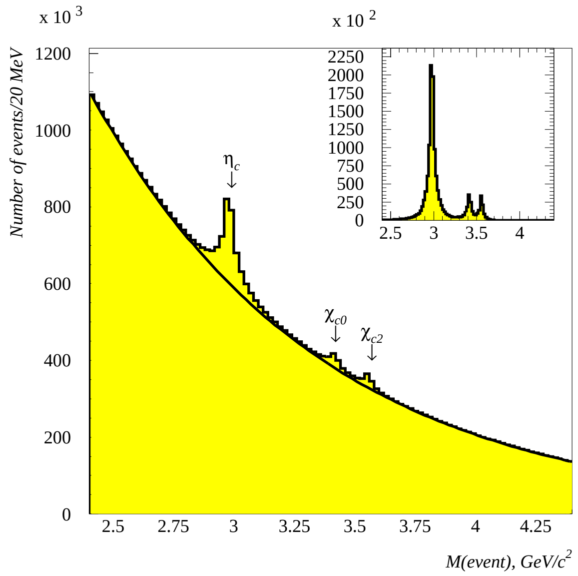

Figure 2.34. Mass spectrum of secondary particles with identification of charged kaons from all decays of η_c, χ_{0c} and χ_{2c} states produced in two photon processes during 10^6 sec runs with $CaCa$, the total transverse momentum of the system, $P_t < 30\ MeV/c$.

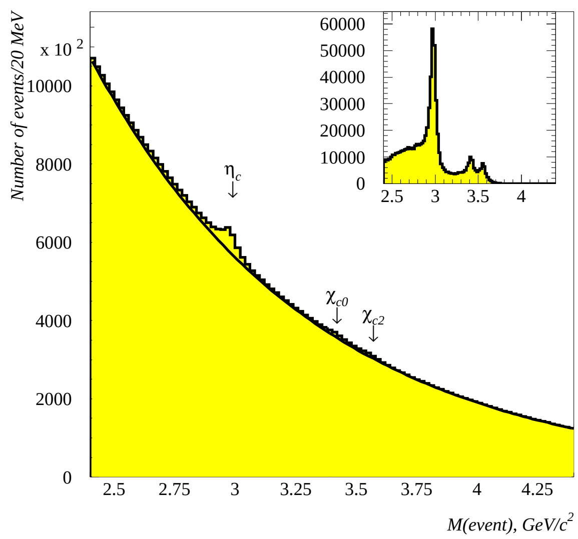

Figure 2.35. The same as in the previous figure but without charged kaon identification.

of the background to bottonium event ratio already for the η_b (Table 2.6). But if FELIX is upgraded with central detectors which include particle identification for charged kaons, we can expect detection of some several thousands of the η_b decays. Isolation of them from the minimum-bias events via looking for η_b in special decay modes, as already achieved in the case of η_c at LEP [175], may be attained.

2.5. The astroparticle connection

FELIX, a full acceptance LHC detector with the capability of observing events over the full range of pseudorapidity at LHC energies, can contribute significantly to cosmic ray astrophysics and to the resolution of some of its outstanding problems, and it will open previously inaccessible regions of parameter space to quantitative study where cosmic ray experiments have hinted at unusual physics.

- The modeling of particle interactions is an essential, integral part of operating and extracting results from cosmic ray, high energy gamma ray and neutrino detectors. As far as possible, it is highly desirable to replace the conjectured models with experimental data. FELIX is unique in covering the energy and rapidity range explored by high energy cosmic ray detectors and relevant to observations of cosmic ray muons and neutrinos. Its data will remove the ambiguity of results extracted from the data of current and future non-accelerator experiments.

- Unlike conventional central detectors, FELIX can search for a variety of unusual phenomena associated with the production of very forward particles in cosmic ray interactions with collision energy in excess of $\sim 10^3$ TeV (one PeV), i.e. $\sqrt{s}$ larger than 1 TeV. Proton-nucleus and nucleus-nucleus interactions will be studied as well as p-p collisions. Cosmic ray experimentalists have, for many years, reported observations at these energies and at large η which appear inconsistent with known and expected strong-interaction particle physics. A statement heard often at conferences and repeated in the conclusions of papers is that "There is persuasive evidence that there is a fundamental change in the character of strong interactions above 10^{16} eV" (4.3 TeV c.m.)[177]. Certainly, to date, there are no hard accelerator data to contradict that statement! The reason is simply that high energy particle detectors cover only the central region of pseudorapidity ($\eta - \phi$) phase space and, to date, even this only at lower energies.

2.5.1. Forward physics and energy flow: accelerators and cosmic rays

Cosmic ray observations are dominated by the energy flow in nucleon-nucleon collisions, as energy-sensitive detectors of nuclear and electromagnetic cascades are critical in triggering and analyzing cosmic ray data. The energy flow, in turn, very strongly weights the most forward-produced particles. The number distribution as a function of pseudorapidity η (in effect equivalent to rapidity y), $dN/d\eta$, when weighted by energy ($EdN/d\eta$) is approximately $e^y dN/d\eta$. The LHC c.m. energy of 14 TeV corresponds to a proton of about 100 PeV on a stationary nucleon target, with rapidity ranging up to 19.2 for forward nucleons. The flux of cosmic rays falls very rapidly with energy; the differential flux dN/dE falling approximately as E^{-3} above a PeV. A plot of the integral flux is shown in Fig. 2.36.

Direct observations of interactions of primary cosmic rays via balloon or satellite payloads have been limited to exposures measured in square meter-days, and hence to energies below a PeV. Knowledge of strong interactions from cosmic rays of energies greater than this comes primarily from mountain top observations, under 5 to 7 nuclear interaction mean free paths of atmospheric overburden, and from observations of the electromagnetic cascades (air showers) and muons at about sea level or (for muons) underground.

2.5.2. The origin of cosmic rays

The energy spectrum and composition of cosmic rays can be understood, up to perhaps a PeV, in terms of acceleration by the blasts of supernova shocks exploding into the interstellar medium of our galaxy. Although the slope of the cosmic ray spectrum increases above a PeV, particles with energies in excess of 10^{20} eV have been observed. The break in the spectrum above a PeV is believed to be related to the onset of a different acceleration mechanism. Where and how cosmic rays with energy well in excess of 1 PeV are accelerated is one of the most interesting problems in cosmic ray astrophysics.

The difficulty in formulating convincing models for the acceleration of charged particles with energies well above a PeV has inspired speculations wherein the highest energy cosmic rays are produced

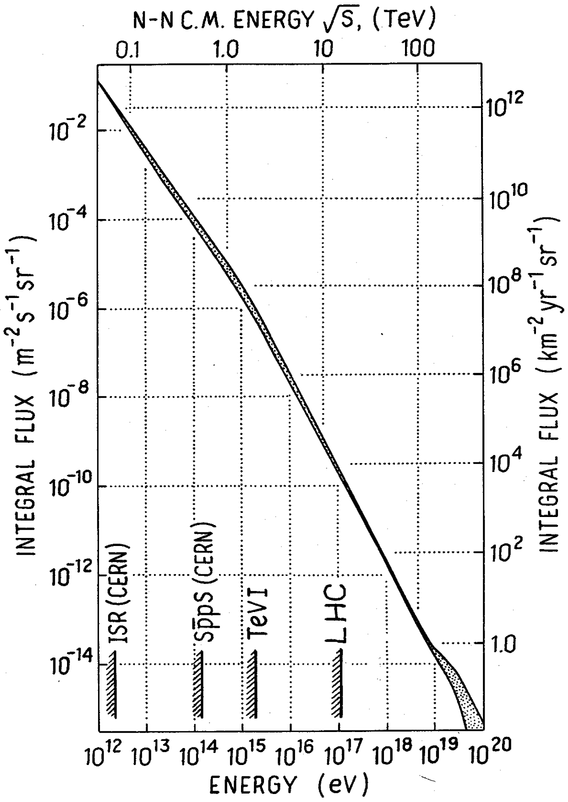

Figure 2.36. The integral flux of high energy cosmic rays. Note the change in slope of the spectrum near 10^{15}eV. The equivalent nucleon-nucleon energies of hadron colliders is noted on the abscissa.

in a "top-down" mechanism, e.g. the decay of X-particles[178]. Sources of these particles would be topological defects formed in the early universe at the time of GUT phase transitions. Energy is no longer a problem: the characteristic energy scale associated with such a scenario is the GUT scale (10^{13} TeV).

Topological defects illustrate how cosmic ray experiments may probe aspects of particle physics which cannot be addressed with accelerators. It is therefore reasonable to argue that the question of the origin of the highest energy particles in the universe is of sufficient importance to merit the support of accelerator experiments which are able to resolve ambiguities in the interpretation of the cosmic ray observations. FELIX, more than any other accelerator experiment, has the capability to provide measurements directly relevant to the analysis of cosmic ray experiments.

2.5.3. Understanding cosmic rays: particle physics beyond the reach of accelerators

Above energies of a few hundred TeV, the mix of atomic weights in primary cosmic rays is not known, and almost surely changes with energy. The simulation models used to understand observations deep in the atmosphere generally assume Feynman scaling and nearly constant inelasticity; over a wide range of energies, these assumptions are subject to logarithmic corrections as embodied, for instance, in "QCD-inspired" models[179].

In almost any model of particle interactions, over 90% of the primary cosmic ray energy eventually appears in the electromagnetic component. This electromagnetic part of the cascade can be modeled with considerable confidence and therefore yields a robust lower limit to the particle energies. (The "Long Flying Component" could lead to a significant underestimate of the primary energy, as discussed below.)

It is, of course, necessary to understand the physics of the first interactions, including effects due to nuclear primaries, in order to unambiguously model air showers in their entirety and to separate the effects of primary composition from interaction dynamics. Proponents of new particle thresholds [180] have a collection of unusual phenomena; so-called "anomalies", to bolster their claims. The critical point is that an LHC detector sensitive to all (including very large) rapidities will provide the critical particle physics information required to more unambiguously extract the cosmic ray composition and energy from air shower experiments.

2.5.4. New particle thresholds and "anomalies"

There is a spectrum of remarkable anomalies reported in the cosmic ray literature. These hint at unusual physics, not anticipated by the Standard Model, and observed at energies and/or regions of η outside the range of existing accelerator observations. These anomalies may be divided into two groups; inclusive phenomena - wherein inclusive distributions of certain cosmic ray data conflict with expectations based on existing accelerator data, and anomalous individual events - smaller numbers of exotic events containing unexpected features.

It must be pointed out that exaggerated claims or experimental mistakes have rarely been the source of cosmic ray anomalies. The possible fates of an anomaly are that: i) it is the first hint of new physics, (like the discovery of charm in cosmic rays) ii) it is eventually understood in terms of known physics (puzzling observations are scattered over the cosmic ray literature which, after their identification at accelerators, are understood as manifestations of parton jets) or iii) it reflects an insufficient understanding of the measurements which are often very indirect. Because of the characteristic millibarn cross-sections associated with many of these "anomalies", they should be readily observed by FELIX; luminosity and running time will not be limitations.

One should not forget that, in 1971, Niu, et al. reported cosmic ray observations from balloon-borne emulsion chambers of unstable, decaying hadrons which were clearly not hadrons containing the S quark or other known particles [181]. After the discovery of Charm in 1974, Gaisser and Halzen showed clearly that Niu's particles were D mesons (containing the Charm quark) [182]; Niu's masses, lifetimes, and other properties had by then been confirmed from accelerator experiments.

The first set of anomalies are those which appear as inclusive phenomena, and which therefore are apparent in the distributions of all events in certain classes (e.g., above a given energy).

- Anomalous Mean Free Path, the Long Flying Component:

  The Russians have operated a lead/ionization chamber calorimeter of 36 square meters area at a mountain station on Tien-Shan at an elevation of 3340 meters. A high-energy hadron entering the calorimeter will interact at some depth; neutral pions produced in this interaction will initiate EM cascades resulting in a prompt build-up of ionization and permitting identification of the initial interaction depth. Secondary hadrons then interact at greater depths, each initiating its own EM and hadronic cascade. The resulting ionization *vs.* depth shows a peak followed by an exponentially falling ionization with depth, where the slope is a function of the interaction mean free path and the inelasticity of the produced secondaries. From calculations and models, this exponential slope should be only a weak function of the energy of the incident hadron.

  The observations show that the exponential characterizing the ionization *vs.* depth of the cascade from a cosmic ray hadron becomes flatter (the attenuation length greater) as the incident hadron becomes more energetic, for energies above about 10 TeV [183]. A compilation of results of attenuation length *vs.* incident energy is in Fig. 2.37. The group argues that the explanation for this phenomenon could be the production of charmed hadrons in the forward direction at high energies. At low energy, the charmed particle decay length is short compared to the characteristic cascade development, and there is little effect on cascades. However, for energies well above 10 TeV, the charmed hadron decay length becomes comparable to the depth of a Pb calorimeter, and this would lead to the observed lengthening of the cascade profile and large energy depositions deep in the calorimeter.

  They conclude that the data can be explained by forward (high-x) production of charmed hadrons with a probability of 30% per interaction above about 10 TeV. The Russian-Japanese emulsion chamber group working at the Pamirs site has published data from their chambers supporting the Tien-Shan results

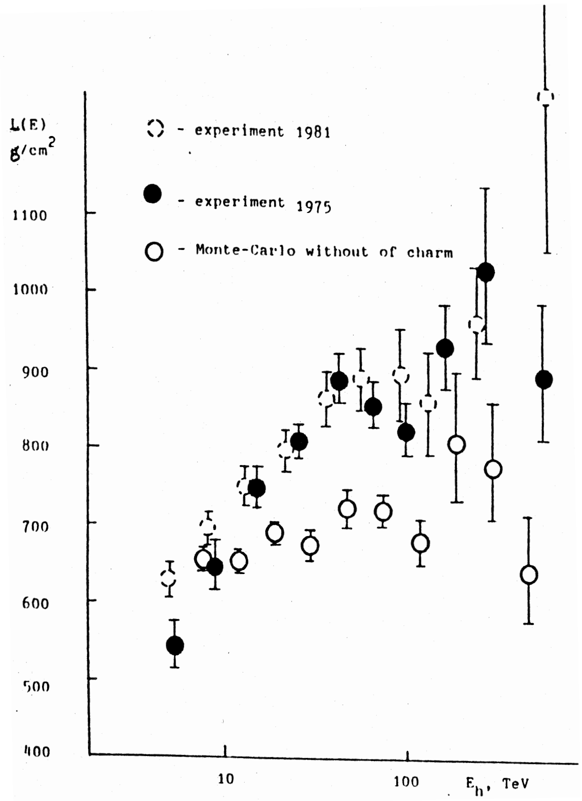

Figure 2.37. Compilation of the ionization attenuation length, L(E), data for the Russian lead calorimeter [183]. The Monte Carlo simulation based on established lower-energy models is plotted as open circles.

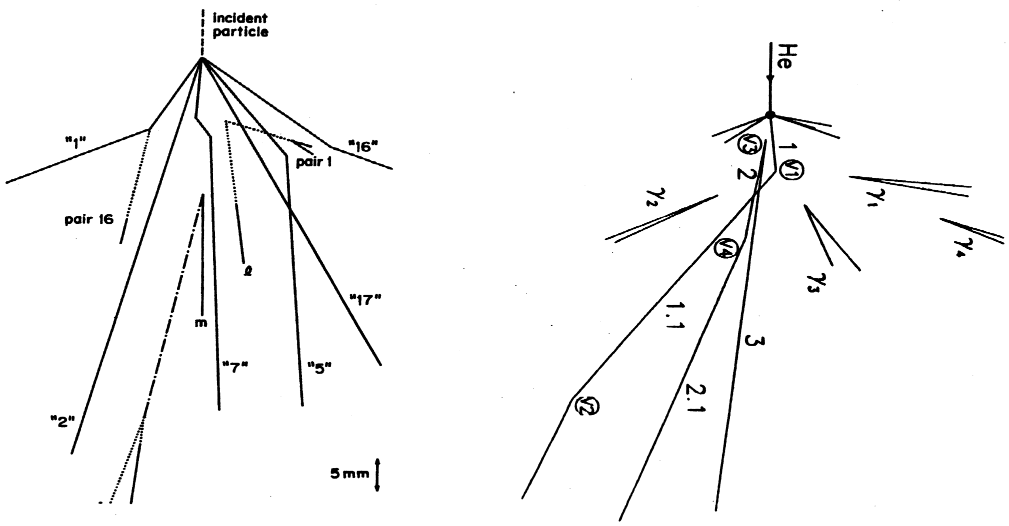

Figure 2.38. Emulsion chamber observation of the associated production of heavy quarks. Event (A) appears to show the decay of 5 quarks. One of the quarks, presumably a b, undergoes a b *to* c cascade decay. Event (B) shows an event wherein four γ conversions point to a decay in flight. Note in both figures a 100:1 (approximately) transverse-longitudinal scale difference. Only tracks relating to the decay processes are shown; other secondaries are not shown in the interest of clarity.

[184]. Yakovlev and White have also interpreted certain observed anomalies in the observations of extensive air showers in support of the 'long-flying component' [180].

- Anomalous Heavy Flavor Production:

  There have been numerous other indications that the production of heavy flavors (charm and bottom quark states) are enhanced at high energies in the far forward direction. The strongest evidence for this comes from the JACEE collaboration. In recent publications [185], they report the analysis of a subset of 15 events with incident energies of over a TeV per nucleon wherein the number of secondaries was less than 50 per event (at energies of tens of TeV, a heavy primary cosmic ray may produce hundreds of secondaries in a collision with an emulsion nucleus). Within these 15 events, they observed 64 secondary vertices (kinks, vees, 3-prong vertices, etc.) within their chamber. Two events are especially striking, each showing a kink (decay in flight) of a secondary with 4 gamma vertices pointing back to the kink. As the chambers are only a fraction of a radiation length in depth, the observed gammas are compatible with a total of about 10 gammas produced at each vertex. The observed gammas do not pair to fit π^0s. These decays do not match any known charm or bottom hadrons. A diagram of the relevant tracks from one of the events is shown in Fig. 2.38(B). An interesting event with 5 (apparently) heavy quarks produced and containing no γ's from the decay vertices is also reproduced in Fig. 2.38(A). One must appreciate that these, as well as other observed cosmic ray events, must be produced with cross-sections of millibarns, which makes exotic explanations such as WW production followed by $t\bar{b}$ decay, in the context of the Standard Model, quite irrelevant. However White [180] suggests just this mechanism and events such as this in support of his "color sextet" model.

- Anomalous Attenuation of Secondary Hadrons

  The Chacaltaya-Pamir Collaboration has reported hadrons with anomalously short mean free path in their emulsion chambers [186]. The interaction length, ΔT, is defined as the distance between the top of the chamber and the initiation of an electromagnetic cascade deeper than 6 radiation lengths into the chamber, which signals the vertex of a hadronic interaction.

  From the study of γ-initiated cascades, the group can determine the distance between the

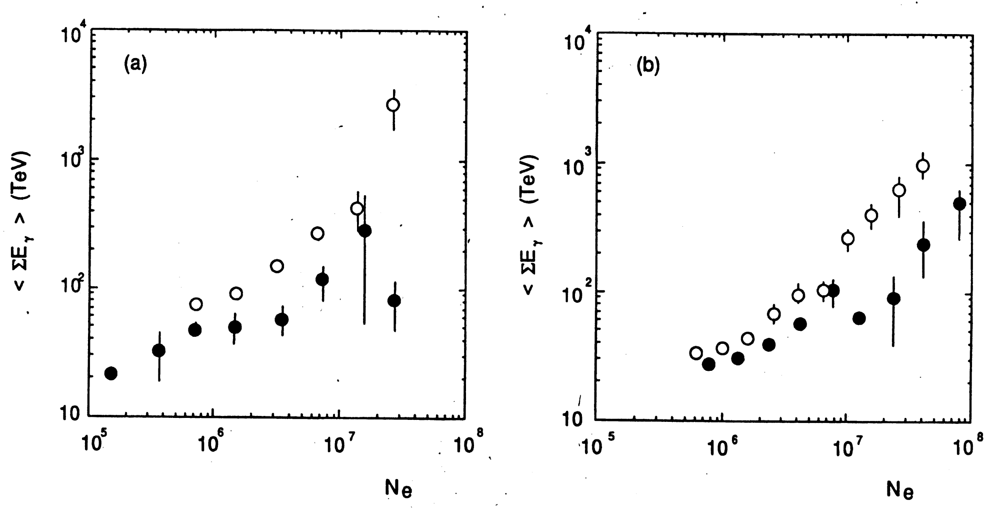

Figure 2.39. Correlation between air shower size, $N(e)$, and visible energy in emulsion chamber families, ΣE_γ. The left graph is from the Chacaltaya results and the right graph from the Tien-Shan experiment. Filled circles are data and open circles are Monte Carlo simulations.

observed maximum of the electromagnetic cascade and its initiating vertex. The distribution of ΔT is then exponential. However the slope of this exponent is significantly greater than that for single unaccompanied hadrons seen in the same chambers and corresponds to a cross section in lead much larger than known from accelerator experiments. The attenuation length is 170 g/cm^2, whereas 252 g/cm^2 is expected.

- Energy Fraction of Air Showers in Emulsion Chamber Families:

  The Japanese emulsion chamber group working at Mt. Chacaltaya has reported that, for extensive air showers produced by incident cosmic rays of over 10 PeV, the energy visible in families in their emulsion chambers is not proportional to the incident energy as determined by the air shower array. They show that the visible energy in electromagnetic cascades (from incident electrons and γ's as well as incident hadrons) increases less rapidly than the total number of electrons in the air shower. Their results are summarized in Fig. 2.39, where results from the Russian HADRON experiment at Tien-Shan, which reached the same conclusions, are also presented [187].

- Scaling and Inelasticity

The inelasticity, K, is defined as $K = (1 - E_l/E_o)$, where E_l is the energy of the leading final-state hadron, and E_o is the incident energy. At energies below a TeV (laboratory), $\langle K \rangle \simeq 0.5$, and Feynman scaling of the forward-produced particles holds. At energies at and above a PeV, however, the situation is much less clear. Costa and Halzen[188] have shown that the inclusive distribution of hadrons *vs.* energy observed at mountain elevations can be reproduced with a Monte Carlo simulation using the known primary spectrum, Feynman scaling, inelasticity only slowly increasing (as predicted by QCD), and a reasonable mass spectrum of primaries ($\langle A \rangle = 7.3$) (see Fig. 2.40). Ohsawa and Wlodarczyk[189], on the other hand, argue that the cosmic ray data support a fall in inelasticity with energy (see Fig. 2.41), and that the data from UA-7, as well as cosmic ray data, demonstrate a departure from scaling. The particular inclusive distributions referenced above, in the case of the anomalous fraction of air shower energy in observed emulsion chamber families, also suggest new physics. This discussion ignores the ambiguities associated with nuclear effects. These are usually finessed by using the superposition model for air shower simulations: the interaction of a primary cosmic ray nucleus with A constituent nucleons and energy E, is modeled as A independent nucleons,

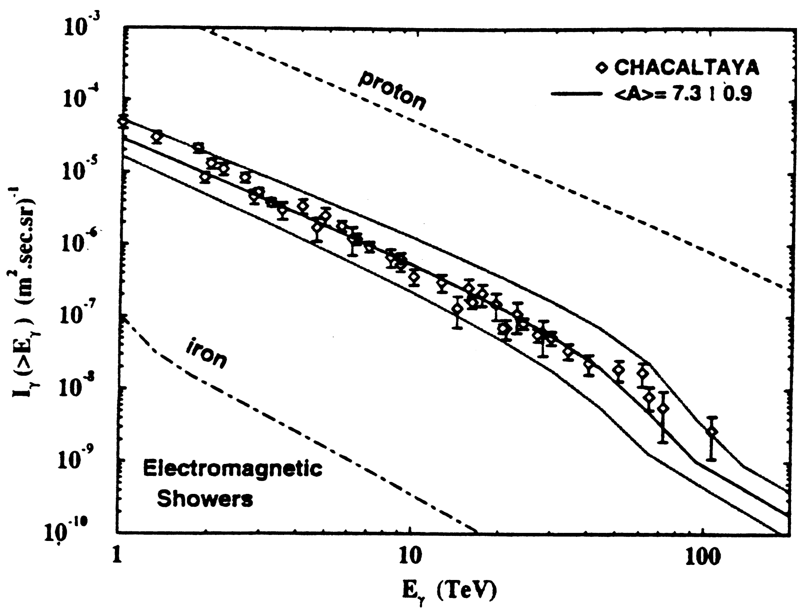

Figure 2.40. Integral energy spectra of electromagnetic showers (◇) detected at Mt. Chacaltaya compared to a calculation assuming Feynman scaling for the productions of neutral pions in the very forward direction [188]. These gamma rays initiate a cascade with the photon energy distribution shown in the figure. Dashed lines: $\langle A \rangle = 1$ (proton) and 56 (iron); solid line: $\langle A \rangle = 7.3 \pm 0.9$, dotted lines: calculated from uncertainties in A and γ.

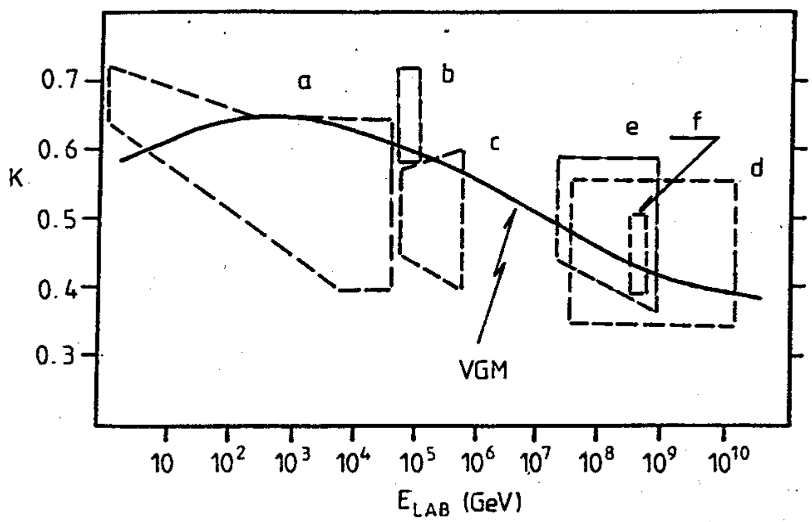

Figure 2.41. Energy dependence of average inelasticity, $\langle K \rangle$, in hadron-air nucleus collisions. (a) evaluated from hadronic flux measured at different depths in the atmosphere, (b) from $h - ^{12}C$ collisions from analysis of Pamir emulsion chambers, (c) from zenith-angle distribution of hadrons, (d) from fluctuations in the depth of air shower maxima, and (e) and (f) from the joint analysis of the Akeno and Fly's Eye data respectively. The solid line is a calculated 'valon-gluon model' [189].

each with energy E/A. Whereas the model is likely to adequately reproduce average properties of the shower, it almost certainly underestimates fluctuations. The LHC will be able to accelerate nuclei and will provide FELIX with the relevant data on nucleus-nucleus as well as proton-nucleus collisions, to both better interpret the cosmic ray data and study this area of physics which is also of great intrinsic interest.

The phenomena noted below are observed in a fraction of high energy cosmic ray interactions studied and (with the exceptions noted) do not impact inclusive distributions.

- Centauros and Anti-Centauros:

  Several events have been reported from the Brazilian-Japanese Collaboration, first about 25 years ago, wherein an interaction in the air 50 to about 500 meters above the detector gave rise to a large number of charged hadrons and zero or very few γ's (or electrons). The separation between the electromagnetic component (γ's and electrons) and charged hadrons is quite clean, based on the depth of initiation of the electromagnetic cascade in the lead of the chamber[190]. In one particularly striking Centauro event, 49 hadrons are observed to interact in the detector but only 1 γ or electron. From estimates of the hadrons which penetrated without interaction and interactions in the air above the chamber, the authors estimate that 74 hadrons were produced and (probably) no neutral pions. By particle physics standards these events are not rare; an estimate of the probability of producing a Centauro in an interaction of one PeV or above is about 1%.

  The Japanese - American Cooperative Emulsion - chamber Experiment, JACEE, has flown emulsion chambers with balloons near the top of the atmosphere. At least two events have been observed which have been referred to as "Anti-Centauros". Here a region of η–ϕ phase space is seen containing an anomalous number of γ-induced showers and a dirth of charged particles. In one such event, 32 γ cascades are observed within a circle of radius 0.7 in η–ϕ space with only 1 charged track. Another event (reported in 1993), has 27 γ's with $\eta > 6$ (and these from conversions in only 0.8 radiation lengths), while only 6 charged tracks fall in the same kinematic range [191].

  These Centauro and Anti-Centauro events have been interpreted as manifestations of Disoriented Chiral Condensates[192]. Another interpretation of the Chacaltaya Centauro events suggests that they are due to fragments of heavy primary cosmic rays. However the survival probability of heavy primary nuclei to this depth in the atmosphere appears much too low to account for the number of Centauros reported.

  Another suggested source of these phenomena are "Strangelets" (hadronic matter containing comparable fractions of up, down, and strange quarks). Were they a component of primary cosmic rays, they could penetrate deeply into the atmosphere and decay, evaporating into nucleons [193].

- Chirons, Halo Events, and Mini-Clusters:

  For some years the Brazilian-Japanese collaboration, working with emulsion chambers on Mt. Chacaltaya, have reported a class of events they refer to as "Chirons" [194]. The two best examples are events where the event vertex is found by triangulation to be in the air within 500 meters above the chambers. These events are characterized by clean hadronic cascades (not clustered among E-M cascades from atmospheric showering of γ's in the intervening atmosphere) with average transverse momenta of 2 to 3 GeV/c. This is interesting in itself. Even more unusual is the fact that about half of these hadronic cascades are seen, on close inspection, to contain two or more internal cascades, clearly identified as initiated by hadrons. The relative transverse momenta within each minicluster are anomalously small: 20 or 30 MeV/c. They are also said to have an anomalously high hadron/γ ratio.

  Events are also often observed which are characterized by a dense blackening of the emulsion over a small area (due to an electromagnetic cascade which had begun development in the air above the chamber) containing within it several hadronic cores, again spaced very closely together. These authors suggest again that the relative transverse momenta of the hadrons within these miniclusters are in the 20–30 MeV/c range, as in the Chirons. These are called "Halo" events [195].

  The cosmic ray community has been very intrigued with the observation that in many of these multi-halo events, the halos are aligned. Halos are electromagnetic showers produced by the most energetic π^0 in jets. Parton-parton scattering naturally leads to the alignment of the final state nucleon fragment with two or more parton jets [196]. However the Russian Group reports that the observed alignment is significantly greater than can be accommodated by the QCD theory. It is intriguing that the data discussed here pertain to the highest energy parton jets ever observed.

- Muon Bundles

  Events have been reported wherein bundles of muons are observed with very small lateral separation, as if produced in a process with very small relative transverse momenta (as in the Chiron miniclusters). In one event, 5 parallel muons are observed within a radius of 10 cm. If produced at an elevation of 10 km above the detector, they have an angular spread of only 10 μ-radians [197].

This list of anomalies is incomplete. The anomalies are all associated with very high energy data and, even where they overlap with existing collider energies, they represent very far forward phenomena which have not been studied by existing detectors. Because the target (or possibly both beam and target) is a nucleus, there is also the possibility that cosmic ray anomalies are associated with nuclear effects. The FELIX detector is the only instrument that can thoroughly explore these claims.

References

[1] A.H. Mueller and G.P. Salam, Nucl. Phys. **B475** (1996) 293.

[2] M.Arneodo, et al, Report of the working group on “Light and Heavy Nuclei in HERA”, *Future Physics at HERA*, G. Ingelman, pp. 887-926; A. De Roeck and R. Klanner, eds. DESY (1996).

[3] L.N. Lipatov, Yad. Fiz. **23**, 642 (1976) [Sov. J. Nucl. Phys. **23**, 338 (1976)]; E.A. Kuraev, L.N. Lipatov and V.S. Fadin, Zh. Eksp. Teor. Fiz. **71**, 840 (1976) [Sov. Phys. JETP **44**, 443 (1976)]; **72**, 377 (1977) [**45**, 199 (1977)]; Ya.Ya. Balitsky and L.N. Lipatov, Yad. Fiz. **28** 1597 (1978) [Sov. J. Nucl. Phys. **28**, 822 (1978)].

[4] G. Camici and M.Ciafaloni, Phys. Lett. **B395** (1997) 118; L. P. A. Haakman, O. V. Kancheli, J. H. Koch, *The BFKL Pomeron with running coupling constant: how much of its hard nature survives?*, hep-ph/9707262. L. Lipatov and V. Fadin Contribution to LEPTON-PHOTON Conference, Hamburg 1997.

[5] D. Treleani, *Minijets as a Probe of the Hadronic Many-Body Parton Structure at LHC*, FELIX Note, (http://www.cern.ch/FELIX).

[6] L. McLerran and R. Venugopalan, Phys. Rev. **D49** (1994) 2233; **D49** (1994) 3352; **D50** (1994) 2225. A. Kovner, L. McLerran and H. Weight, Phys. Rev.**D52** (1995) 3809; **D52** (1995) 6231.

[7] B. L. Ioffe, Phys. Lett. **30** (1968) 123.

[8] L. C. H. Llewellyn Smith, Nucl. Phys. **A 434** (1985) 356.

[9] B. Blättel, G. Baym, L.L. Frankfurt, and M. Strikman, Phys. Rev. Lett. **71** (1993) 896.

[10] L. Frankfurt, A. Radyushkin, and M. Strikman, Phys. Rev. **D55** (1997) 98.

[11] ZEUS collaboration, Paper pa02-028 submitted to the XXVIII. International Conference on High Energy Physics, Warsaw, July 1996.

[12] E. Eichten, I. Hinchliffe, K. Lane and C. Quigg, Rev. Mod. Phys. **56** (1984) 579; **58** (1986) 1065.

[13] CTEQ Collaboration, *Handbook of Perturbative QCD Version 1.0*, April 1993.

[14] A.D. Martin, R.G. Roberts, W.J. Stirling Phys. Lett. **B387** 419-426, 1996

[15] S. Heppelmann and R. Bagdasaryan, hep-ph/9704252.

[16] S.Abachi *et al.*, (D0) Phys. Rev. Lett. **77** (1996) 5011.

[17] K. Goulianos, Phys. Lett. **B358** (1995) 379, Erratum: Phys. Lett. **B363** (1995) 268.
K. Goulianos, *Renormalized diffractive cross-sections at HERA and the structure of the pomeron*, Talk given at 7th Rencontres de Blois: Frontiers in Strong Interactions - 6th International Conference on Elastic and Diffractive Scattering, Blois, France, 20–24 June 1995, hep-ph/9512291

[18] S. Erhan *et al.*, *UA8: Measurements of Single Diffraction at* $\sqrt{s} = 630\,\mathrm{GeV}$*; Implications for the Pomeron Flux Factor*, to be published.

[19] G. Ingelman and P.E. Schlein, Phys. Lett. **B152** (1985) 256.

[20] A. Donnachie and P.V. Landshoff, Nucl. Phys. **B303** 634 (1988).
A. Donnachie and P.V. Landshoff, Phys. Lett. **191B** 309 (1987), ERRATUM-ibid. **198B** 590 (1987.

[21] A. Hebecker, *Diffractive parton distributions in the semiclassical approach*, preprint DAMTP-97-10, hep-ph/9702373.
W. Buchmüller and A. Hebecker, Phys. Lett. **B355**, 573 (1995).

[22] A. Edin, G. Ingelman, and J. Rathsman, *Unified description of rapidity gaps and energy flows in DIS final states*, hep-ph/9605281.
A. Edin, G. Ingelman, and J. Rathsman, Phys. Lett. **B366** 371 (1996).

[23] J. Bartels and M. Wüsthoff, Z. Phys. **C66** (1995) 157

[24] M. Genovese, N.N. Nikolaev, and B.G. Zakharov, Phys. Lett. **B380** 213 (1996).
N.N. Nikolaev and B.G. Zakharov, J. Exp. Theor. Phys. **78** 598 (1994) [Zh. Eksp. Teor. Fiz. **105** 1117 (1994)].
N. Nikolaev and B.G. Zakharov, Z. Phys. C53, 331 (1992).

[25] J.D. Bjorken, *Rapidity gaps in deep inelastic scattering*, hep-ph/9601363.
J.D. Bjorken, Phys. Rev. **D47** 101 (1993).

[26] L. Dick, V. Karapetian, R. Barni, and G. Preparata, *Diffraction in deep inelastic scattering: the hadronic nature of quarks*, hep-ph/9608217.

[27] A. Berera and D.E. Soper, Phys. Rev. **D53** 6162 (1996).
A. Berera and D.E. Soper, Phys. Rev. **D50** 4328 (1994).

[28] Z. Kunszt and W.J. Stirling,*Hard diffractive scattering: partons and QCD*, talk given at Durham Workshop on HERA Physics: Proton, Photon, and Pomeron Structure, Durham, England, 17–23 Sep 1995, and at International Workshop on Deep Inelastic Scattering and Related Phenomena (DIS 96), Rome, Italy, 15–19 Apr 1996, hep-ph/9609245.

[29] H. Abramowicz, L. Frankfurt, M. Strikman DESY-95-047, Mar 1995. 60pp. Published in SLAC Summer Inst. 1994:539-574.

[30] J. C. Collins, *Notes on diffractive hard scattering at FELIX*, FELIX Note (http://www.cern.ch/FELIX).

[31] J. C. Collins, L. Frankfurt and M. Strikman, Phys. Lett. **B307** (1993) 161; A. Berera and J.C. Collins, *Double Pomeron Jet Cross Sections* preprint PSU/TH/162, hep-ph/9509258, to be published in Nucl. Phys. B.

[32] J. C. Collins, in preparation.

[33] See, for example, Refs. [28,34–36,38]

[34] T. Gehrmann and W.J. Stirling, Z. Phys. **C70** (1996) 89.

[35] K. Golec-Biernat and J. Kwieciński, Phys. Lett. **B353** (1995) 329.

[36] L. Alvero, J.C. Collins, J. Terron and J. Whitmore, *Diffractive Hadronic Production of Jets and Weak Bosons*, hep-ph/9701374.

[37] H1 Collaboration, *A Measurement and QCD Analysis of the Diffractive Structure Function* $F_2^{D(3)}$, submitted to ICHEP'96, H1 preprint pa02-061; A. De Roeck, in the Proceedings of the DIS96 Workshop on "Deep Inelastic Scattering and Related Topics", April 15 - 19, 1996, Rome.

[38] J. C. Collins, J. Huston, J. Pumplin, H. Weerts and J. Whitmore, Phys. Rev. **D51** (1995) 3182.

[39] L. Frankfurt, M. Strikman, Phys. Lett. **B 64**, 1914 (1989).

[40] UA8 Collaboration, (A. Brandt *et al.*), Phys. Lett. **B297**, 417 (1992).

[41] D0 Collaboration, S. Abachi *et al.*, Phys. Rev. Lett. **72** (1994) 2332; CDF Collaboration, F. Abe *et al.*, Phys. Rev. Lett. **74** (1995) 855; D0 Collaboration, S. Abachi *et al.*, Phys. Rev. Lett. **76** (1996) 734.

[42] J. D. Bjorken, Int. J. Mod. Phys. **A7**, 4189 (1992); Phys. Rev. **D47**, 101 (1993); D. Zeppenfeld, *Developments in perturbative QCD: Challenges from collider physics*, hep-ph/9603315.

[43] O. J P. Eboli, E. M. Gregores, and F. Halzen, *(No)Color in QCD: Charmonium, charm and rapidity gaps*, hep-ph/9611258.

[44] A.D. Martin, M.G. Ryskin, V.A. Khoze, it Dijet hadroproduction with rapidity gaps and QCD double logarithmic effects DTP-97-34, May 1997. 15pp. e-Print Archive: hep-ph/9705258

[45] B.Abbott (for D0) DOCONF-97-10, Conf-97/180-E (FNAL).

[46] ZEUS Collaboration, M. Derrick *et al.*, Phys. Lett. **B369** (1996) 55.

[47] L. Frankfurt, L. Mankiewicz, A. Radyushkin, M. Strikman, in preparation.

[48] L. L. Frankfurt, G. A. Miller and M. Strikman, Ann. Rev. of Nucl. and Particle Phys. **44** (1994) 501.

[49] G. Bertsch, S.J. Brodsky, A.S. Goldhaber, J. Gunion, Phys. Rev. Lett. **47**, 297 (1981).

[50] L. Frankfurt, G.A. Miller, and M. Strikman, Phys. Lett. **B304** 1 (1993).

[51] B.K.Jennings and G.A.Miller, Phys.Rev. **C50** (1994) 3018.

[52] R. Weiss-Babai, representing Fermilab E791 collaboration, proceedings of Hadron97 conference, BNL (1997) to be published.

[53] L. Frankfurt, M. Strikman, in Proceedings of Baryons'95, Edi. B. F. Gibson, P. D. Barnets, J. B. McClelland, W .Weise, World Scientific, 1996, p.211.

[54] R. Rubinstein *et al.*, Phys. Rev. **D30** (1984) 1413.

[55] S. J. Brodsky, J. Ellis, M. Karliner Phys. Lett. **206B**: 309, 1988

[56] G.A. Schuler, *Quarkonium production and decays*, CERN-TH-7170-94 [hep-ph/9403387]

[57] E. Braaten, S. Fleming and T.C. Yuan, Ann. Rev. Nucl. Part. Sci. **46** (1996) 197

[58] M. Beneke,*Non-relativistic effective theory for quarkonium production in hadron collisions*, CERN-TH/97-55, hep-ph/9703429.

[59] M. Ciafaloni, Nucl.Phys. **B296** (1987) 249; S. Catani, F. Fiorini and G. Marchesini, Nucl.Phys. **B336** (1990) 18.

[60] A.H. Mueller and H. Navelet, Nucl. Phys. **B282**, 727 (1987).

[61] The D0 Collaboration (S.Abachi *et al.*), Phys. Rev. Lett. **77**, 598 (1996).

[62] V. Del Duca and C.R. Schmidt, Phys. Rev. D **49**, 4510 (1994); Phys. Rev. D **51**, 2150 (1995); Nucl.Phys. **B** (Proc.Suppl.) **39C**, 137 (1995); W.J. Stirling, Nucl. Phys. **B423**, 56 (1994).

[63] J.R. Forshaw, M.G. Ryskin, Zeit. Phys. **C68**, 137 (1995).

[64] J. Bartels, J.R. Forshaw, H. Lotter, M. Wüsthoff, Phys. Lett. **B 375**, 301 (1996).

[65] N. Paver and D. Treleani, Nuovo Cim. **70A:** 215, 1982.

[66] CDF Collaboration (F. Abe *et al.*). FERMILAB-PUB-97-094-E, Apr 1997. Submitted to Phys. Rev. D

[67] L. Ametller and D. Treleani, Int. J. Mod. Phys. **A3**:521, 1988. .

[68] UA1 Collaboration (C. Albajar *et al.*) Nucl. Phys. **B309**: 405, 1988

[69] Yu.L. Dokshitser, V.A. Khoze, A.H. Mueller, S.I. Troian, BASICS OF PERTURBATIVE QCD. 1991. Gif-sur-Yvette, France: Ed. Frontieres (1991) 274 p

[70] Y. Azimov, Y. Dokshitzer, V. Khoze, and S. Troyan, Z. Phys. **C27** 65 (1985); **C31** 213(1986).

[71] F. Abe et. al. (CDF Collaboration), Phys. Rev. **D50** (1994) 5562; S. Abachi et. al. (D0 Collaboration) Fermilab Conf-95/182-E; E. Varelas, Fermilab Conf-95/181-E.

[72] R. Orava and V. Khoze, *FELIX as a Partonometer* Felix Note.

[73] B. Andersson, G. Gustafson, and T. Sjostrand, Z. Phys. **C6** 235 (1980).

[74] A. Donnachie and P.V. Landshoff, Nuclear Physics **B267** (1986) 690

[75] A. B. Kaidalov,L. A. Ponomarev,K. A. Ter-Martirosyan, Yad. Fiz. **44** (1986)722

[76] J.-R Cudell, K. Kang, Sung Ku Kim, *Simple model for total cross sections*, hep-ph/9701312

[77] Particle Data Group, Phys. Rev. **D54** (1996) page 193

[78] E710 collaboration: N. Amos et al, Phys. Lett **B243** (1990) 158 CDF collaboration: F.Abe et al,Phys. Rev. **D50** (1994) 5550.

[79] J. A. Jaroszkiewicz and P. V. Landshoff, Phys. Rev. **D10** (1974) 170.

[80] C. Bourreley, F. Soffer, T.T. Wu Phys. Rev. Lett **54** (1985) 757; Z. Phys. C **37** (1988) 369; Phys. Lett. **B315** (1993) 195.

[81] M.G. Sotiropoulos, G.Sterman Nucl. Phys. **B425**:489-515, 1994

[82] A. H. Mueller and W. K. Tang, Phys. Lett. **B284** :123-126, 1992.

[83] M. Islam, *pp elastic scattering in FELIX: physics goals*, FELIX Note (http://www.cern.ch/FELIX).

[84] V. N. Gribov and I. Ya. Pomeranchuk, Phys. Rev. Lett. **8** (1962), 343; **8** (1962) 412.

[85] F. Abe *et al.* (CDF) Phys. Rev. **D50**: 5535-5549, 1994 and private communication of K. Goulianos.

[86] A. B. Kaidalov, Phys. Rep. **50**: 157-226, 1979, and *Soft hadronic interaction at LHC. Proposal for FELIX.*, FELIX Note (http://www.cern.ch/FELIX).

[87] G. Alberi, G. Goggi, Phys. Rept. **74**:1-207, 1981

[88] R. Weiner, in Ref. [93].

[89] M. I. Podgoretskii, Sov. J. Part. Nucl. **20**, (1989) 266; D. H. Boal, C. K. Gelbke and B. K. Jennings, Rev. Mod. Phys. **62** (1990) 553; I. V. Andreev, I. M. Dremin, B. Bijajima and N. Suzuki, Int. J. Mod. Phys. **A10** (1995) 3951.

[90] T. Brooks et.al. (Minimax Collaboration) Phys. Rev. **D55** 5667 (1997).

[91] See the contributions, e.g. of I. Sarcevic, M. Greiner, and M. Biyajima in Ref. [93].

[92] International Symposia on Multiparticle Dynamics: 1996 (to be published); 1995 ed.D. Bruncko, L. Sandor, and J. Urban; 1994, ed. A. Giovannini, S. Lupia, and R. Ugoccioni (World Scientific).

[93] Proceedings of the 7th International Workshop on Multiparticle Production, “Correlations and Fluctuations”, ed. R. Hwa, W.Kittel, W. Metzger, and D. Schonaus, World Scientific, 1997.

[94] A. Bialas and R. Peschansky, Nucl. Phys. **B273** (1986) 703

[95] B. Buschbeck, in Ref. [92].

[96] A. Belogianni et.al. (WA91 collaboration); Phys. Lett. (to be published).

[97] A. Giovannini and R. Uguccioni, *Multiparticle production structure in hh collisions at 14 TeV*, FELIX Note (http://www.cern.ch/FELIX).

[98] UA5 collaboration : R. E. Ansorge et al, Z. Phys. C **37**(1988) 191 ; Phys. Rep. **154** (1987) 247.

[99] A.Capella, *Long-range (forward-backward) rapidity correlations at LHC*, FELIX Note (http://www.cern.ch/FELIX).

[100] A. B. Kaidalov, In QCD at 200 TeV, ed. by L. Cifarelli and Yu. Dokshitzer, Plenum Press, N. Y. and London, 1992, p.1 A Capella et al, Phys. Lett. **B337** (1994) 358; E. Gotsman, E. M. Levin and U. Maor, Phys. Rev. **D49** (1994) 4321.

[101] V. A. Abramovsky, V. N. Gribov and O. V. Kancheli, Yad. Fiz. **18** (1973) 595.

[102] F. W. Bopp, A. Capella, J. Ranft and J. Tran Thanh Van, Z. Phys.C **51** (1991) 99.

[103] I. Dremin et.al., Mod. Phys. Letts. **A5** 1743 (1990).

[104] F. Halzen and J. Morris, Phys. Rev. **D42** 1435 (1990) and references therein.

[105] P. Seyboth, in Ref. [93]

[106] M.A. Faessler, Annals Phys. **137**:44,1981

[107] L. Frankfurt and M. Strikman, Phys. Rept. **76**:215-347,1981.

[108] A. H. Mueller and Jian-wei Qiu, Nucl. Phys. **B268**:427,1986

[109] M. Arneodo, A. Bialas, M.W. Krasny, T. Sloan, M. Strikman In *Hamburg 1995/96, Future physics at HERA* 887-926.

[110] L. Frankfurt, W. Koepf, M. Strikman, Phys. Rev. **D54**:3194-3215, 1996

[111] H.Abramowicz, L.Frankfurt, M. Strikman Published in SLAC Summer Inst.1994:539-574.

[112] S. J. Brodsky, L. Frankfurt, J. F. Gunion, A. H. Mueller and M. Strikman, Phys. Rev. **D50** (1994) 3134.

[113] L. Frankfurt, M. I. Strikman , S. Liuti, Phys. Rev. Lett. **65**:1725, 1990

[114] D. M. Alde, et al, Phys. Rev. Lett. **64**:2479-2482, 1990.

[115] M. Strikman and D. Treleani, in preparation

[116] F. Abe et al, FERMILAB-PUB-97-094-E, Apr 1997.

[117] J. W. Cronin, H. J. Frisch, M. J. Shochet, J. P. Boymond, P. A. Piroue, Phys. Rev. Lett. **31**:1426-1429, 1973

[118] R. Baier, Yu. L. Dokshitzer, A. H. Mueller, S. Peigné and D. Schiff, **B483** (1997) 291.

[119] R. Baier, Yu. L. Dokshitzer, A. H. Mueller, S. Peigné and D. Schiff, Nucl. Phys. **B484** (1997) 265; and references therein.

[120] A. H. Mueller, Nucl. Phys. **A610** (1996) 459c.

[121] B. G. Zakharov, hep-ph/9704255, preprint LPTHE-Orsay 97-09.

[122] S. Gavin and R. Vogt, hep-ph/9610432; and references therein.

[123] D. Kharzeev, M. Nardi and H. Satz, hep-ph/9702273, preprint BI-TP 97/02.

[124] S. J. Brodsky, Tao Huang, G.Peter Lepage Presented at 9th SLAC Summer Inst. on Particle Physics, Stanford, Calif., Jul 27 - Aug 7, 1981. Published in SLAC Summer Inst.1981:87

[125] L. L. Frankfurt, M. I. Strikman, Nucl. Phys. **B250**:143-176, 1985.

[126] S. J. Brodsky, P. Hoyer, A. H. Mueller, Wai-Keung Tang, Nucl.Phys. **B369**:519, 1992.

[127] A. Berera, M. Strikman, W. S. Toothacker, W. D. Walker, J. J. Whitmore, Phys. Lett. **B403** (1997) 1.

[128] K. Geiger, hep-ph/9701226; *Particle production in pA collision at the LHC with QCD-based event-generator models*, FELIX Note (http://www.cern.ch/FELIX); J. Ellis, K. Geiger, H. Kowalski, Phys. Rev. **D54**: 5443-5462, 1996

[129] S.M. Schneider, W. Greiner, G. Soff, Preprint GSI-92-56.

[130] S.Kawabata, Proc.of the Joint Intern. Lepton-Photon Symp. and Europhysics Conf. on High Energy Physics, Vol.2, p.53, Geneva, 1991.

[131] F.del Aguila et al. Preprint CERN-TH. 6205/91, August 1991; Phys.Lett. B271 (1991) 256.

[132] G. Altarelli and R. Barbieri, Phys.Lett. **B253** (1990) 161.

[133] J. Ellis, G.L. Fogli and E. Lisi, preprint CERN-TH-95-202, July 1995.

[134] J. Erler and P. Langacker, Phys.Rev.**D52** (1995) 441.

[135] J. Ohnemus, T.F. Walsh, P.M. Zerwas, Phys.Lett., **B328** (1994) 369.

[136] S. Klein and E. Scannapieco, LBNL-40457, June, 1997, to appear in the Proceedings of Photon '97, hep-ph/9706358; S. Klein and E. Scannapieco, LBL-40485, June, 1997, to appear in the Proceedings of the 6th Conf. on the Intersections of Particle and Nuclear Physics, nucl-th/9707008; S. Klein and E. Scannapieco, STAR Note 243, http://www.rsgi01.rhic.bnl.gov/star/starlib/doc/www/sno/ice/sn0243.html;

[137] K. Hencken, D. Trautmann, G.Baur, Z.Phys. **C68** (1995) 473.

[138] D. Brandt, K. Eggert, A. Morsch, Preprint CERN AT/94-05 (DI).

[139] G.Baur, Z.Phys. **C54** (1992) 419-423.

[140] N. Cahn, J. D. Jackson, Phys. Rev. **D42** (1990) 3690.

[141] C.A. Bertulani, G. Baur, Phys. Rep. **163** (1988) 299.

[142] S.U. Chung, D.P. Weygand and H.J. Willutzki, Intern. Conf. HADRON 91, p.895, Univ. of Maryland, College Park, 1991.

[143] H.L. Bradt and B. Peters. Phys. Rev. **77** (1950) 54.

[144] P.J. Karol, Phys. Rev. **C11** (1975) 1203.

[145] R. Engel, M.A. Braun, C. Pajares and J. Ranft, Z. Phys. **C74** (1997) 687

[146] S.U. Chung, D.P. Weygand, H.J. Willutzki, Informal Report, BNL-46863, November 1991.

[147] F.W. Bopp, et al., Phys. Rev.**D49** (1994) 3236 and

[148] R.Engel, Z.Phys. C66,203 (1996). R.Engel and J.Ranft, Phys.Rev. D54,4244 (1996).

[149] G.A.Schuler and T.Sjostrand, Preprint CERN-TH.7193/94.

[150] L.D. Landau and E.M. Lifshitz, Phys. Zs. Sowjet, **6** 244 (1934).

[151] A.J. Baltz and M. Strikman, *Suppression of Heavy Ion $\gamma\gamma$ Production of the Higgs by Coulomb Dissociation* hep-ph/9705220, 6 May 1997.

[152] A. Alscher, K. Hencken, D. Trautmann, G. Baur, *Multiple electromagnetic electron positron pair production in relativistic heavy ion collisions* nucl-th/9606011, 6 June 1996.

[153] G.A. Schuler and T. Sjostrand, Phys. Lett. **B300** (1993) 169.

[154] A.Bawa et al. $\gamma\gamma$ *Physics* hep-ph/9601317.

[155] L.Frankfurt, M.Strikman, in preparation.

[156] L.L. Frankfurt and M. Strikman, Phys. Rev. Lett. **63** (1989) 1914, Erratum ibid. **64** (1990) 815, and references therein

[157] J.A. Crittenden, DESY-97-068, (hep-ex/9704009) and references therein.

[158] L.L. Frankfurt, W. Koepf and M. Strikman, DESY-97-028, (hep-ph/9702216) references therein.

[159] E. Ackleh, T. Barnes, and F. Close, Phys. Rev. **D46**, 2257(1992).

[160] Z. P. Li, F. Close, and T. Barnes, Phys. Rev. **D43**, 2161(1991).

[161] E. Amsler and F. Close, Phys. Rev. **D53**, 295(1996).

[162] D. Weingarten, contribution to Lattice '97 (to be published).

[163] F. Close, G. Farrar, and Z. P. Li, Phys. Rev.**D55**, 5749 (1997).

[164] A. Wright, private communication regarding Aleph contribution to EPS conference, Jerusalem.

[165] J.Weinstein and N. Isgur, Phys. Rev. **D41**,2236 (1990).

[166] N. Tornqvist, Z. Phys. **C68** 647 (1995).

[167] T. Barnes, Proc. of IX International Workshop on Gamma Gamma Physics, La Jolla (1992), ed. D. Caldwell and H. Paar (World Scientific).

[168] D. Barberis et. al. (WA102 Collaboration), preprints hep-ex/9707021 and hep-ex/9707022.

[169] F. Close and A. Kirk, Phys. Lett. **B397**, 333 (1997).

[170] Ch. Berger and W. Wagner, Phys.Rep. **146** (1987) 1.

[171] Review of Particle Physics, Phys.Rev. **D54** (1996) 1.

[172] G. T. Bodwin et al. Phys. Rev.**D46** (1992) 1914.

[173] W.Kwong et al. Phys.Rev. **D37** (1988) 3210.

[174] M. Consoli, J.H. Field Phys. Rev. **D49** (1994) 1293.

[175] O. Adriani et al. (L3 coll.) , Phys. Lett.**B318** (1993) 575.

[176] K.Hencken, et al. Preprint IHEP 96-38, Protvino, 1996.

[177] Y. Fujimoto and S. Hasegawa, presentations at the *VIII International Symposium on Very High Energy Cosmic Ray Interactions*, Tokyo (1994).

[178] For recent review, see *The Pierre Auger Project Design Report*, Fermilab report (1995) and references therein.

[179] For a review see M. Block *et al.*, Nucl. Phys. B (Proc. Suppl.) **12A**, 238 (1990) and Phys. Rev. **D45**, 839 (1992).

[180] A. R. White, Int. J. Mod. Phys. **A8**, 4755 (1993); A.R. White and K. Kang, *Proceedings of the VII International Symposium on Very High Energy Cosmic Ray Interactions*, Ann Arbor (1992), p.459; A.R. White, *Proceedings of the VIII International Symposium on Very High Energy Cosmic Rays*, Tokyo (1994), p.468; A.R. White, "New Strong Interactions above the ElectroWeak Scale", Argonne preprint ANL HEP CP 94-46 (1994). See also ANL-HEP-PR-97-09 (1997) (unpublished).

[181] K. Niu *et al.*, Prog. Theor. Phys. **46**, 1644 (1971).

[182] T. K. Gaisser and F. Halzen, Phys. Rev. **D14**, 3153 (1976).

[183] V. I. Yakovlev, *Proceedings of the VII International Symposium on Very High Energy Cosmic Ray Interactions*, Ann Arbor (1992), p.154; I.M. Dremin, D.T. Madigozhin, and V.I. Yakovlev, *ibid.*, p.534.

[184] V. I. Yakovlev, "Some Current Problems in Very High Energy Cosmic Ray Physics", to be published in the *Proceedings of the 15th European Cosmic Ray Symposium*, Perpignan, France (1996).

[185] H. Wilczynski *et al.*, *Proceedings of the XXIII International Cosmic Ray Conference*, HE Sessions, Calgary (1993), Vol.4, p.29; H. Wilczynski, "JACEE Results on Very High Energy Interactions", to be published in the it Proceedings of the IX International Symposium on Very High Energy Cosmic Ray Interactions, Karlsruhe (1996).

[186] T. Arisawa, *et al.*, (Chacaltaya and Pamir Collaboration), Nuclear Physics B **424**, 241 (1994).

[187] V. V. Arabkin, *et al.*, *Proc. XXII International Cosmic Ray Conference*, Dublin (1991), Vol.4, pp.269 and 273.

[188] C. G. S. Costa, F. Halzen and C. Salles, Phys. Rev. D **52**, 3890 (1995); Phys. Rev. D **54**, 5558 (1996).

[189] A. Ohsawa *Proceedings of the VII International Symposium on Very High Energy Cosmic Ray Interactions*, Ann Arbor (1992) p.466; Z. Wlodarczyk, J. Phys. G. Nucl. Part. Phys. **19** p. 133 (1993), and **21** p.281 (1995).

[190] C. M. G. Lattes *et al.*, Physics Reports **65**, p.151 (1980); S. Hasegawa, ICRR Report 151-87-5 (1987).

[191] J. J. Lord and J. Iwai, Paper 515, presented at the International Conference on High Energy Physics, Dallas (1992); H. Wilczynski *et al.*, *Proceedings of the XXIV International Cosmic Ray Conference*, HE Sessions, Rome (1995), Vol.1, p.1.

[192] J. D. Bjorken, Int. J. Mod. Phys. A**7** p.4189 (1992).

[193] G. Wilk and Z. Wlodarczyk, J. Phys. G: Nucl. Part. Phys **32**, p.105 (1996), and Nucl. Phys.B (Proc. Suppl.) **52B** p.215 (1997).

[194] J.A. Chinellato, *et al.*, "Chirons", preprint, Waseda University; S.Hasegawa, *Proceedings of the VIII International Symposium on Very High Energy Cosmic Ray Interactions*, Tokyo (1994), p.115; S. Hasegawa and M. Tamada, Nuclear Physics B **474**, 141 (1996).

[195] L. T. Baradzei *et al.* (Chacaltaya and Pamir Collaboration), Nuclear Physics B **370**, 365 (1992)

[196] F. Halzen and D. A. Morris, Phys. Rev. **D52**, 1435 (1990).

[197] S. Miyake *et al.* J. Phys. Soc. Japan **18** (1963).